AD-A069 449 NEW MEXICO STATE UNIV LAS CRUCES DEPT OF PHYSICS F/G 4/1
STUDIES ON THE DEVELOPMENT OF ALGORITHMS FOR THE PREDICTION OF --ETC(U)
DEC 78 A MILLER, G H GOEDECKE, R C SHIRKEY DAAD07-78-C-0063
UNCLASSIFIED NMSU-PHYS-586-78-1 NL

1 OF 2
AD A069419

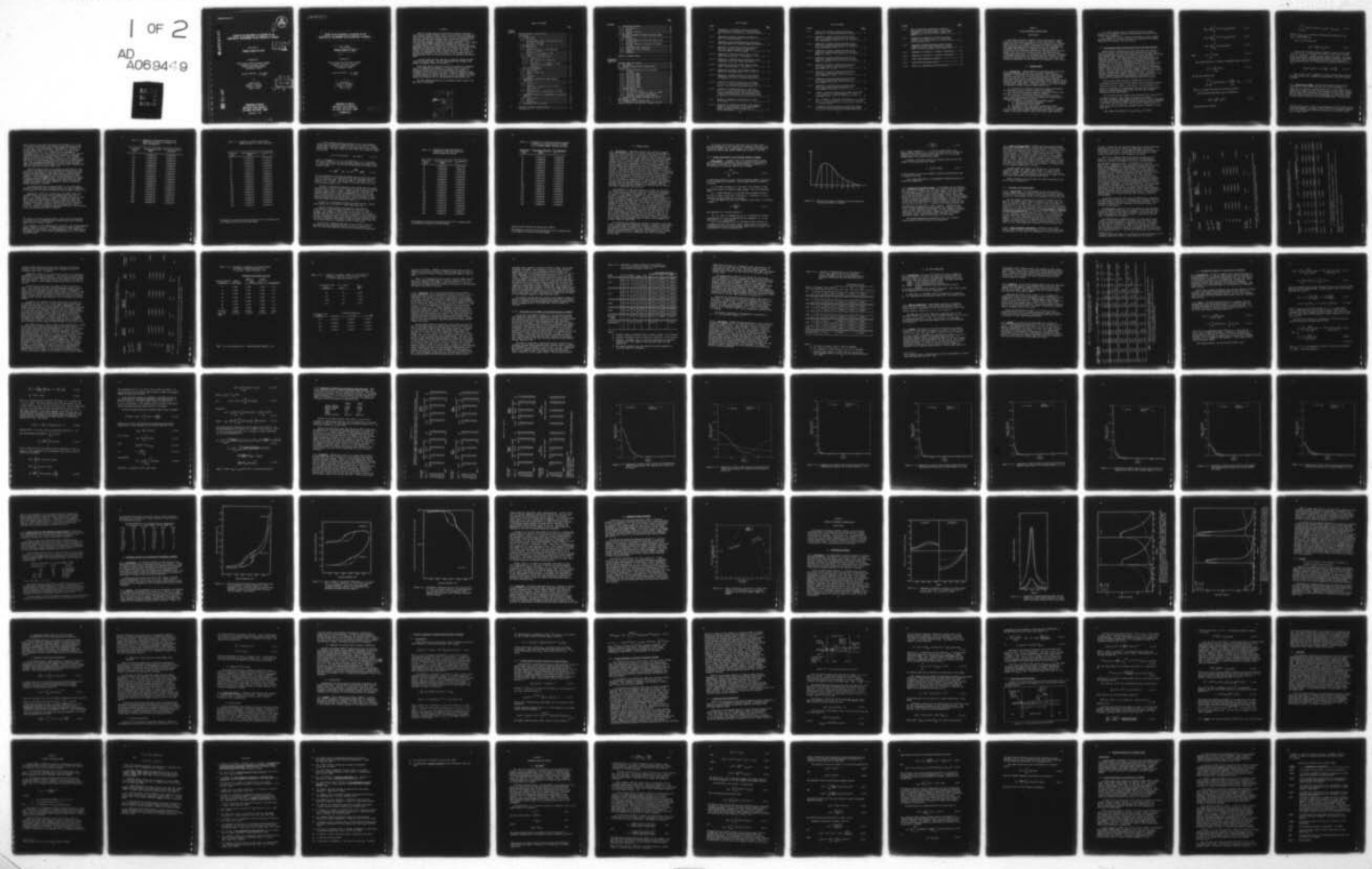

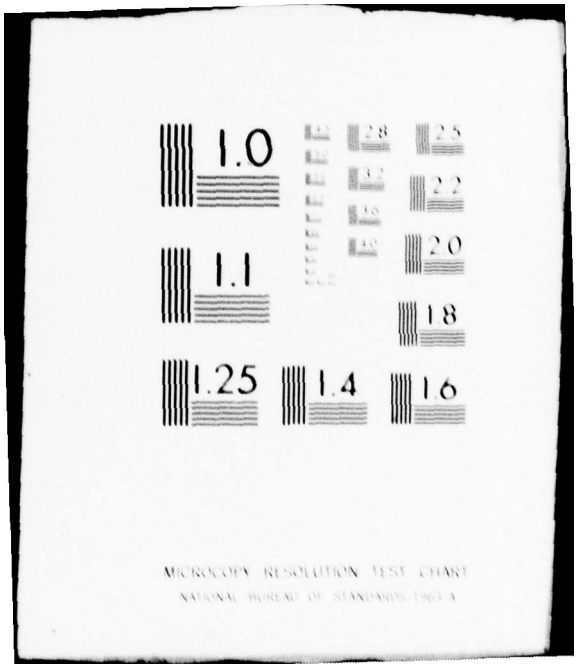
1.0
1.1
1.25
1.4
2.8
2.5
2.2
2.0
1.8
1.6
MICROCOPY RESOLUTION TEST CHART
NATIONAL BUREAU OF STANDARDS 1963 A

NMSU-PHYS-586-78-1

STUDIES ON THE DEVELOPMENT OF ALGORITHMS FOR THE PREDICTION OF TIME-DEPENDENT OPTICAL PROPERTIES OF AEROSOLS

Final Report

CONTRACT DAAD07-78-C-0063

Prepared for

United States Army Electronics Command
Atmospheric Sciences Laboratory
White Sands Missile Range
New Mexico 88002

Contract Monitors: J.B. Mason
J.T. Hall

by

August Miller
George H. Goedecke
Richard C. Shirkey
Yugal K. Behl

DEPARTMENT OF PHYSICS
NEW MEXICO STATE UNIVERSITY
LAS CRUCES, NEW MEXICO 88003

December, 1978

(14) NMSU-PHYS-586-78-1

(6)

STUDIES ON THE DEVELOPMENT OF ALGORITHMS FOR THE PREDICTION OF TIME-DEPENDENT OPTICAL PROPERTIES OF AEROSOLS

(9) Final Report,

CONTRACT/DAAD07-78-C-0063

(15)

Prepared for

United States Army Electronics Command
Atmospheric Sciences Laboratory
White Sands Missile Range
New Mexico 88002

Contract Monitors: J.B. Mason
J.T. Hall

by

(10) August/Miller,
George H./Goedecke
Richard C./Shirkey
Yugal K./Behl

DEPARTMENT OF PHYSICS
NEW MEXICO STATE UNIVERSITY
LAS CRUCES, NEW MEXICO 88003

(11) December, 1978

(12) 157 p.

402 005

Preface

This is the final report on activities and research performed under Contract DAAD07-78-C-0063. Most of the work done under the contract has been directed toward searches for ways in which existing ASL aerosol IR transmittance modeling codes could be made computationally more efficient in order to enhance their utility in applications involving time dependent variations in aerosol properties. In the course of those studies, NMSU personnel have examined both rigorous and approximate methods for calculating both single and multiple scattering extinction and scattering effects, and have devised a new version of the NMSU/ASL code AGAUS which permits the user to "trade-off" overall accuracy for significantly faster program execution. The latter code has also been modified in such a way that it can be easily used for generating data which can be used directly by the ASL Smoke Obscuration Model.

A serious effort has also been made to generate improved documentation for program AGAUS. The new documentation will probably also enhance the general utility of the code.

Other minor efforts under the contract have resulted in modification of the NMSU/ASL code ATRANX [1] to permit users to choose an additional line-profile (the Van Vleck-Weisskopf line shape), to reorganize certain portions of the code to decrease computation times, to permit users of the aerosol sub-code to allow for changes in particle sizes with changes in relative humidity, and the integration of a more sophisticated Galatry code for the generalized Voigt profile case.

The work summarized above will be presented in more detail in the main body of this report.

TABLE OF CONTENTS

Page

LIST OF TABLES

LIST OF FIGURES

Chapter 1

SINGLE-SCATTERING INVESTIGATIONS

Introduction

This chapter presents a summary of work characterized as single scattering studies which was carried out under the contract. These studies have led to the development of two new versions of the ASL/NMSU single-scattering code (AGAUS), comparisons of several different Mie codes vis a vis computational speed and accuracy, the development of a new analytic approximation for computation of angular intensity distributions for polydisperse aerosols, and some extensions of earlier studies of the way in which relative humidity may affect infrared transmittance predictions. In addition, both newly developed versions of the ASL/NMSU single-scattering code AGAUS have been subjected to further evaluations with respect to the results generated by other codes, and extensive documentation has been prepared as an appendix to this report.

1.1 PROGRAM AGAUS9

1.1.1 Introduction: Program AGAUS9 is an extended version of earlier programs developed by NMSU and ASL code PGAUSS. AGAUS9 has the capability of generating "scattering fractions" with a normalization consistent with that used in the ASL Smoke Obscuration Model (ASLSOM), while retaining the option of generating phase-function expansion coefficients which may be desired for subsequent usage in the ASL multiple scattering code STAR04 (and its derivative codes) or the NMSU/ASL aerosol thermal emission code CLEM70. Additional features to be found in AGAUS9 (as compared to PGAUSS or earlier AGAUS versions) are:

(1) Provision for automatic cycling over a range of wavelengths and averaging of results over such a range of wavelengths.
(2) Provision for treating changes in hygroscopic particle sizes which may occur with variations in relative humidity.
(3) Inclusion of an internal subroutine to provide automatic look-up and/or interpolation of optical constants for liquid water at wavelengths between 0.35 μm and 200 μm.
(4) The addition of two new size-distribution models:
    A) User-supplied Bimodal parameters,
    B) Marshall-Palmer "rain" model.
(5) Conversion of most input data to common data formats.
(6) Replacement of the undocumented ASL "Fog model" by a special version of the "modified gamma" distribution whose control parameters include "liquid water content" rather than droplet number densities.

(7) Options whereby users can either define particle number densities or let them be calculated from mass density and mass concentration input parameters.

(8) Addition of internal checks to warn users if certain computed quantities seem to be failing to converge, and extended error messages associated with failures in the Mie routine.

1.1.2 Relationships between Scattering Fractions and Phase Functions

Among the major objectives of the work done under this contract was the conversion of the ASL/NMSU single scattering code AGAUS into a form which produced the types of data required by the ASL Smoke Obscuration Model (ASLSOM) while retaining the variety of options previously developed for AGAUS. That conversion required that AGAUS be given the additional capabilities of predicting (a) attenuation coefficients or cross-sections in units of square meters per milligram of aerosol material, and (b) so-called "scattering fractions" per unit aerosol mass. Unfortunately, the available documentation for the Mie code used in ASLSOM's parent code was not very clear as to the precise relationships between "scattering fractions" and the customary quantities used in Mie theory. That fact made the conversion of AGAUS a great deal more tedious and time consuming than it might otherwise have been. In order to attempt to avoid future possible confusions on those relationships, they will be summarized below before proceeding to a discussion of the evaluation of the versions of AGAUS developed under this contract.

The so-called "phase functions", denoted here by $P_f(\mu)$ and "scattering fractions" $S_f(\theta)$ are both derived from the average scattered intensities $(I_1+I_2)/2$ defined in Mie theory. The two quantities are related to one another for calculations associated with a single wavelength by a simple multiplicative factor, but they have different interpretations and applications.

Let $I(\alpha,m,k,\theta)$ be the average of the intensities $i_1(\theta)$ and $i_2(\theta)$ for scattering at angle θ from a sphere whose Mie-size parameter is $\alpha = 2\pi r/\lambda$, and whose complex index of refraction is $n = m-ik$. Furthermore, let $n(r)dr$ be the relative number of aerosol particles with radii between r and $(r+dr)$, and let $Q_{ext}(\alpha,m,k)$ and $Q_{sca}(\alpha,m,k)$ respectively be the total extinction and scattering efficiency factors as defined by van de Hulst [2].

Now, define the quantities $\bar{I}$, $\bar{C}_{ext}$ and $\bar{C}_{sca}$ as follows:

$$\bar{C}_{ext} = \frac{1}{N_T} \int_{r=o}^{\infty} \pi r^2 \, n(r) \, Q_{ext}(\alpha,m,k)dr, \qquad (1.1\text{-}1)$$

$$\bar{C}_{sca} = \frac{1}{N_T} \int_{r=o}^{\infty} \pi r^2 \, n(r) \, Q_{sca}(\alpha,m,k)dr, \qquad (1.1\text{-}2)$$

$$\bar{I}(\theta) = \frac{1}{N_T} \int_{r=o}^{\infty} I(\alpha,m,k,\theta)n(r)dr, \qquad (1.1\text{-}3)$$

where $$N_T = \int_{r=o}^{\infty} n(r)dr. \qquad (1.1\text{-}4)$$

The "phase-function" as defined in program(s) AGAUS is given by

$$P_f(\theta) = \frac{\lambda^2}{\pi \, \bar{C}_{ext}} \bar{I}(\theta) \ , \qquad (1.1\text{-}5)$$

and has the property that

$$\int_{\phi=o}^{2\pi} \int_{\theta=o}^{\pi} P_f(\theta)d\phi \; d(\cos\theta) = 4\pi \frac{\bar{C}_{sca}}{\bar{C}_{ext}} \equiv 4\pi\tilde{\omega}_o \ , \qquad (1.1\text{-}6)$$

where $\tilde{\omega}_o$ is called "the albedo for single scattering."

The "scattering fractions" $S_f(\theta)$ are defined by

$$S_f(\theta) = \left(\frac{\lambda}{2\pi}\right)^2 N_T \, \bar{I}(\theta), \qquad (1.1\text{-}7)$$

and $S_f(\theta)$ has the property

$$\int_{\phi=o}^{2\pi}\int_{\theta=o}^{\pi} S_f(\theta)\, d\phi\, d(\cos\theta) = \bar{C}_{sca}\cdot N_T = (C_{sca})_{total}, \quad (1.1\text{-}8)$$

wherein $(C_{sca})_{total}$ is the total scattering cross-section per unit mass of aerosol material.

Thus, it will be seen that

$$S_f(\theta) = (\frac{1}{4\pi} N_T \bar{C}_{ext}) P_f(\theta). \quad (1.1\text{-}9)$$

The ASL Smoke Obscuration Model (ASLSOM) is coded with the assumption that $(C_{sca})_{total}$ as derived from $S_f(\theta)$ will have units of square meters per milligram. ASL/NMSU programs AGAUS9 and AGAUS10, (see below) on the other hand are coded in what are basically CGS units. Conversion from $I(\theta)$ to $S_f(\theta)$ in the ASLSOM normalization therefore requires a unit-conversion factor for λ^2 from μm to m, and for N_T from cm^{-3} to m^{-3}, i.e.,

$$[\lambda(\mu m)]^2\, N_T(cm^{-3}) \times (10^{-6}\, \frac{m}{\mu m})^2 \times 10^6\, \frac{cm^3}{m^3}. \quad (1.1\text{-}10)$$

Thus, a factor 10^{-6} is required to convert the scattering fractions from the internal units of NMSU/ASL program AGAUS to the units expected by ASLSOM.

1.1.3 Evaluation of AGAUS9: Once the relationships between the Mie intensities, i_1 and i_2 described above were clearly elucidated, it seemed that it would be a straightforward task to convert AGAUS from the computation of phase functions to the calculation of scattering fractions. When the appropriate conversions were completed, the new version, AGAUS9, was run using, as nearly as could be determined, the same aerosol model for which results were found in the SOM documentation.* The particular

*The label SOM is used to refer to the document entitled "The Effectiveness of Obscuring Smokes", by Johnson, Forney and Dolce, an unpublished description of the JTCG/ME smoke obscuration model which was supplied to NMSU by R.B. Gomez of ASL.

model used was a log normal distribution for WP smoke ($\bar{r}$ = 0.37 μm, σ = 1.54 μm), 200 particle radii between minimum and maximum values of 0.005 and 1.0 μm, respectively, a mass density of 1.87 gm/cc, a particle number density of 1.276345×10^3 cm^{-3}, and complex index of refraction m = 1.43 - 0i. Computations were performed at 7 wavelengths (0.40, 0.45, 0.50, 0.55, 0.60, 0.65 and 0.70 μm), and the scattering fractions were arithmetically averaged over wavelength. Some of the results are presented in Table 1.1.1. Only a cursory examination of that table is needed to observe that the AGAUS9 results were not in very good agreement with those found in the SOM documentation. This comparison was something of a shock, because the basic AGAUS code had previously been found to give much better agreement with other Mie codes than is seen in Table 1.1.1.

Because thorough reviews of the program listings failed to shed any light on the reasons for such large apparent discrepancies it was decided that comparisons of computations made at a single wavelength (rather than after averaging over several wavelengths) were highly desirable. The problem there was that the SOM documentation did not contain any single wavelength results. Since that avenue for testing of AGAUS9 was closed, some other approach was needed, and was found through the courtesy of ASL which supplied a copy of the Radiation Research Associates' code MIE-2.

The aerosol model used to generate Table 1.1.1 was then passed through both AGAUS9 and the ASL supplied MIE-2 code using a wavelength of 0.40 μm only. The results of those two runs are shown in Table 1.1.2.*

Examination of Table 1.1.2 reveals that the AGAUS9 results and the MIE-2 results are in much better agreement than those seen in Table 1.1.1. Whereas Table 1.1.1 shows discrepancies even in the first digit at many scattering angles, Table 1.1.2 shows that AGAUS9 and MIE-2 agree to at least five and often six significant digits--the nominal accuracy which is used in terminating Mie series calculations in AGAUS9. It appears, therefore, that the disagreements found in Table 1.1.1 should be interpreted as casting doubts on the results quoted in the SOM documentation rather on AGAUS9.**

*The results of the ASL supplied version of MIE-2 have been multiplied by a factor of 10^2 to offset different normalizations used in SOM and AGAUS9 and ASL's version of MIE-2.

**It is possible, but not demonstrated at this point, that the discrepancies might be traced to the use of a "single-precision" version of MIE-2 in generating the data listed in the SOM documentation. Both AGAUS9 and the ASL supplied version of MIE-2 used in generating table 1.1.2 are "double-precision" codes.

Table 1.1.1 Comparison of Scattering Fractions from AGAUS9 and SOM Report as Averaged for a Seven Wavelength Run.

Scattering Angle	Scattering Fractions (NMSU)	Scattering Fractions SOM report
0	0.5840074-02	0.530822-02
10°	0.3385669-02	0.294243-02
20°	0.1236144-02	0.961893-03
30°	0.5525204-03	0.419528-03
40°	0.2882904-03	0.254840-03
50°	0.1637546-03	0.176892-03
60°	0.9840574-04	0.114931-03
70°	0.6277324-04	0.706178-04
80°	0.4262488-04	0.445657-04
90°	0.3097364-04	0.309732-04
100°	0.2429897-04	0.249208-04
110°	0.2086846-04	0.237614-04
120°	0.2023009-04	0.265251-04
130°	0.2267312-04	0.330425-04
140°	0.3014750-04	0.446135-04
150°	0.4592933-04	0.637035-04
160°	0.6781825-04	0.883152-04
170°	0.4512012-04	0.678717-04
180°	0.6003613-04	0.836141-04

Table 1.1.2 Comparison of Results from Runs of AGAUS9 and MIE2 at a Single Wavelength.

Scattering Angle	Scattering Fractions (NMSU)	I^{*}_{avg} (RRA-MIE2)
0°	8.215439-03	8.215442-03
10	3.341243-03	3.341238-03
20	8.565565-04	8.565530-04
30	4.126651-04	4.126640-04
40	2.452253-04	2.452247-04
50	1.503114-04	1.503111-04
60	9.399925-05	9.399906-05
70	6.098411-05	6.098398-05
80	4.167272-05	4.167267-05
90	3.019892-05	3.019886-05
100	2.333270-05	2.333268-05
110	1.957286-05	1.957282-05
120	1.854355-05	1.854351-05
130	2.096545-05	2.096542-05
140	2.942918-05	2.942910-05
150	4.947500-05	4.947498-05
160	8.643879-05	8.643865-05
170	6.208783-05	6.208780-05
180	7.644555-05	7.644557-05

*The RRA-MIE-2 results have been multiplied by 10^2 to normalize them in the same way as found in the SOM document.

To avoid drawing erroneous conclusions on the cross-agreements between results produced by AGAUS9 and MIE-2 on the basis of a single aerosol model, additional comparisons were made using a quite different aerosol model. The model chosen for this "test" was a "modified" gamma distribution:

$$f(r) = Ar^{\alpha} \exp(-Br^{\gamma}), \quad \text{[for MIE-2]} \qquad (1.1\text{-}11)$$

with $A = 1.0396 \times 10^{6}$, $\alpha = 7.5$, $B = 28.333333$ and $\gamma = 1.0$. The input data used by AGAUS9 are the particle number density N_T and mode radius r_c, rather than A and B, but the various quantities are related to one another through:

$$r_c = \left(\frac{\alpha}{\gamma B}\right)^{1/\gamma} \quad \text{and} \quad N_T = AB^{-\left(\frac{\alpha+1}{\gamma}\right)} \Gamma\left(\frac{\alpha+1}{\gamma}\right). \qquad (1.1\text{-}12)$$

For this comparison the minimum and maximum particle radii were taken to be 0.01 μm and 1.5 μm, respectively, and 200 individual values of particle radii were used. The run was made at a wavelength of 0.6 μm using $m = 1.53 - 0.006i$. Some results of the first runs of this type will be found in Table 1.1.3.

Contrary to the excellent agreement found between MIE-2 and AGAUS9, the data found in Table 1.1.3 did not agree as well as had been expected being good only to about 4 digits. Further analysis indicated that the most probable source of these disagreements lay in the fact that AGAUS9 and MIE-2 did not choose the values of particle radii actually used in the calculation in the same way. Slight alterations to remove these differences were then made in AGAUS9, and the calculations were repeated, yielding the data presented in Table 1.1.4.

In Table 1.1.4 discrepancies between the AGAUS9 and MIE-2 results again appear only in the fifth or sixth significant digit.

The above results indicate once again that code AGAUS9 is quite capable of yielding results which are as reliable as those of MIE-2. The changes in AGAUS9 needed to bring about the level of agreement seen in Table 1.1.4 involved only the choice of the values of the 200 radii used, and illustrates that the method of choosing the radii can have a significant effect on the values of the scattering fractions even when a relatively large number of radii are used. That matter will be discussed further in a subsequent section of this report.

At this point, AGAUS9 has been shown to be as valid as MIE-2 in the computation of scattering fractions, so that the conversion of AGAUS into an ASLSOM compatible form has been successfully accomplished.

Table 1.1.3 Comparison of Scattering Fractions Calculated by MIE-2 and AGAUS9 for a Modified Gamma Distribution

Scattering Angle	Scattering Fractions (NMSU)	I^{*}_{avg} (RRA-MIE2)
0°	9.254421-08	9.254768-08
10	7.620680-08	7.620913-08
20	4.470319-08	4.470374-08
30	2.156754-08	2.156747-08
40	1.038258-08	1.038255-08
50	5.626184-09	5.626226-09
60	3.415889-09	3.415935-09
70	2.236736-09	2.236776-09
80	1.555144-09	1.555170-09
90	1.149602-09	1.149602-09
100	9.113908-10	9.114065-10
110	7.876338-10	7.876470-10
120	7.656564-10	7.656688-10
130	8.657526-10	8.657658-10
140	1.074210-09	1.074245-09
150	1.193137-09	1.193200-09
160	1.134702-09	1.134755-09
170	1.502157-09	1.502236-09
180	1.969069-09	1.969203-09

*The RRA-MIE-2 results have been multiplied by 10^2 to normalize them in the same way as found in the SOM document.

Table 1.1.4 Comparison of Scattering Fractions Produced by MIE-2 and a Special Version† of AGAUS9 for a "Modified Gamma" Distribution Model.

Scattering Angle	Scattering Fractions (NMSU)	I^*_{avg} (RRA-MIE2)
0°	9.254772-08	9.254768-08
10	7.620918-08	7.620913-08
20	4.470380-08	4.470374-08
30	2.156751-08	2.156747-08
40	1.038257-08	1.038255-08
50	5.626233-09	5.626226-09
60	3.415938-09	3.415935-09
70	2.336777-09	2.336776-09
80	1.555171-09	1.555170-09
90	1.149623-09	1.149622-09
100	9.114071-10	9.114065-10
110	7.876480-10	7.876470-10
120	7.656697-10	7.656688-10
130	8.657668-10	8.657658-10
140	1.074245-09	1.074245-09
150	1.193200-09	1.193200-09
160	1.134755-09	1.134755-09
170	1.502236-09	1.502236-09
180	1.969203-09	1.969203-09

†particle radii selected the same way as in MIE-2.

*The RRA-MIE-2 results have been multiplied by 10^2 to normalize them in the same way as found in the SOM document.

1.2 PROGRAM AGAUS10

1.2.1 Introduction: Experience acquired over a period of several years with various versions of the single scattering codes PGAUSS and AGAUS has revealed that users of such codes often tend to be over-conservative in their choice of the number of radii at which Mie calculations are performed. Many single scattering codes (including PGAUSS, AGAUS9, and R.R.A.'s MIE-2) require that the user specify some input parameter such as the total number of radii to be used. Unless a user has had a great deal of experience with choosing such parameters for various types of size distributions, there is a tendency to use many more radii than may be needed to obtain results at acceptable levels of accuracy. Since the overall running time of Mie codes may be greatly reduced by reducing the number of particle sizes treated, it is desirable to have a code in which one specifies an acceptable level of accuracy and which then uses only as many particle radius values as are needed to satisfy that requirement. The concept of a Mie code written along that line is not new and, in fact, ASL already has a code of that nature but it is one which is limited solely to log-normal size distributions. In view of the fact that substantial savings in computer time might be obtained, while maintaining a great deal of versatility, NMSU has developed a special version of AGAUS9 called AGAUS10 which is based on the sorts of compromises indicated above.

Code AGAUS10 is in many ways identical to AGAUS9, but the method for choosing values for particle radius and the scheme for integration over a size distribution is quite different. Rather than specifying the number of radii (NRADI for AGAUS9), the user of AGAUS10 must specify a "convergence" level DELTA. The quantity DELTA represents the minimum fractional accuracy that is acceptable for certain results of a run. In operation, AGAUS10 then runs through the Mie calculations and integrations over size using only a few particle radii and obtains first estimates of extinction coefficients, etc. The size intervals are then reduced to one-half their former value and new estimates are calculated. If the new and old estimates agree to within (DELTAx100) percent, then AGAUS10 ceases to treat additional particle sizes and proceeds to its final calculations. If the new estimate does not agree with the "old" one to within (DELTAx100) percent, the size interval is again cut in half and the calculations and comparisons are repeated. The cycling occurs repetitively until either the convergence criterion is satisfied or until some pre-coded maximum number of values (513 for AGAUS10) for particle radius have been used.

It is believed that AGAUS10 will represent a substantial advancement in ASL's aerosol modeling capabilities because it contains a large variety of size distributions, the possibility of modeling mixtures of aerosols with different optical properties, treats changes in particle size with variable relative humidity, is compatible with ASLSOM, and will probably provide substantially shorter computation times than most existing aerosol codes.

In the next few sections of this report will be found a more detailed description of the theoretical and numerical techniques which distinguish AGAUS10 from its predecessors, and comparisons between the results and running times AGAUS9, AGAUS10 and the R.R.A. code MIE-2.

1.2.2 Further Description of the "Halving" Methods of AGAUS10

Basic Concept. A general idea of how program AGAUS10 operates can be obtained by considering a numerical method for determining the area under a curve g(R) vs R such as that sketched in figure 1.2.1. The objective is to evaluate numerically an integral

$$G = \int_{R=o}^{R=\infty} g(R)\, dR \qquad (1.2\text{-}1)$$

to some desired agree of accuracy using the smallest number of values of R for the numerical calculations. The procedure adopted in AGAUS10 is as follows:

(1) An initial estimate G_1 of the value of the integral is made using three values of R labeled by Roman numeral I and the "trapezoidal rule".

(2) A second estimate G_2 is then made using increments ΔR which are half as large as those used in getting G_1. In getting G_2, the two additional R-values labeled II are utilized.

(3) The values of G_2 and G_1 are compared to each other by calculating a quantity

$$\delta = \frac{|G_2 - G_1|}{|G_2|} \qquad (1.2\text{-}2)$$

and comparing it to a pre-set quantity Δ.

If $\delta < \Delta$, then it is assumed that G_2 is a "sufficiently" accurate representation of G, and the computations are terminated. If, on the other hand, $\delta > \Delta$, one proceeds.

(4) A third estimate G_3 of G is then made by again cutting the increments ΔR to half its previous value. This results in the addition of computations at the four new R-values labeled III in the figure 1.2.1. A new value of δ is then calculated from

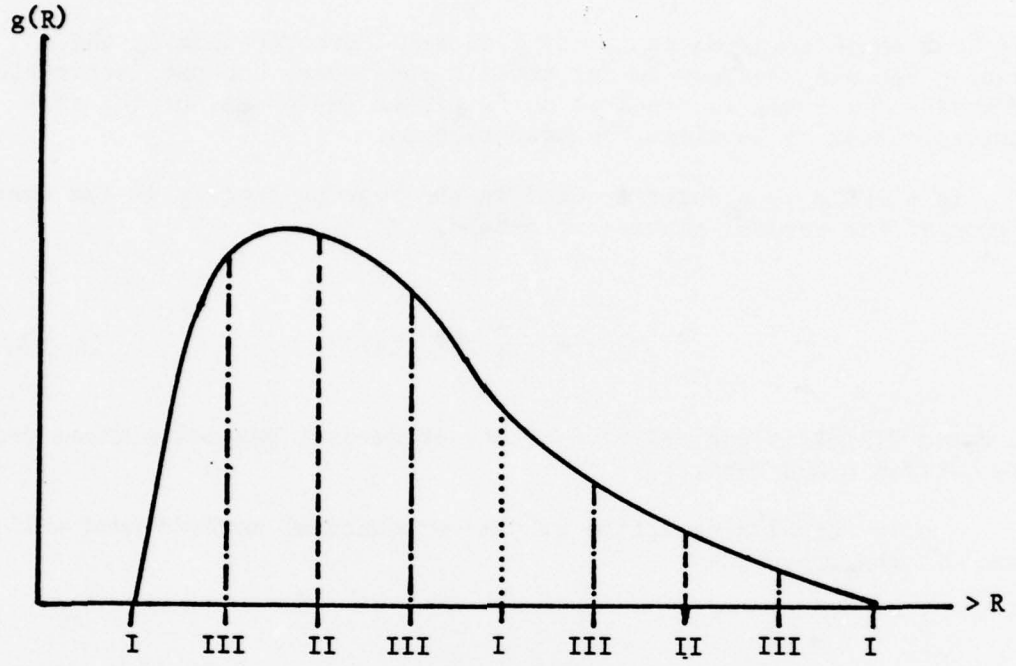

Figure 1.2.1 Sketch of how values of particle radii are selected in the halving procedure of AGAUS10.

$$\delta = \frac{|G_3 - G_2|}{G_3} , \qquad (1.2\text{-}3)$$

and δ is again compared to Δ. If δ is still greater than Δ, the spacing between R-values is cut in half once more, and the "estimation-comparison" process is repeated until either (a) $\delta < \Delta$, or (b) some maximum number of R-values has been reached.

In AGAUS10, the quantity used in the testing process is the total volume of the aerosol particles, namely,

$$V = \int \frac{4}{3} \pi R^3 \, f(R) dR, \qquad (1.2\text{-}4)$$

in which $f(R)dR$ is the relative number of aerosol particles whose radii lie between R and R+dR.

A more formal description of the mathematical methods used will be found in the appendices.

1.2.3 Extensions to the Basic Concept: It may happen that the function g(R) illustrated in figure 1.2.1 will have a form which is much "smoother" over some range of R-values than over other ranges. Strict application of the halving procedure to such a situation could easily lead to the use of many more R-values in one of those ranges than are really needed because of the behavior of g(R) in other R-ranges. Such a situation seems especially likely with asymmetric size-distributions. One way of attempting to avoid un-needed computations in various R-ranges is to split the regions used in halving loops into several distinctive "intervals"--say, R_A to R_B, R_B to R_C, R_C to R_D, ..., and to do the halving operations and convergence tests separately for each "interval". AGAUS10 has been coded to permit separate halving computations and convergence testing for up to eight "intervals" of that type. In fact, however, the present coding uses two radius "intervals" (ranges) for those distributions f(R) known to show a single maximum, four "intervals" for bi-modal distribution models, and just one interval for other models.

The detailed mathematical description of the use of multiple size-intervals will also be found in the appendices.

1.2.4 Usage of Program AGAUS10: AGAUS10 has been developed somewhat concurrently with AGAUS9, and a strenuous effort has been made to make their input and output data more or less identical. It is believed that the objective has generally been fulfilled, but a few differences in input data exist. In particular, AGAUS9 requires the user to supply a value (NRADI) for the number of radii to be used in a run, whereas AGAUS10 requires that the user specify a value for the convergence level Δ (DELTA). Those input data are arranged, however, so that the same set of data cards can be used as input to either program: AGAUS9 will ignore any given value of DELTA, and AGAUS10 will ignore the user supplied value of NRADI--except for the case IDSTP = 0, in which f(R) is to be supplied externally by the user.

Programs AGAUS9 and AGAUS10, for the most part, use the same subroutines (ANGLE, GAUS, GUSET, MIEGX, WATER), or slight variants (AG9PT3 is the same as AGXPRT except in title; the same is true of AG9PRT and AGXPRT). Non-interchangeable routines are the main programs, subroutines AG9PT1/AGXPT1 and routines AG9PT2/AGXPT2.

Sample compatible input data decks for several distribution types will be found in appendix A.4.

1.2.5 Evaluation of Program AGAUS10

1.2.5.1 Introduction: In the development of the actual coding of program AGAUS10, continuous testing and comparison of results produced by the new codes and those yielded by other single scattering codes was carried out. The findings of a few such comparisons will be given next.

The supplementary codes used for evaluation of AGAUS10 were the NMSU/ASL code AGAUS9, and the Radiation Research Associates code, MIE-2, which was supplied to NMSU by ASL. In order to avoid the problem of deciding which of the three codes was "correct" in the event that no two agreed well, all codes were run using aerosol models for which independent results could be found in Deirmendjian's book Electromagnetic Scattering on Spherical Polydispersions [3]. The specific models used for comparison runs were Deirmendjian's cloud models C.1 and C.3 at a wavelength of 0.7 μm. Additional comparison runs were made at 10.6 μm using an NMSU simulated hygroscopic smoke model [1] and several values of relative humidity. The latter comparisons involved only program AGAUS9 and AGAUS10. The objectives of all comparisons were not only to show that AGAUS10 was working properly, but also to determine whether or not it would, in fact, offer significant reductions in overall running time.

1.2.5.2 Water Cloud Model Comparisons: Comparison runs of codes AGAUS9, AGAUS10 and MIE-2 for cloud models C.1 and C.3 were made using the same range of radii quoted for Deirmendjian's tables T.36 and T.30.

In order to assure that any conclusions drawn about relative computation times would be valid in the context of ASLSOM usage, scattering fractions were calculated at 2° increments between scattering angles of 0° and 180° in these runs. AGAUS10 was also run for model C.1 using several different values of the convergence level DELTA.

Table 1.2.5.1 presents some of the results obtained for cloud model C.1. The scattering fraction entries for the "Deirmendjian" column were obtained by averaging his P_1 and P_2, and multiplying by the appropriate conversion factor. The AGAUS10 run listed used DELTA = 0.01. Examination of the tabulated data shows that none of the three runs yields exactly the same extinction coefficient that was printed by Deirmendjian, but all were within 0.3% of his results. Unfortunately, Deirmendjian's table T.36 did not include angles at 2° increments, so only forward and backward scattering fractions could be inferred accurately. It will be seen that all three codes gave scattering fractions which agreed well in the $\theta = 0°$ direction, but the results are obviously not identical. The variations are, however, quite a bit larger at other scattering angles, although the variations are really not terribly large when their magnitudes compared to that of the forward scattering. For this particular model, it will be noted that AGAUS10's convergence criterion led to its use of more radii than were used with the other codes. It will also be seen that MIE-2 handled the 40 radii faster than did AGAUS9. MIE-2's speed advantage over AGAUS9 probably results from the fact that MIE-2 uses a non-uniform spacing of particle radii--a procedure which leads to a significantly smaller number of Mie calculations which must be done at large Mie size-parameters.

It should be noted that the version of AGAUS10 used in generating the results shown in Table 1.2.5.1 performed its "convergence test" on the total aerosol volume and not on the scattering fractions. (Results obtained by checking on both volume and the scattered intensity at 90° will be given below.)

Although AGAUS10 appears to offer no computation speed advantage if the user KNOWS how many radii are "enough", it does have the useful feature (not found in either MIE-2 or AGAUS9) of giving the user some idea of how many radii were really required to achieve some minimum level of confidence in its results.

By repeating runs of AGAUS10 and Model C.1 using various values of DELTA, it has been possible to learn more about the sensitivities of the extinction coefficient and scattering fractions to the number of radii used in a calculation. Table 1.2.5.2 contains the results of a few runs of that type. The first four entries represent runs in which the quantity which was tested for convergence was the total volume of the aerosol particles.† The fifth and sixth entries are the results

†Volume was used rather than, say, extinction cross-section because its R^3 dependence appeared to make it a "more sensitive" test quantity.

Table 1.2.5.1 Comparisons of Results and CPU Times for Three Single Scattering Codes - Cloud Model C.1. (λ = 0.7 μm.)

Quantity	AGAUS-9 (NMSU/ASL)	AGAUS-10 (NMSU/ASL (Delta - 0.01)	MIE 2 (RRA)	Deirmendjian T.36
K_{ext} (km^{-1})	16.7512	16.7223	16.780	16.73
K_{sca} (km^{-1})	16.7512	16.7223	16.780	16.73
Scattering Fractions				
θ				
0°	2.2438E0	2.2404E0	2.2534E0	2.237E0
44°	1.952E-3	1.784E-3	1.0875E-3	
90°	6.1552E-5	4.8011E-5	5.6898E-5	
136°	1.8252E-4	1.9026E-4	2.1120E-4	
180°	8.9722E-4	8.3856E-4	8.9161E-4	8.457E-4
CPU Time (Seconds)	86.86	82.81	75.35	
No. of Radii	40	50	40	440

*Notes AGAUS9 and AGAUS10 scattering fractions at 0°, when converted to phase functions have values of 1683. as compared to Deirmendjian's values of 1680.

Table 1.2.5.2 Comparison of AGAUS10 Results Obtained with Four Convergence Test Levels Using Cloud Model C.1. (λ = 0.7μm)

Convergence Level	NRADI	CPU (Seconds)	K_{ext} (km^{-1})	Scattering Fractions 0°	44°	90°	136°	180°
0.05	26	45.28	17.47	2.4521E0	1.1280E-4	5.2019E-5	1.8805E-4	7.4914E-4
0.01	50	82.81	16.72	2.2404E0	1.1784E-3	4.8011E-5	1.9026E-4	8.3856E-4
0.005	66	127.93	16.74	2.2395E0	1.1697E-3	5.6570E-5	1.9095E-4	8.7430E-4
0.001	130	245.13	16.73	2.2370E0	1.1815E-3	5.4473E-5	1.8960E-4	8.2393E-4
*0.05	98	220.91	16.73	2.2369E0	1.1814E-3	5.5012E-5	1.9213E-4	8.3975E-4
**0.005	513	143.73	16.75	2.2411E0		5.5880E-5		8.8647E-5

Notes: a) In these runs, the quantity which was tested for convergence was the total volume of the aerosol particles.
b) In these runs, scattering fractions were calculated at 2° increments.

*Special Version of AGAUS10 with convergence checks on scattered intensity at 90° as well as on volume.

**Similar to * case, but only 5 angles used.

of runs in which testing was done on both volume and the scattered intensity of 90°; note that the sixth entry represents a run at 45° increments rather than 2° increments.

Examination of Table 1.2.5.2 shows that the value of the extinction coefficient is not nearly as sensitive to the choice of particle radius values as are the scattering fractions at fairly large scattering angles, especially near 90°. The 90° results show "oscillations" of as much as 15% as the number of radii changes through the set {26, 50, 66, 98, 130, and 513}.

It should also be noted that the AGAUS9 and MIE-2 runs shown in Table 1.2.5.1 used only 40 radii, while Deirmendjian evidently used 440 radii. Even with that vastly larger number of radii, Deirmendjian's results are not so different from the present results to warrant, in many applications, an additional increase in computation time of a factor of eleven. It was, in fact, observations of that type gleaned from earlier usage of AGAUS versions, that eventually led to the decision to develop AGAUS10.

A similar set of comparative results obtained for cloud model C.3 are presented in Table 1.2.5.3. For this model, AGAUS9 and MIE-2 were run with the same number of radii as was used by Deirmendjian. This example illustrates the way in which AGAUS10 can offer definite decreases in CPU time over codes requiring the user to make an a priori decision as to the number of radii needed. Using only 66 radii, AGAUS10 produced an extinction coefficient to within better than 1% of Deirmendjian's value (with which AGAUS9 and MIE-2 results are identical to the four digits given by Deirmendjian). AGAUS10, (with DELTA = 0.01), however, ran nearly four times faster than either AGAUS9 or MIE-2. Furthermore, the AGAUS10 run at DELTA = 0.01 yielded scattering fractions which, at worst, differed from those found by AGAUS9 and MIE-2 by the order of 10%.

Cloud models such as C.1 and C.3 used at short wavelengths (≈ visible) are severe tests of single scattering codes because they typically involve some rather large Mie size-parameters ($\alpha \approx 110$ for the C.1 model). Calculations performed at infrared wavelengths for smaller particles than found in typical clouds are not quite so demanding. That fact is illustrated partially, by Tables 1.2.5.4 and 1.2.5.5, which were compiled using an NMSU hypothetical model for a hygroscopic smoke having the particle size-distribution of white phosphorous smoke. The model used here was denoted as model A' in an earlier document [1]. Table 1.2.5.4 shows extinction coefficients obtained from AGAUS9 (using 100 radii), and AGAUS10 (using DELTA = 0.01) at seven different values of relative humidity. It also presents the results of a run of a special version of AGAUS10 (labeled AGAUSXL) in which the RRA Mie-routine DOWN42 was used instead of routine MIEGX. It will be seen that AGAUS10 (and AGAUSXL) needed only 34 radii to reach extinction coefficients within 0.2% of those found by AGAUS9, but the AGAUS9 run used 340% more computer

Table 1.2.5.3 Comparisons of Results and CPU Times for Three Single Scattering Codes - Cloud Model C.3. (λ = 0.7μm).

Quantity	AGAUS-9 (NMSU/ASL	AGAUS-10* (NMSU/ASL)		MIE 2 (RRA)	Deirmendjian T.60
		Δ = .01	Δ = .001		
K_{ext} (km^{-1})	3.0212	3.0078	3.0151	3.0218	3.021
K_{sca} (km^{-1})	3.0212	3.0078	3.0151	3.0218	3.021
Scattering Fractions*					
θ					
0°	5.3970E-2	5.3569E-2	5.3796E-2	5.3946E-2	5.396E-2
44°	2.1276E-4	2.1398E-4	2.1220E-4	2.1182E-4	
90°	2.0787E-5	2.1668E-5	2.2180E-5	2.0366E-5	
136°	3.5852E-5	3.2756E-5	3.4983E-5	3.5562E-5	
180°	2.0350E-4	1.7792E-4	1.9798E-4	2.0269E-4	1.649E-4
CPU Time* (Seconds)	289.79	71.49	131.5	266.36	
No. of Radii	280	66	130	280	280

*Notes: a) All runs calculated Scattering Fractions at 2° increments between 0° and 180°.

b) The quantity tested for convergence was the total aerosol volume.

Table 1.2.5.4 Comparisons of Results from Programs AGAUS9 and AGAUS10 for NMSU Smoke Model A' at λ = 10.6 μm. (Relative humidity = 0%)

	Extinction Coefficients (per km)			
Relative Humidity (percent)	AGAUS9 (100 radii)	AGAUS 10 (34 radii) [Delta - 0.01]	AGAUSXL (34 radii) [Delta - 0.01]	% Difference*
0	0.1838	0.1835	0.1835	0.16
75	0.2801	0.2797	0.2797	0.18
80	0.3020	0.3016	0.3016	0.17
85	0.3340	0.3335	0.3335	0.27
90	0.3887	0.3882	0.3882	0.15
95	0.5350	0.5343	0.5343	0.15
99	1.9295	1.9268	1.9268	0.15
Total CPU Time	34.34 sec	9.83 sec	34.98 sec	71.4

*NOTE: per cent differences are: |(AGAUS9-AGAUS10)/AGAUS9| x 100.

Table 1.2.5.5 Comparison of AGAUS10 Results for Four Different Convergence Levels and a Simulated Smoke Model - λ = 10.6 μm. (Relative humidity = 0%).

Convergence Level (DELTA)	No. of Radii used	K_{ext} (km^{-1})
.05	18	1.8277
.01	34	1.8353
.005	50	1.8345
.001	130	1.8377

Convergence Level (DELTA)	Scattering Fractions		
	θ = 0°	θ = 90°	θ = 180°
.05	1.5574E-6	6.9366E-7	1.2326E-6
.01	1.5610E-6	6.9555E-7	1.2365E-6
.005	1.5605E-6	6.9533E-7	1.2361E-6
.001	1.5621E-6	6.9613E-7	1.2376E-6

time than did AGAUS10. AGAUSXL's results were quite close to those of AGAUS10, but the relative slowness of DOWN42 brought the total time to treat 34 radii up to nearly the same time needed by AGAUS9 to treat 100 radii.

Table 1.2.5.5 demonstrates how the user's choice of DELTA affected runs of the simulated smoke model at a relative humidity of 0%. For that model, changes in the number of radii from 18 to 130 (a factor of seven!) did not change either the extinction coefficient or the scattering fractions by more than 0.3 percent.

1.2.5.3 Discussion: One of the decisions which had to be made for program AGAUS10 was that of determining just which "quantity" or set of quantities should be used in the test for convergence to within the level DELTA. The one which was finally chosen was the total volume of the aerosol particles. The volume was chosen because, being dependent on the cubes of the radii, it might be a little more conservative choice than the extinction coefficient, although, as seen in Tables 1.2.5.1 and 1.2.5.2, it is a less conservative test quantity than the scattered intensity at, say, $\theta = 90°$. Present experience is limited, but the use of the volume seems to be a good compromise unless highly precise scattering fractions are needed. If the latter situation arises in a particular application, users of the code should have no difficulty in coding in their own preferred test quantity. The quantities which are available at present are extinction, scattering and backscattering cross-sections and the average intensities at various angles. Careful study of the source listing for subroutine AGXPT2 will reveal how such changes can be made.

A major surprise which was revealed by these studies was the fact that the code MIE-2 used less computer time to handle cloud models C.1 and C.3 than AGAUS9 needed (for the same number of radii). The reason for the surprise was that the basic Mie routine DOWN42 used by MIE-2 was known to be usually appreciably slower than routine MIEGX (see section 1.3). It was, in fact, that difference in speed which caused AGAUSXL (see above, and Table 1.2.5.4) to require more than three times as long to treat the smoke model than AGAUS10 needed. The reason for MIE-2's evident computation time advantage over AGAUS9 has been alluded to above (section 1.1), and appears to be the result of the differences in the ways in which the values of radii (at which the Mie calculations are to be done) are chosen in the two codes. In MIE-2, the interval between successive values of particle radius is doubled as each additional value is assigned (at least for the generalized Khirgian-Mazin distribution), while AGAUS9 uses a constant increment. The MIE-2 method therefore uses far fewer large values of radius than the AGAUS9 method does. That difference, and the fact that the time required within the Mie subroutines DOWN42 and MIEGX increases rapidly with the size to

wavelength ratio, appears to account for MIE-2's (small) running time advantage over AGAUS9. That difference in how the radii are chosen definitely accounts for the disagreements between the MIE-2 and AGAUS9 values for the scattering fractions for cloud models C.1 and C.3 (that disagreement is quite appreciable [see Table 1.2.5.1] in some cases). The latter conclusion has been verified by direct runs with a version of AGAUS9 which uses the MIE-2 method for choosing the radii (the AGAUS9/MIE-2 disagreements moved out to the fifth or sixth digit). The running time of the special version of AGAUS9 was 240 seconds as compared to 266 seconds for MIE-2, demonstrating that the use of fewer large radii significantly decreases running time. That alteration of AGAUS9 has not been made permanent, although the changes needed are not particularly troublesome, because it is not really clear that the MIE-2 method of doubling the interval does not also carry along an implication that a larger number of radii (than needed with AGAUS9) would be needed to secure adequate sampling of larger particles sizes.

The questions raised above are, however, made somewhat academic by AGAUS10 for many applications requiring single scattering calculations because of AGAUS10's clear speed advantage in handling distributions for which no a priori guide as to how many radii will be "enough" is available.

1.2.5.4 Some Effects of the Number of Size-Intervals Used in AGAUS10

In the early development of AGAUS10, it was tentatively assumed that computation times might be substantially reduced by breaking the total ranges of R-values to be treated into more than one "size-interval" and then performing the halving calculations and tests separately within each size interval. That assumption was based upon the belief that the use of a single interval could result in unneeded computations in some size ranges brought about by slow convergence in other ranges. Consequently, all types of distribution functions which were known to be "peaked", were split into two size-intervals: (a) one with radii smaller than the one at which the distribution was a maximum, and (b) one containing all larger values of particle radii. In some of the test runs, however, it was found that the interval containing the smaller radii required more halvings than the other interval, but contributed only a small fraction of the total extinction effects--thereby perhaps wasting computation time.

The effect of using just a single size interval, instead of two intervals, has been briefly explored using a special version of AGAUS10, and Deirmendjian's cloud models C.1 and C.3 at $\lambda = 0.7$ μm. Computations were made with several different values for the convergence level (Δ). Table 1.2.5.6 compares some of the results found with the special version (AGAUS10S), and the regular version. The scattering fraction

Table 1.2.5.6 Comparison of Results Produced for Cloud Model C.1 (λ = 0.7 μm) by Several Variants of Program AGAUS10, and Different Convergence Levels (Δ).

DELTA	*	NI	NRADI	K_{ext}	CPU	Scattering Fractions 0°	90°	180°
0.05	a	2	26	17.47	45.28	2.4521	5.2019E-5	7.4914E-4
	b	1	9	16.70	21.06	2.2353	6.9736E-5	1.2946E-3
	c	1	9	16.70	note-d	2.2353	6.9736E-5	1.2946E-3
0.01	a	2	50	16.72	82.81	2.2404	4.8011E-5	8.3856E-4
	b	1	17	16.77	38.72	2.2438	7.0311E-5	1.0222E-3
	c	1	129	16.74	note-d	2.2386	5.6969E-5	9.1422E-3
0.005	a	2	66	16.74	127.93	2.2395	5.6570E-5	8.7430E-4
	b	1	17	16.77	37.78	2.2438	7.0311E-5	1.0222E-3
0.001	a	2	130	16.73	245.13	2.2370	5.4473E-5	8.2393E-4
	b	1	33	16.76	75.71	2.2398	6.8529E-5	9.3237E-4
"Reference Case"	c	2	513	16.75	noted-d	2.2411	5.5880E-5	8.8647E-4
Deirmendjian		1	440	16.73	--	2.2370	--	8.457E-4

*Notes

a) "Normal" AGAUS10; convergence tests on aerosol volume; 2 size interval.

b) AGAUS10S; convergence tests on extinction coefficient; 1 size interval.

c) AGAUS10S; convergence tests on extinction coefficient and scattered intensity at θ = 90°; number of size intervals given in column labeled "NI".

d) 45° angular increment runs; CPU times not directly comparable to other runs made at 2° increments.

computations were made at 2° increments in most cases shown in the table, and the column labeled "NI" explicitly shows the number of size-intervals used. Also shown, and labeled "REF. CASE", are results obtained with an AGAUS10 run which used all 513 available values of particle radii.

The results seen in Table 1.2.5.6 indicate that the special version (AGAUS10S) found the convergence of the extinction coefficient to be satisfied with a substantially smaller number of particle sizes than the "normal" version required. That fact also meant that AGAUS10S required only one-third to one-half as much computation time to satisfy the different convergence levels as AGAUS10 needed. It thus appears that the initial assumption that two intervals would be preferable to one interval may be false. However, a closer examination of the table shows that AGAUS10S yielded substantially larger scattering fractions (away from 0°) than did AGAUS10, with the latter code's values being closer to the "REF. CASE" values at all choices of Δ.

About the only conclusions which can be drawn at this point are that the NI = 1 version is by far the most efficient when only k_{ext} is of interest, and that the NI = 2 version is preferable, in spite of its slower speed, if high accuracies are needed for the scattering fractions at large scattering angles. From another vantage point, however, the discrepancies between the NI = 1 and NI = 2 scattering fractions at $\theta = 90°$ and $\theta = 180°$ are an insignificant fraction of the $\theta = 0$ values.

A few similar comparisons for Deirmendjian's cloud model C.3 at $\lambda = 0.7$ μm are given in Table 1.2.5.7

1.2.5.5 Conclusions: AGAUS10 has been demonstrated to offer substantial decreases in computation time, at selectable levels of accuracy, over either code AGAUS9 or MIE-2. That advantage is gained by letting the program itself determine the number of radii to be used to achieve a given level of convergence for a specific "test quantity", rather than relying upon a user's guess. It also has the additional property, unlike MIE-2 and AGAUS9, that the user can obtain some idea of the absolute accuracies to be expected from the results of a particular run. There is probably room for further improvements, of AGAUS10, however. The rather short existence of the code (less than four months in its present general form) has not permitted the exploration of many of its aspects--such as optimizing the number of radius intervals used with the various types of distributions, or of modifying it to handle mixtures of aerosol components which have different size distributions as well as optical properties.

Table 1.2.5.7 Comparison of AGAUS10 Results for Cloud Model C.3 (λ = 0.7 μm) Using One and Two Size Intervals, Several Convergence Levels, and Convergence Tests on Extinction Coefficient and Scattering Fractions at 90°.

DELTA	NI	NRADI	K_{ext}	CPU[a]	Scattering Fractions 0°	90°	180°
0.1	--	--	--	--	--	--	--
	1	33	3.042	34.81	5.4626E-2	2.2433E-5	2.5350E-4
0.05	--	--	--	--	--	--	--
	1	65	3.041	68.71	5.4583E-2	2.2435E-5	2.3498E-4
0.01	2	66	3.008	71.49	5.3569E-2	2.1668E-5	1.7792E-4
	1	65	3.041	72.67	5.4583D-2	2.2435E-5	2.3498E-4
0.005	--	--	--	--	--	--	--
	1	65	3.041	72.06	5.4583E-2	2.2435E-5	2.3498E-4
0.001	2	130	3.015		5.3796E-2	2.2180E-5	1.9798E-4
	1	129	3.041	16.86[b]	5.4585E-2	2.1382E-5	2.3500E-4
.0001	1	513	3.021	62.83[b]	5.3985E-2	2.0643E-5	2.0382E-4
Deirmendjian		280	3.021	?	5.396E-2	--	2.025E-4

Notes:

a) CPU times in seconds, using 2° angular increments.

b) Not comparable to other runs due to use of 45° increments.

c) Cases for which dashes (--) appear were not run for NI=2 and convergence tests on both K_{ext} and the scattered intensity at θ = 90°.

1.3 MIE CODE COMPARISONS

1.3.1 Introduction: As a part of the search for ways of speeding up Mie-type calculations of aerosol extinction and scattering, NMSU has conducted a series of studies of the comparative computational speeds and results using three separate computer codes. The three codes were:

MIEGS - an ASL forward-recursion routine,
BMIEGS - an ASL backward-recursion routine,
and, DOWN42 - a Radiation Research Associates downward recursion routine.

In the table accompanying this section of the report, those three routines will be referred to as M, B and R, respectively.

In some cases, an "extended" version[†] of MIEGS will be denoted as M'. All computations were performed on WSMR Univac 1108 computer system B.

1.3.2 Range of Comparisons: These studies used Mie size-parameter values ($\alpha = 2\pi r/\lambda$) of 1,10,20,40,60,80,100,200,300,500 and 1000, and complex indices of refraction ($n = m-ik$) in the forms k=0, $\frac{m}{2}$ and m, and m had the explicit values m = 1.2, 1.4, 1.6, 1.8 and 5.0.

The quantities which were computed for comparison were the Mie efficiency factors Q_{ext} and Q_{sca}, and the average intensity $I_{ave} = (I_1+I_2)/2$ at scattering angles 0°, 45°, 90°, 135° and 180°. CPU times were determined using a system supplied timing routine for each combination of α, m and k.

1.3.3 Results: The results of the above calculations are presented in Table 1.3.1 which shows the values of α, m and k for which all the results (Q_{ext}, Q_{sca}, and I_{avg}) agreed to better than one (1) percent. For each α, n and k combination the identification letters M, B, R or M' (see above) appear in order of increasing computation time. If a particular routine's outputs disagreed with those of the other routines by more than 1% but were within 10% of the other results, that routine carries an asterisk. If a label (B, M or R) does not appear at all, then either it would not run at all (failed in a mode leading to termination by the computer system itself), or did not even achieve the

[†]The "extended" version of MIEGS was one in which the dimensions of certain arrays were extended from 500 to 1500.

10% agreement level. Where no entry at all appears for some (α,m,k) combinations, it means that all three failed at the machine detectable level. Finally, entry points showing only a single identifying letter and a question mark represent cases in which the other two routines failed to run at all or gave such widely differing outputs that no cross-checking was possible.

1.3.4 Discussion: In all cases for which complete runs were obtainable routine MIEGS executed faster than BMIEGS which in turn used less computer time than DOWN42. BMIEGS typically required twice as much CPU time as did MIEGS. DOWN42 required from five to twelve times as much CPU time as was needed by MIEGS.

Based upon the results shown in Table 1.3.1, it appears that routine MIEGS offers the best performance (accuracy and speed) for size parameters up to about 100 if the imaginary part k of the index of refraction is less than about m/2. Routine DOWN42, however, appears to be very reliable in all the cases in which it did not fail at the machine level, while BMIEGS seemed to have the most limited reliability. None of the codes tested proved to be capable of handling the complete range of parameters used in this study.

Since the entries shown in Table 1.3.1 for each (m,k and α) combination are in order of increasing computation times, that table itself can be used as a guide for selecting the routine most likely to be preferable for use under various situations.

1.3.5 Remarks: As a part of this study, NMSU also evaluated the so-called "Deirmendjian approximations" [3] for the calculation of the Q_{ext}'s. Those approximations were found to be valid in the regions defined by Deirmendjian, but they did not prove to be faster in execution than MIEGS except in the range $1 < \alpha < 20$. The computational advantages of the Deirmendjian's approximations over routines MIEGS were so small and so restricted in applicability (unusable for angular intensity calculations, for example) that NMSU sees little advantage to their use in any situation in which MIEGS can be used.

Table 1.3.1 Regions of Agreement of Mie Routines to Within 1% or Better
(in order of increasing computation time)

INDEX OF REFRACTION		MIE SIZE ~ PARAMETER (α)										
Real	Imaginary	1	10	20	40	60	80	100	200	300	500	1,000
1.20	0.00	M,B,R	M,B,R	M,B,R	M,B,R	M,B*,R	M,R	M,R	M,R	M,R	M*,R*	M*,R*
1.20	0.60	M,B,R	M,B,R	M,B,R	M,B,R	M,B,R	M,B,R	B,R	B,R	R?	R?	
1.20	1.20	M,B,R	M,B,R	M,B,R	M,B,R	M*,B,R	M*,B,R	B,R	R?	R?		
1.40	0.00	M,B,R	M,B,R	M,R	M,R	M,R	M,R	M,R	M,R	M,R	M,R	M,R
1.40	0.70	M,B,R	M,B,R	M,B,R	M,B,R	M,B,R	M,B,R	M,B,R	B,R	R?	R?	
1.40	1.40	M,B,R	M,B,R	M,B,R	M,B,R	M,B,R	M,B,R	M*,B,R	R?	R?		
1.60	0.00	M,B,R	M,B*,R	M,R	M,R	M,R	M,R	M,R	M,R	M,R	M'?	M'?
1.60	0.80	M,B,R	M,B,R	M,B,R	M,B,R	M,B,R	M,B,R	M,B,R	B,R	R?		
1.60	1.60	M,B,R	M,B,R	M,B,R	M,B,R	M,B,R	M,B,R	M*,B,R	R?			
1.80	0.00	M,B,R	M,B*,R	M,R	M,R	M,R	M,R	M,R	M,R	M,R	M'?	M'?
1.80	0.90	M,B,R	M,B,R	M,B*,R	M,B,R	M,B,R	M,B,R	M,B,R	M*,B,R	R?		
1.80	1.80	M,B,R	M,B,R	M,B*,R	M,B,R	M,B,R	M,B,R	M*,B,R	R?			
5.00	0.00	M,B,R	M?	M?	M?	M?	M?	M*,R*	M?	M?		
5.00	2.50	M,B,R	M,B*,R	M,R	M,R	M,R	M,R	M?	M?			
5.00	5.00	M,B,R	M,B*,R	M,R	M,R	R?	R?					

NOTES: 1) Entries with an asterisk did not yield 1% agreement, but did yield results which were within 10% of those found with other routines.

2) Entries followed by ? represent cases in which other codes failed to run at all or no cross-checking was possible.

1.4 APPROXIMATION METHODS FOR PHASE FUNCTION PREDICTION

1.4.1 Introduction: In order to surmount some of the difficulties in determining the 'true' or computed phase function NMSU has developed two alternate methods of reducing the computational load. The first method, to be explained in section 1.4.5, is essentially a tabular one: given a particular aerosol model this method will look up precomputed scattering fractions and interpolate over wavelength if necessary. The second method, to be described below, is the construction of approximate phase functions.

We have used the Henyey-Greenstein phase function (hereafter referred to as HG), a new analytic phase function which we shall refer to as Goedecke's phase function (hereafter referred to as GG), and a combination of the HG and GG phase function which we shall refer to as the HG-GG phase function.

1.4.2 Theory: The analytic HG phase function is dependent upon one parameter, g, called the asymmetry factor: $g = \langle\cos\theta\rangle/\tilde{\omega}_o$, where θ is the scattering angle and $\tilde{\omega}_o$ is the albedo for single scattering. For isotropic scattering g = 0, while for pure forward scattering g = 1. In our notation the analytic HG phase function is:

$$\bar{P}(\mu) = \tilde{\omega}_o \frac{1-g^2}{(1+g^2 - 2g\mu)^{3/2}} \qquad (1.4\text{-}1)$$

$$= \tilde{\omega}_o \sum_{n=o}^{\infty} (2n+1) g^n P_n(\mu) \equiv \sum_{n=o}^{\infty} \bar{\omega}_n P_n(\mu), \qquad (1.4\text{-}2)$$

where $\bar{P}(\mu)$ is the approximate phase function at $\mu = \cos\theta$, and the $P_n(\mu)$'s are the Legendre polynomials. Using direct integration it is an easy matter to show that $g = \tilde{\omega}_1/(3\,\tilde{\omega}_o)$. Very often the HG phase function is much too large for angles close to the forward or incident directions ($\mu \approx 1$) compared to the computed, or 'true', phase function found by using Mie theory.

The GG phase function has the following analytic form:

$$\bar{P}(\mu) = \tilde{\omega}_o \left\{ \frac{\alpha}{2} \frac{1-g_1^2}{(1+g_1^2-2g_1\mu)^{3/2}} + (1 - \frac{\alpha}{2}) \frac{1}{(1+g_1^2-2g_1\mu)^{1/2}} \right\}, \quad (1.4\text{-}3)$$

$$= \tilde{\omega}_o \sum_{n=o}^{\infty} (\alpha n+1) g_1^n P_n(\mu) \equiv \sum_{n=o}^{\infty} \bar{\omega}_n' P_n(\mu), \quad (1.4\text{-}4)$$

where the parameters have the same meaning as before; g_1 and α may be chosen and fixed by the following method. We simultaneously solve the following equations for g_1 and α:

$$\bar{P}(1) \equiv p = \tilde{\omega}_o \left\{ \frac{\alpha}{2} \frac{1 + g_1}{(1-g_1)^2} + (1 - \frac{\alpha}{2}) \frac{(1-g_1)}{(1-g_1)^2} \right\}, \quad (1.4\text{-}5)$$

$$\tilde{\omega}_1 = \bar{\omega}_1' = \tilde{\omega}_o(\alpha+1)g_1 \quad \text{or} \quad \tilde{\omega}_2 = \bar{\omega}_2' = \tilde{\omega}_o(2\alpha+1)g_1^2, \quad (1.4\text{-}6a,b)$$

where $p \equiv$ value of actual phase function at $\mu = 1$. In some cases $\alpha > 2.0$, which means that in these cases the phase function can (and sometimes does) take on negative values for some μ. This usually occurs for $\mu < 0$ only, where the phase function is small compared to its values for μ near 1.0.

The HG-GG phase function is a combination of the HG and GG phase functions and has the following analytic form:

$$\bar{\bar{P}}(\mu) = \begin{cases} \tilde{\omega}_o \left[\frac{\alpha}{2} \frac{1-g_2^2}{(1+g_2^2-2g_2\mu)^{3/2}} + (1 - \frac{\alpha}{2}) \frac{1}{(1+g_2^2-2g_2\mu)^{1/2}} \right], & 1 \geq \mu \geq \mu_1, \\ \tilde{\omega}_o \beta \frac{1-g_2^2}{(1+g_2^2-2g_2\mu)^{3/2}}, & \mu_1 \geq \mu \geq -1. \end{cases} \quad (1.4\text{-}7a,b)$$

Here, g_2, α, β, μ_1 are parameters that must be fixed and are evaluated as follows: solve simultaneously

$$\bar{\bar{P}}(1) \equiv p \frac{\tilde{\omega}_o}{(1-g_2)^2}\left[\frac{\alpha}{2}(1+g_2) + (1-\frac{\alpha}{2})(1-g_2)\right], \qquad (1.4\text{-}8)$$

$$\tilde{\omega}_2 = \tilde{\omega}_o(2\alpha+1)g_2^2. \qquad (1.4\text{-}9)$$

Note: $\tilde{\omega}_1 = \tilde{\omega}_o(\alpha+1)g_2$ will not work for all cases; i.e., no real g_2 for $0 \le g_2 \le 1$ exists. The above equations yield the same values of g_2 and α that we had for g_1 and α for the GG function alone. Since we expect that, for $\mu<\mu_1$, the actual phase function, and therefore the HG part of the HG-GG phase function, is very small compared to its values for $\mu>\mu_1$, we take these values of g_2 and α as our working values. We then take μ_1 to be that value of μ for which the GG function first goes negative. β is found by matching the GG part of the phase function to the HG phase function at $\mu = \mu_1$. This yields

$$\beta = \frac{\alpha}{2} + (1-\frac{\alpha}{2})(1+g^2-2g\mu_1)/(1-g^2) > 0. \qquad (1.4\text{-}10)$$

Therefore $\bar{P}(\mu) > 0$ for all μ and is a continuous function of μ. We must now determine the $\bar{\bar{\omega}}_n[\bar{\bar{P}}(\mu)] = \sum_{n=o}^{\infty} \bar{\bar{\omega}}_n P_n(\mu)]$:

$$\bar{\bar{\omega}}_n = \frac{2n+1}{2}\int_{-1}^{1} \bar{\bar{P}}(\mu)\, P_n(\mu)d\mu. \qquad (1.4\text{-}11)$$

If $\mu_1>-1$, none of the $\bar{\omega}_n$ will exactly match the computed or 'true' ω_n. Since it is most important that an approximate phase function have the correct $\tilde{\omega}_o$, we redefine

$$\bar{P}(\mu) \equiv \frac{\tilde{\omega}_o}{\bar{\bar{\omega}}_o}\bar{\bar{P}}(\mu); \text{ then if we write,}$$

$$\bar{P}(\mu) = \sum_{n=o}^{\infty} \bar{\omega}_n P_n(\mu), \text{ we have}$$

$$\bar{\omega}_n = \frac{2n+1}{2}\int_{-1}^{1} \bar{P}(\mu)\, P_n(\mu)d\mu = \tilde{\omega}_o\left(\frac{\bar{\bar{\omega}}_n}{\bar{\bar{\omega}}_o}\right). \qquad (1.4\text{-}12)$$

This guarantees that $\bar{\omega}_o = \tilde{\omega}_o$, but $\bar{\omega}_2$ will not match $\tilde{\omega}_2$ exactly. As long as the HG part of the HG-GG phase function is small, the mismatch between $\bar{\omega}_2$ and $\tilde{\omega}_2$ will be small.

In all the above cases it is necessary to calculate only two of the coefficients in the Legendre expansion of the phase function, $\tilde{\omega}_o$ and $\tilde{\omega}_1$ or $\tilde{\omega}_o$ and $\tilde{\omega}_2$. This may be done directly in terms of the a_n and b_n coefficients of the Legendre series occurring in Mie theory without evaluating the exact phase function of any angle.

We want the phase function for incident natural light to satisfy

$$\int \bar{P}(\mu)d\Omega = 4\pi\tilde{\omega}_o = 2\pi \int_{-1}^{1} P(\mu)d\mu = 4\pi \frac{C_{scat}}{C_{ext}} , \qquad (1.4\text{-}13)$$

where C is the total cross section for scattering and extinction, respectively. In the notation of van de Hulst (1958, Chs. 2,9),

$$C_{scat} = \frac{1}{k^2} \int F(\theta,\phi)d\Omega. \qquad (1.4\text{-}14)$$

So, if we put

$$P(\mu) = \frac{K}{2\pi} \int_{o}^{2\pi} F(\theta,\phi)d\phi , \qquad (1.4\text{-}15)$$

then

$$\int P(\mu)d\Omega = K\, k^2\, C_{scat}, \qquad (1.4\text{-}16)$$

or

$$K = \frac{4\pi}{k^2\, C_{ext}} , \qquad (1.4\text{-}17)$$

and therefore

$$P(\mu) = \frac{2}{k^2\, C_{ext}} \int_{o}^{2\pi} F(\theta,\phi)d\phi. \qquad (1.4\text{-}18)$$

Now $F(\theta,\phi) = i_1(\theta)\sin^2\phi + i_2(\theta)\cos^2\phi$, hence

$$P(\mu) = \frac{1}{k^2 C_{ext}}[i_1(\theta) + i_2(\theta)], \qquad (1.4\text{-}19)$$

where $i_{1,2}(\theta) = |S_{1,2}(\theta)|^2$,

and $$S_1(0) = S_2(0) = \frac{1}{2}\sum_{n=1}^{L\to\infty}(2n+1)(a_n+b_n). \qquad (1.4\text{-}20)$$

Therefore,

$$P(1) = \frac{1}{k^2 C_{ext}}\frac{1}{2}\left|\sum_{n=1}^{L}(2n+1)(a_n+b_n)\right|^2 = \frac{2}{k^2 C_{ext}}|S_1(0)|^2, \qquad (1.4\text{-}21)$$

where $$C_{ext} = \frac{4\pi}{k^2}\,\mathrm{Re}\left[\frac{1}{2}\sum_{n=1}^{L\to\infty}(2n+1)(a_n+b_n)\right] = \frac{4\pi}{k^2}\,\mathrm{Re}[S_1(0)]. \qquad (1.4\text{-}22)$$

This allows direct calculation of P(1) in terms of the a_n and b_n. We now need expressions for $\tilde{\omega}_1$ and/or $\tilde{\omega}_2$ in terms of the a_n and b_n. These are given by Chu and Churchill [4]. In terms of the Mie coefficients a_n, b_n, these expressions are:

$$\tilde{\omega}_1 = \frac{3}{x^2 Q_{ext}}\sum_{n=1}^{\infty}\left[\frac{2n(n+2)}{(n+1)}(a_n a_{n+1}^* + b_n b_{n+1}^* + a_{n+1}a_n^* + b_{n+1}b_n^*) + \frac{2(2n+1)}{n(n+1)}(a_n b_n^* + a_n^* b_n)\right], \qquad (1.4\text{-}23)$$

$$\tilde{\omega}_2 = \frac{4}{x^2 Q_{ext}}\sum_{n=1}^{\infty}\left[\frac{5}{2}\frac{(n(n+1)-3)^2(2n+1)}{n(n+1)(2n+3)(2n-1)}\mathrm{Re}(a_n^* a_n + b_n^* b_n)\right.$$

$$+ \frac{15}{2}\frac{n(n+3)}{(2n+3)}\mathrm{Re}(a_{n+2}^* a_n + b_{n+2}^* b_n)$$

$$\left. + \frac{15}{n+1}\mathrm{Re}(a_{n+1}^* b_n + b_{n+1} a_n^*)\right], \qquad (1.4\text{-}24)$$

where $x = 2\pi r/\lambda$, $Q_{ext} = C_{ext}/(\pi r^2)$, and r is the particle radius.

1.4.3 Comparison of Results for the Analytic Phase Functions: Three models have been chosen to compare the analytic phase functions (HG, GG and HG-GG) with the 'true' or computed phase function. These models and selected wavelengths at which comparisons were made are: simulated white phosphorus [1] at 1.06 and 10.6 microns; fog models WSMRF1, and WSMRF2 at wavelengths of 2.5, 10.0 and 11.0 microns: the parameters for each of the two fog models are tabulated below.

	WSMRF1	WSMRF2
Radius, Minimum	1.0μm	0.4μm
Radium, Maximum	40.0μm	12.0μm
Radius, Mode	10.0μ	4.0μm
Alpha	3.0	6.0
Gamma	1.0	1.0
Particle Density	20.0 cm^{-3}	100.0 cm^{-3}

Because the GG_1 phase function, which uses $\tilde{\omega}_o$, $\tilde{\omega}_1$ and $P(\mu=1)$ to match the computed phase function, will not always work, it has been abandoned, and GG_2 will be used instead and referred to simply as GG: the GG function matches $\tilde{\omega}_o$, $\tilde{\omega}_2$ and $P(\mu=1)$.

Values of the analytical phase functions HG and HG-GG, along with the computed phase functions are presented graphically in figures 1.4.3.1 through 1.4.3.8. A visual inspection of these figures shows that the HG-GG analytic phase function matches the computed phase function far better than the HG phase function near zero degrees, and that the HG-GG function apparently provides a better overall fit to the computed phase function than the HG function. Because the scales of the graphs usually do not permit sufficient resolution near 180°, the values of the computed and analytic phase functions are presented in table 1.4.3.1 (two pages) at selected angles. Table 1.4.3.1 also presents the differences between the computed and analytic phase functions at the selected angles, and also the root mean square error for the points considered.

1.4.4 Discussion: Inspection of table 1.4.3.1 shows that the HG-GG analytic phase function is superior to the HG analytic phase function at angles near zero degrees. However, as one approaches 180° the HG function sometimes provides a better fit to the computed phase function. Since for most of the distributions examined the backscatter is far less than the forward scattering, it becomes important to analytically fit the computed phase function more closely near the forward direction of scattering relative to the backscatter direction. Additionally, since the HG analytic function fits the computed phase function best near 180° and the HG-GG analytic function is comprised of the GG function near 0° and the HG function near 180°, we again find that the HG-GG analytic function will fit well near 180°. The root mean square

Table 1.4.3.1

Comparison of Computed and Analytic Phase Function Values at Selected Angles for Fog Models WSMRF1, WSMRF2 and Simulated White Phosphorous, at Various Wavelengths.

Wavelength 2.5 μm	Model WSMRF1					Model WSMRF2				
	Phase function values*					Phase function values*				
Angle (°)	True†	HG	HG-GG	Δ_1^+	Δ_2^*	True†	HG	HG-GG	Δ_1^+	Δ_2^+
1.51	706.61	137.77	595.47	568.84	111.14	134.80	68.17	133.20	66.63	1.60
25.08	2.51	2.31	1.00	.20	1.51	3.59	3.56	2.56	.03	1.30
50.66	.32	.32	.23	.00	.09	.49	.55	.43	-.06	.06
74.26	.07	.12	.13	-.05	-.06	.13	.20	.18	-.07	-.05
99.84	.02	.06	.09	-.04	-.07	.06	.10	.11	-.04	-.05
125.41	.09	.04	.08	.05	.01	.09	.06	.08	.03	.02
150.98	.08	.03	.07	.05	.01	.09	.05	.07	.04	.02
174.58	.11	.03	.07	.08	.04	.17	.05	.07	.12	.10
178.49	.16	.03	.07	.13	.09	.23	.05	.07	.18	.16
RMS# =				189.61	37.05				22.21	.64

Wavelength 10.0 μm	Model WSMRF1					Model WSMRF2				
	Phase function values*					Phase function values*				
Angle (°)	True†	HG	HG-GG	Δ_1^+	Δ_2^+	True	HG	HG-GG	Δ_1^+	Δ_2^+
1.51	97.34	257.63	94.08	-160.29	3.26	14.12	60.63	12.86	-46.51	1.26
25.08	1.42	.92	1.71	.50	-.29	4.32	2.07	3.97	2.25	.35
50.66	.14	.12	.17	.02	-.03	.38	.30	.68	.08	-.30
74.26	.03	.04	.03	-.01	.00	.08	.11	.09	-.03	-.01
99.84	.01	.02	.00	-.01	.01	.03	.05	.00	-.02	.03
125.41	.01	.01	.00	.00	.01	.02	.04	.00	-.02	.02
150.98	.01	.01	.00	.00	.01	.02	.03	.00	-.01	.02
174.58	.01	.01	.00	.00	.01	.02	.02	.00	.00	.02
178.49	.00	.01	.00	-.01	.01	.02	.02	.00	.00	.02
RMS# =				53.43	1.09				15.52	.45

Table 1.4.3.1 (con't)

Wavelength 11.0 μm		Model WSMRF1				Model WSMRF2				
		Phase function values*				Phase function values*				
Angle (°)	True†	HG	HG-GG	Δ_1^+	Δ_2^+	True†	HG	HG-GG	Δ_1^+	Δ_2^+
1.51	80.75	361.00	76.07	-280.25	4.68	7.14	31.08	6.39	-23.94	.75
25.08	.87	.52	1.44	.35	-.57	2.61	1.28	2.34	1.33	.27
50.66	.07	.07	.12	.00	.05	.26	.19	.45	.07	-.19
74.26	.02	.02	.00	.00	.02	.05	.07	.07	-.02	.00
99.84	.01	.01	.00	.00	.01	.02	.03	.01	-.01	.01
125.41	.00	.01	.00	-.01	.00	.01	.02	.01	-.01	.00
150.98	.00	.01	.00	-.01	.00	.01	.02	.01	-.01	.00
174.58	.00	.01	.00	-.01	.00	.01	.02	.01	-.01	.00
178.49	.00	.01	.00	-.01	.00	.01	.02	.01	-.01	.00
RMS# =				93.42	1.57				7.99	.27

Wavelengths 1.06 μm and 10.6 μm		Model WP(1.06 μm)				Model WP(10.6 μm)				
		Phase function values*				Phase function values*				
Angle (°)										
4.24	15.15	26.52	14.40	-11.37	.75	.11	.07	.14	.04	-.03
26.32	5.58	4.26	5.55	1.32	.03	.10	.07	.14	.04	-.04
48.47	1.15	1.00	1.53	.15	-.38	.07	.07	.09	.00	-.02
76.16	.26	.32	.29	-.08	-.03	.05	.07	.06	-.02	-.01
98.16	.13	.18	.02	-.05	.11	.05	.06	.05	-.01	.00
126.00	.10	.11	.02	-.01	.08	.06	.06	.04	.00	.02
148.14	.12	.09	.02	.03	.10	.07	.06	.04	.01	.03
175.76	.17	.08	.02	.09	.15	.08	.05	.04	.03	.04
RMS# =				4.05	.31				.02	.03

*Rounded to two decimal points
†Computed via Mie theory
+True minus analytic: 1 = Henyey-Greenstein; 2 = modified Henyey-Greenstein
#RMS ≡ Root Mean Square

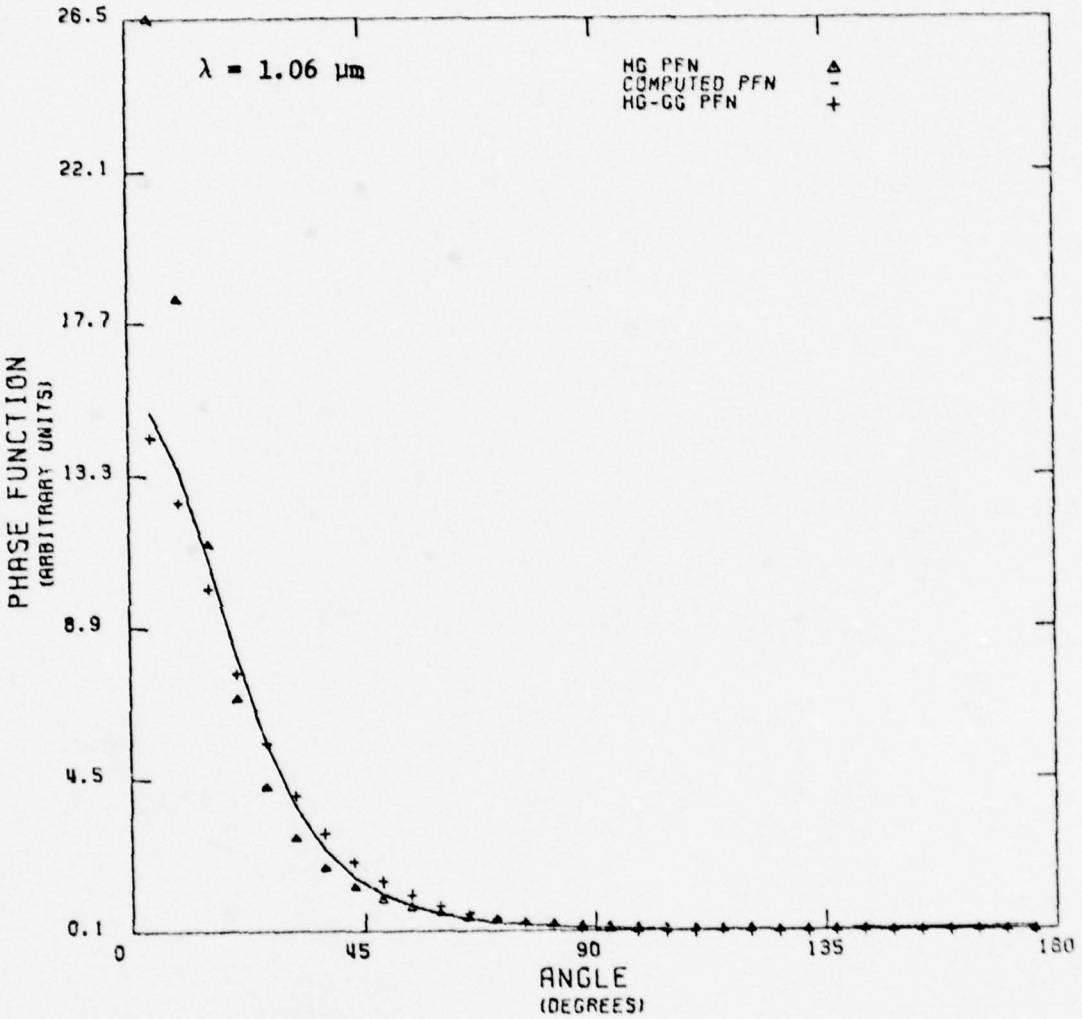

Figure 1.4.3.1 Comparison of analytic phase functions HG and HG-GG with computed phase function for simulated white phosphorous at 1.06 μm.

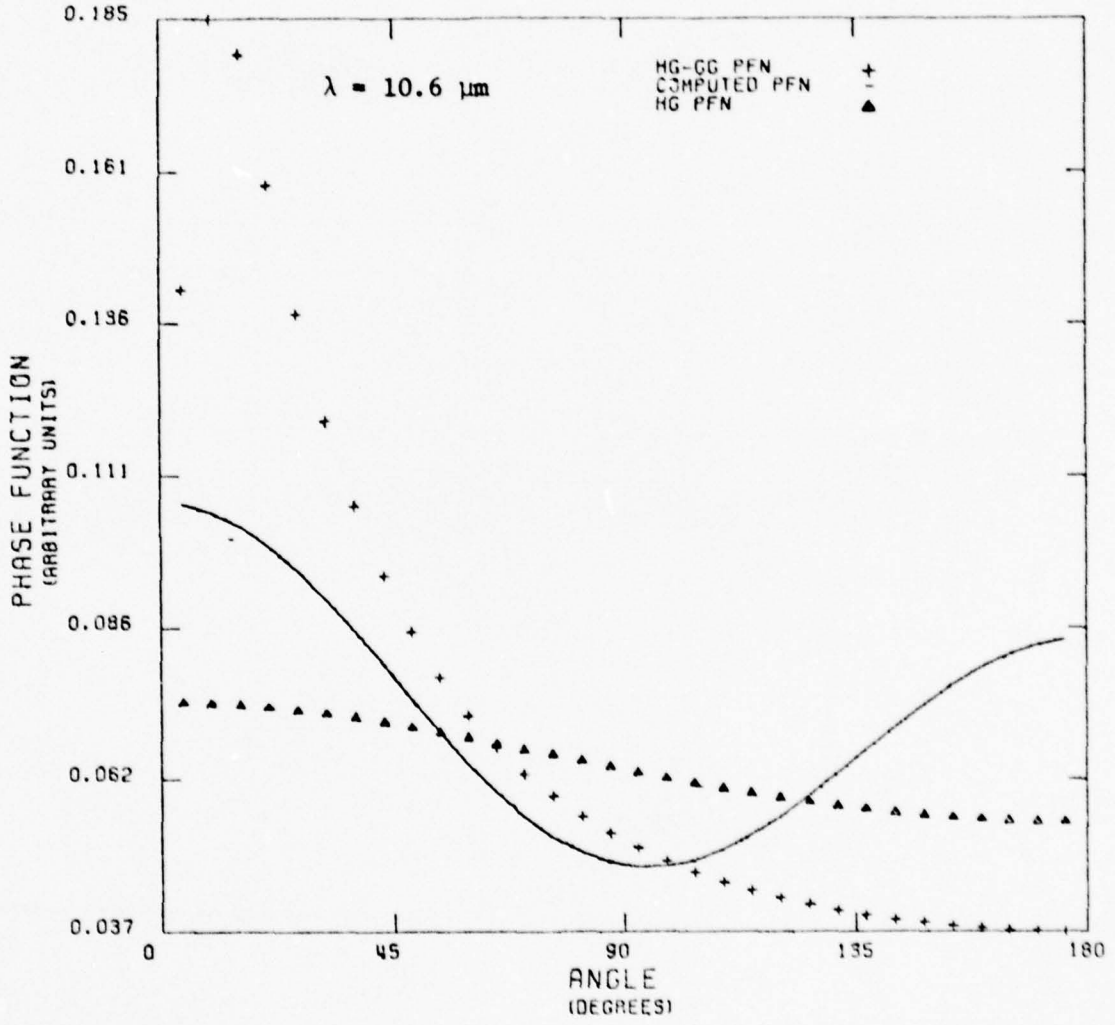

Figure 1.4.3.2 Comparison of analytic phase functions HG and HG-GG with computed phase function for simulated white phosphorous at 10.6 μm.

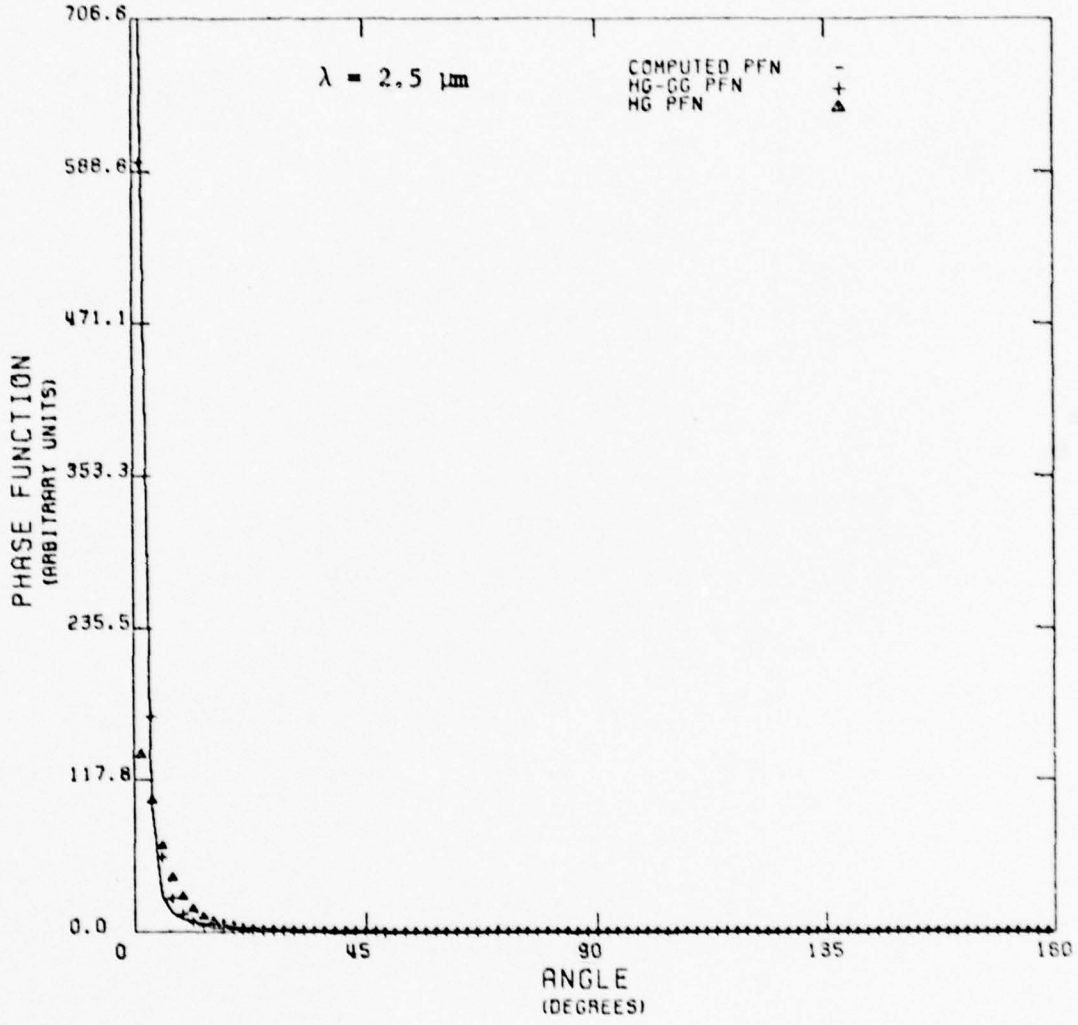

Figure 1.4.3.3 Comparison of analytic phase functions HG and HG-GG with computed phase function for fog model WSMRF1 at 2.5 μm.

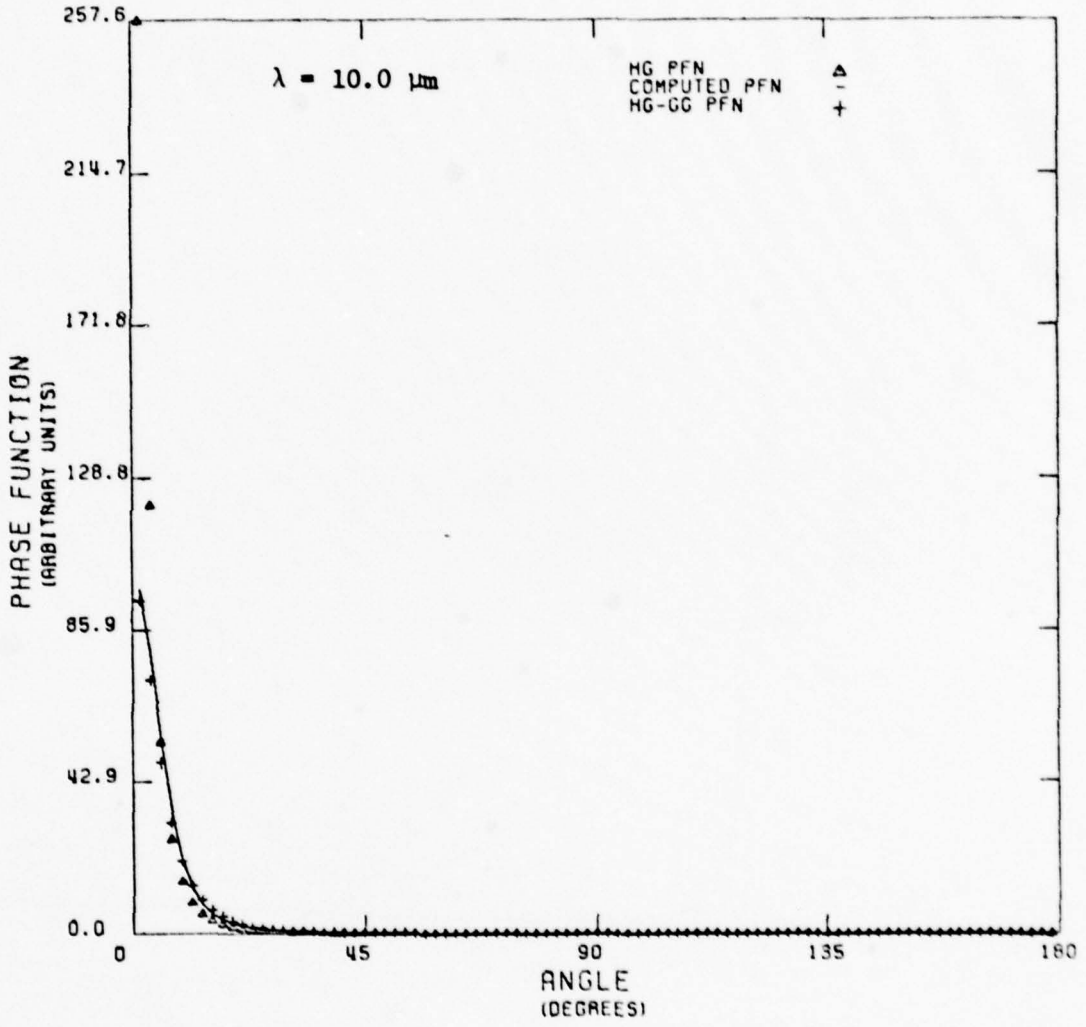

Figure 1.4.3.4 Comparison of analytic phase functions HG and HG-GG with computed phase function for fog model WSMRF1 at 10.0 μm.

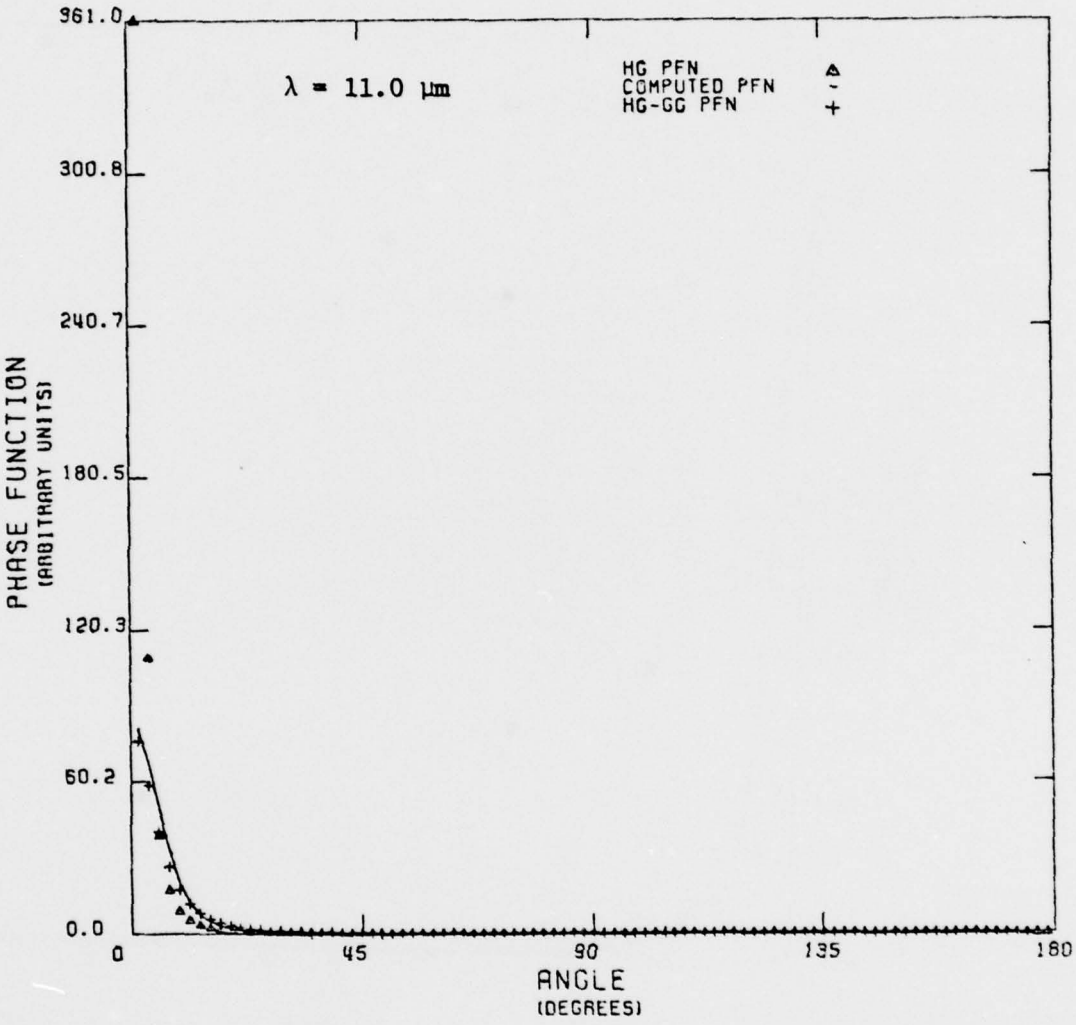

Figure 1.4.3.5 Comparison of analytic phase functions HG and HG-GG with computed phase function for fog model WSMRF1 at 11.0 μm.

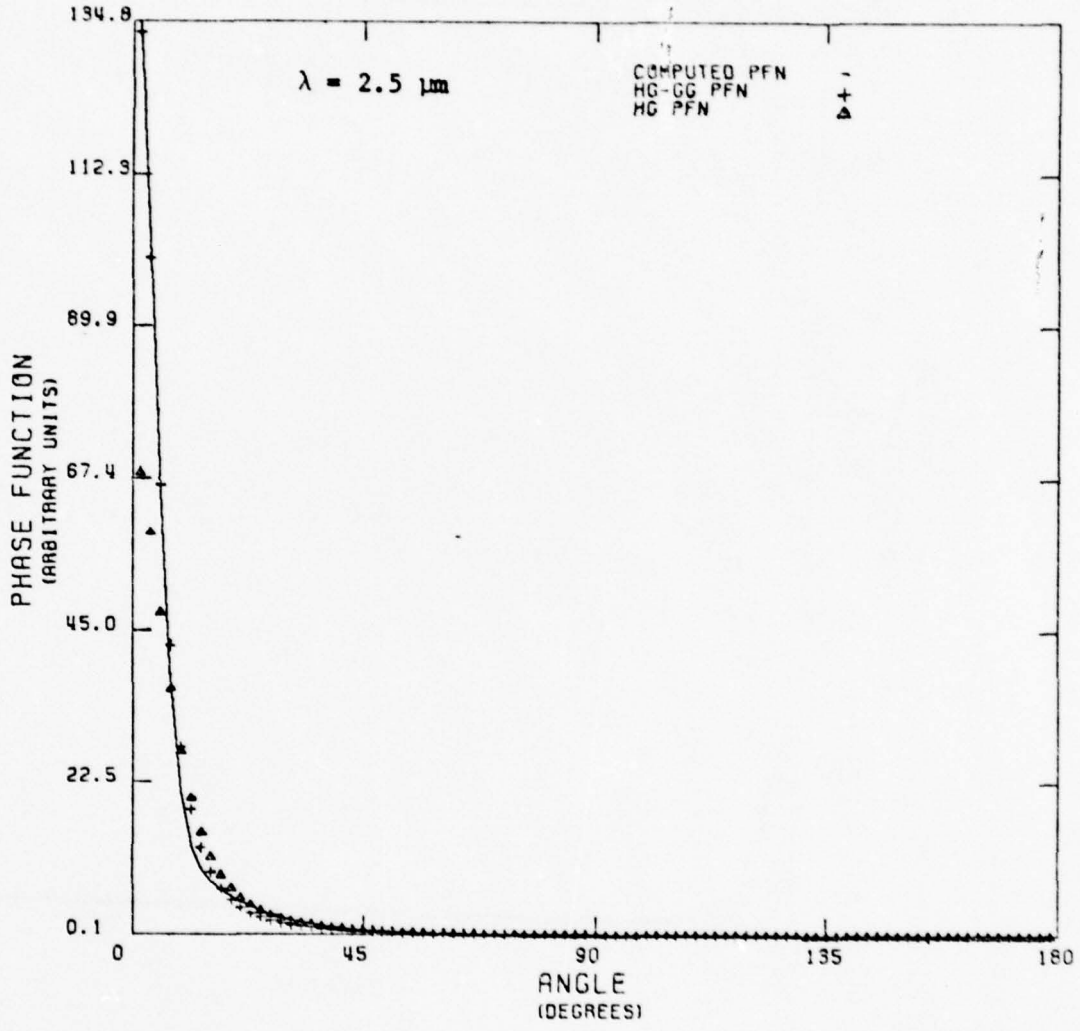

Figure 1.4.3.6 Comparison of analytic phase functions HG and HG-GG with computed phase function for fog model WSMRF2 at 2.5 μm.

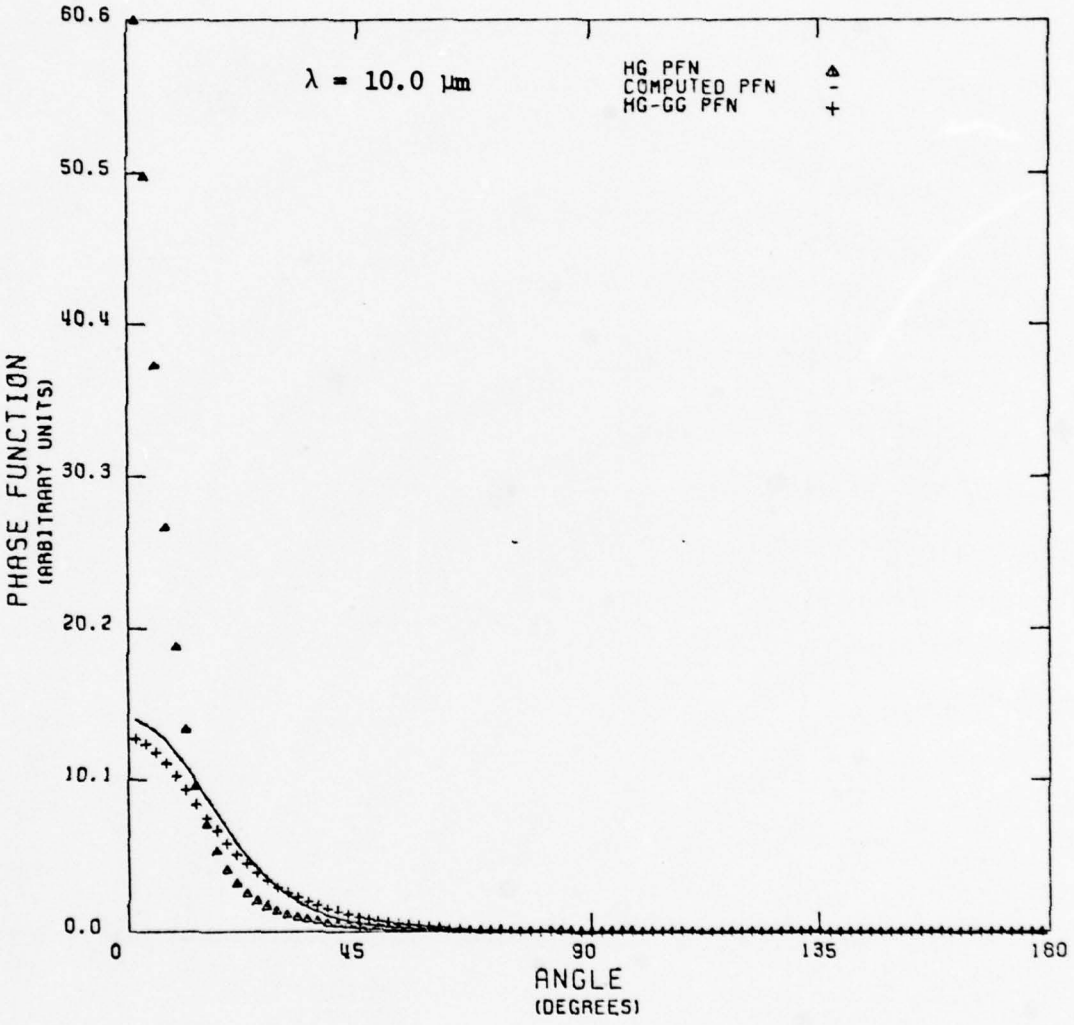

Figure 1.4.3.7 Comparison of analytic phase functions HG and HG-GG with computed phase functions for fog model WSMRF2 at 10.0 μm.

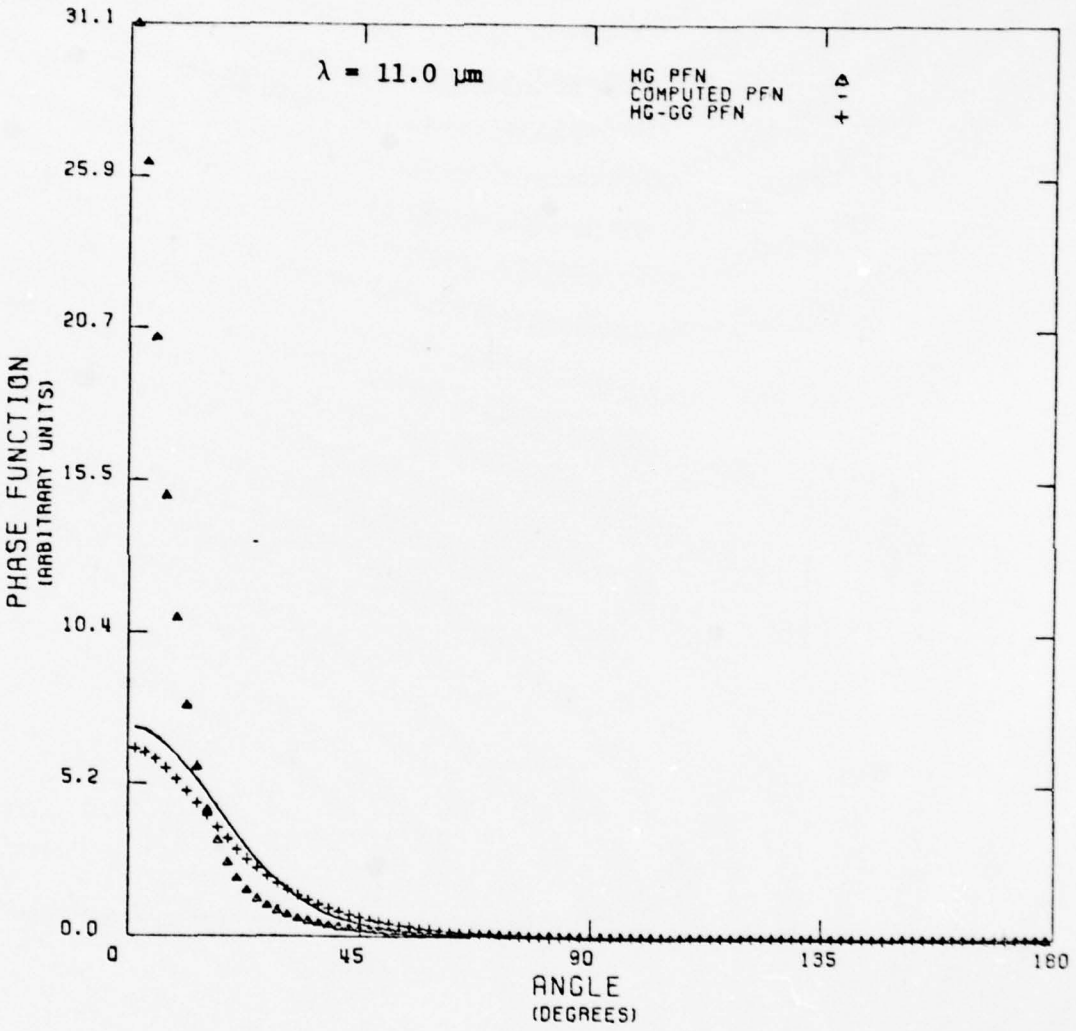

Figure 1.4.3.8 Comparison of analytic phase functions HG and HG-GG with computed phase function for fog model WSMRF2 at 11.0 μm.

error is also presented for the difference between the computed and analytic phase functions, and again indicate that the HG-GG analytic phase function provides a better fit to the computed phase function than the HG analytic phase function. Therefore, it is recommended that if an analytic phase function is to be used it should be the HG-GG function. This is particularly so if the particular regime under consideration is near the incident (forward) direction.

1.4.5 Tabular Method for Determination of Phase Function: Should the user desire more accuracy than the HG-GG analytic phase function provides, it is suggested that the following tabular method be employed. The program for creating such a table is explained in Appendix B.

In order to reduce the computational load in determining the computed phase function needed for the multiple scattering programs, New Mexico State University has constructed a tabular 'look up' method for certain fog models. The fog models have been provided by the Atmcspheric Sciences Laboratory, and are based upon the modified gamma distribution, and have been labeled WSMRF1 and WSMRF2 (see section 1.4.3).

Program AGAUSX has been used to calculate values of the scattering fraction at 2° increments from zero to 180° and at selected wavelengths using the modified gamma/generalized Khirgian-Mazin distribution (type 5 within program AGAUSX). The selected wavelengths for both models are presented below.

Selected Wavelengths for Fog Models WSMRF1, WSMRF2

Wavelength (μm)	Δλ(μm)	Remarks
.55	N.A.	one wavelength
1.06	N.A.	one wavelength
2.5	N.A.	one wavelength
3.0 - 5.0	.25	inclusive*
8.0 - 10.0	.25	inclusive
10.0 - 12.0	.5	inclusive

*e.g., 3.25, 3.50, ... 4.75, 5.0

The control program called FIND is a stand-alone routine or may be incorporated into program ASLSOM as a subroutine. Documentation for program FIND may be found in Appendix B. Program FIND provides scattering fractions and the attenuation coefficient in the proper format for input to ASLSOM at the wavelengths given above or will perform linear interpolation within the wavelength range 0.55 μm to 12.0 μm.

An error analysis has been performed to determine the percent difference between the interpolated phase function and the computed phase function.

The following table should be used with caution, since the percent difference is at the best only a rough indication of the accuracy of the interpolation process.

Percent Difference for Scattering Fraction Interpolation at Wavelength λ for Models WSMRF1 ($\bar{E}_1$) and WSMRF2 ($\bar{E}_2$)

λ(μm)	$\bar{E}_1$(%)	$\bar{E}_2$(%)	λ(μm)	$\bar{E}_1$(%)	$\bar{E}_2$(%)
1.06	16	16	2.5	40	58
3.0	119	241	3.25	100	123
3.5	19	26	3.75	22	9
4.0	11	5	4.25	14	1
4.5	16	6	4.75	16	5
5.0	21	9	8.0	8	7
8.25	3	0	8.50	5	2
8.75	4	0	9.0	5	1
9.25	5	1	9.5	6	2
9.75	3	2	10.0	6	4
10.5	11	8	11.0	30	29
11.5	13	13			

1.5 ADDITIONAL STUDIES OF IR EXTINCTION IN HYGROSCOPIC AEROSOLS

1.5.1 Introduction: In a previous document [1] some results of the modeling of IR extinction in hygroscopic aerosols were reported. During the present contract period, some additional computations have been made to extend the range of relative humidities beyond that used previously and to examine the effects of "hysteresis" in the condensation and evaporation of droplets formed upon hygroscopic condensation nuclei. The new calculations were carried out using the simulated white phosphorous smoke model A' defined in the report referenced above.

Computations were carried out with an early version of program AGAUS9 at wavelengths of 0.55, 1.06, and 3.6 μm. Twelve values of relative humidity were used, and mass accretion coefficients were taken from Hanel [5] for conditions of both increasing and decreasing relative humidities.

1.5.2 Results: The data generated by the new computations are presented in graphical form in figures 1.5.1 through 1.5.3. Figure 1.5.1 shows the absolute extinction coefficients as a function of relative humidity at λ = 0.55 and λ = 1.06 μm. The "arrowheads" indicate the direction in which relative humidity is changing: An arrowhead tilted toward the right represents increasing relative humidity, and an arrowhead tilted toward the left represents decreasing relative humidity. Figure 1.5.1

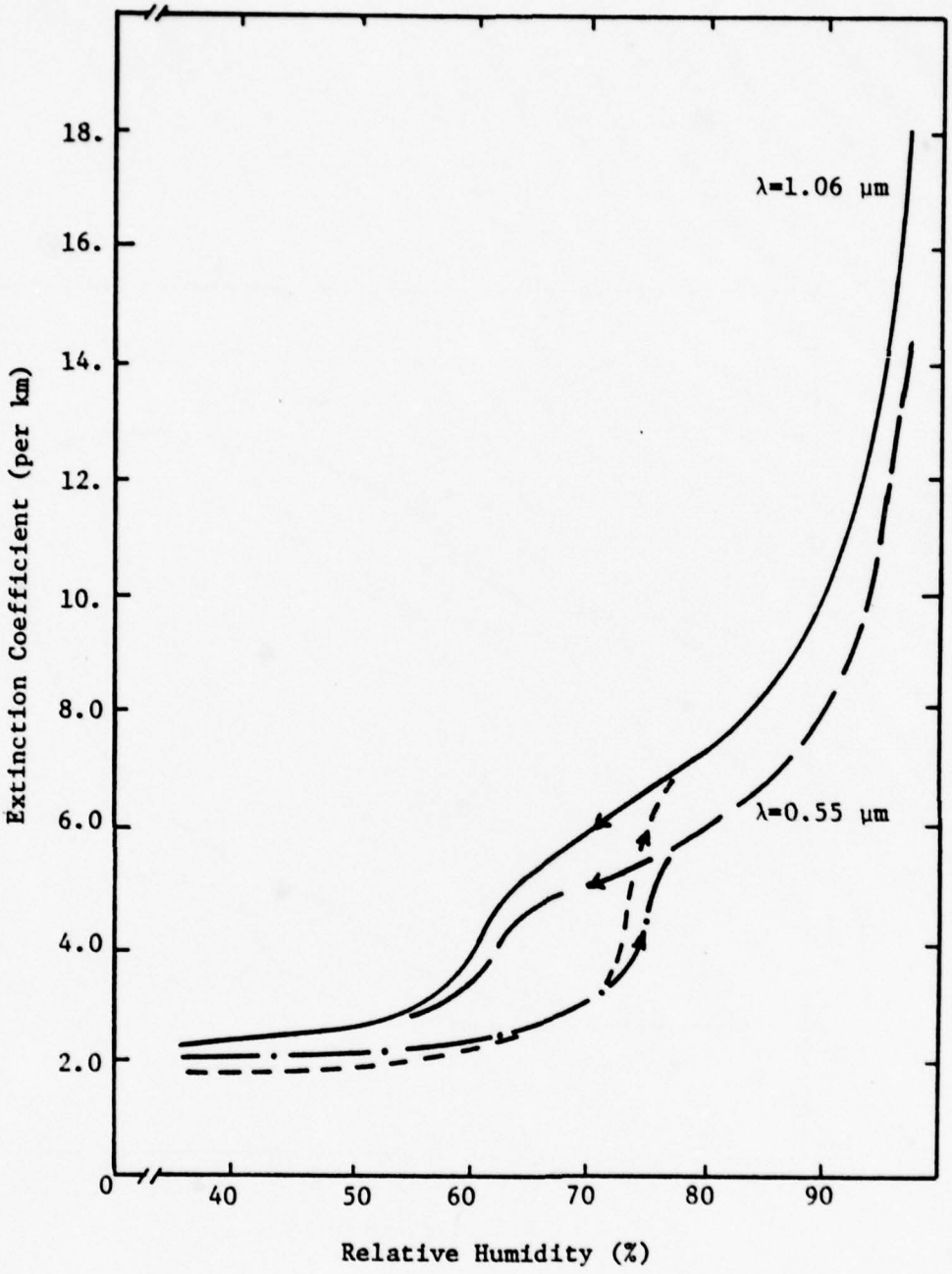

Figure 1.5.1 Computed extinction coefficients for NMSU smoke model A' as a function of relative humidity; λ is the wavelength in μm. The solid curves and broken curves represent conditions of decreasing and increasing relative humidity, respectively.

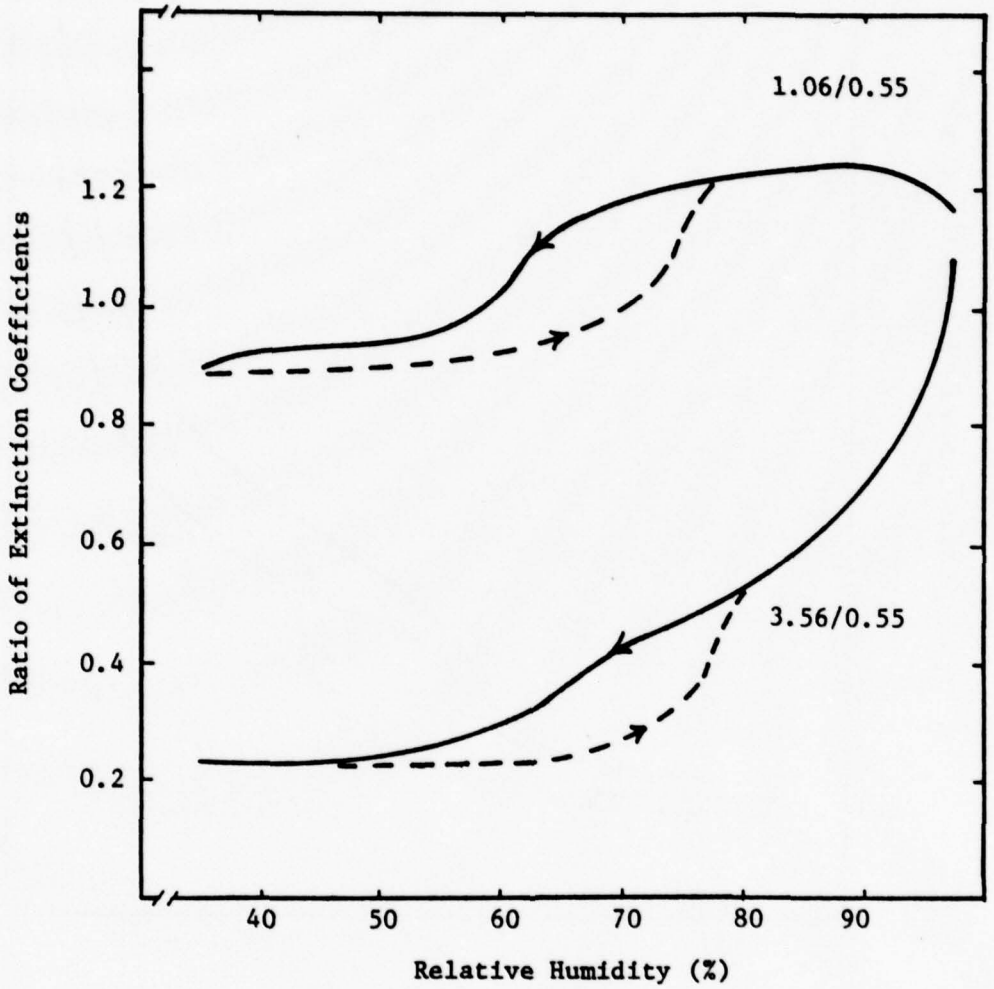

Figure 1.5.2 Ratio of Model A' extinction coefficients at λ = 1.06 μm and λ = 3.56 μm to values at λ = 0.55 μm as a function of relative humidity. The solid curves represent increasing relative humidity, and the dashed curves represent decreasing relative humidity.

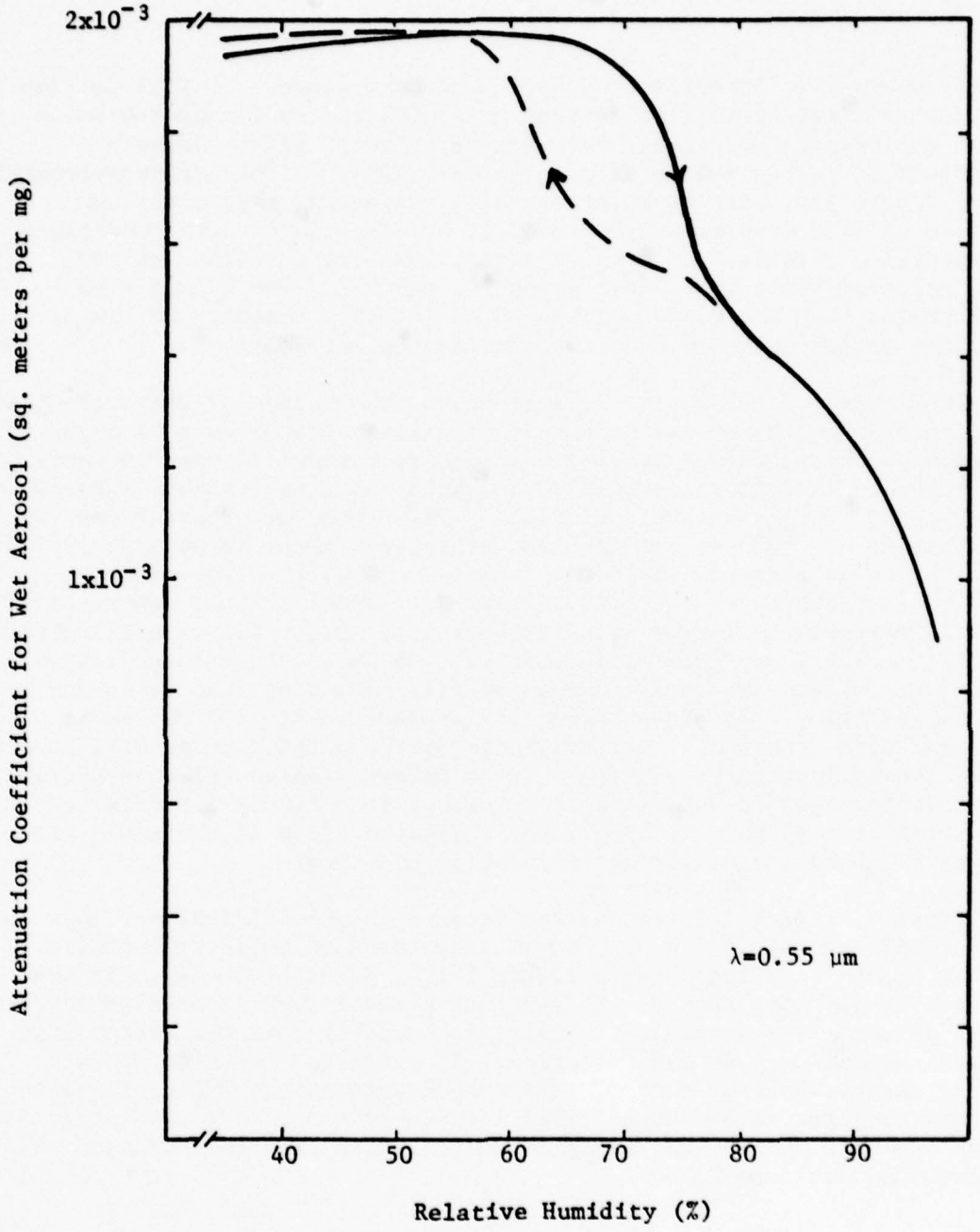

Figure 1.5.3 Attenuation coefficient per unit mass of Wet Aerosol at 0.55 μm vs Relative Humidity for NMSU smoke model A'. The solid curve is for increasing relative humidity and the dashed curves represent decreasing relative humidity.

clearly shows the "hysteresis" effect mentioned above. It will be seen that for relative humidities between about 60% and 75%, that the value of the extinction coefficient may vary by a factor of two between conditions of rising and falling relative humidity. For both wavelengths shown, figure 1.5.1 can be interpreted as suggesting that clearing (associated with droplet evaporation) of a smoke cloud under conditions of decreasing relative humidity is slower than its formation at any given relative humidity between about 50% and 75%. The figure also demonstrates that the sense of changes in relative humidity may be as important as its value in modeling hygroscopic aerosols.

In figure 1.5.2 one will find graphs of the ratios of the extinction coefficients at 1.06 μm and 3.56 μm to those at 0.55 μm as a function of relative humidity, figure 1.5.2 is subject to various interpretations. One inference is that the aerosol model used for these calculations is almost always (all relative humidities $\leq$ 99%) more "transparent" at 3.56 μm than at 0.55 μm, but the same statement cannot be made at 1.06 μm. This particular aerosol, while more transparent at 10.6 μm than at 0.55 μm for relative humidities below about 59%, is comparatively less transparent for larger saturation ratios. Other features discernable from figure 1.5.2 are that extinction at 1.06 μm as compared to its value at 0.55 μm is much less sensitive to relative humidity than it is for 3.56 μm radiation. In other words, the extinction at 1.06 μm can be predicted more accurately from knowledge of the extinction at 0.55 μm than can be the extinction at 3.56 μm when no information on relative humidity is available. One further obvious inference from figure 1.5.2 is that extinction at 1.06 μm will be greater than at 0.55 μm if the smoke cloud is clearing because of decreasing relative humidity.

Finally, figure 1.5.3 shows the attenuation coefficient per unit mass of WET aerosol at λ = 0.55 μm as a function of relative humidity. If that figure is compared with figure 1.5.1, it will be seen that the attenuation per unit mass of the existing aerosol (WET → nuclei + accreted water) is much less sensitive to relative humidity than the attenuation per unit mass of dry aerosol material. It suggests that simultaneous in situ measurements of aerosol mass concentrations and extinction which preserve accreted water should yield less uncertainty or variation in extinction with changes in relative humidity than measurements made on dry aerosol materials alone.

1.5.3 Discussion: The results described above can, of course, be applied in detail only to the aerosol model used in generating them and at the specific wavelengths used. They do suggest, however, that extinction can, under some situations at least, vary by nearly a factor of two at a given relative humidity between conditions of rising and falling relative humidity, and that the relationship between extinction at two different wavelengths may also be dependent on the direction of changes in relative humidity. Consequently it would seem that persons involved in both field measurements and numerical modeling should probably pay more attention to meteorological conditions than they seem to have done in the past.

1.6 WAVELENGTH CHANGE ALGORITHM

A feasibility study has been undertaken at NMSU to determine whether it is possible to determine the extinction at a given wavelength, λ_G, from the extinction at λ = .55 μm for various aerosol distributions. To accomplish this, program AGAUSX has been used to find the extinction coefficient at various wavelengths for three specific aerosol models. The models used were WSMRF1, WSMRF2, (see section 1.4.3) and a modification of WSMRF1 which shall be referred to as model WSMRF3. Model WSMRF3 is identical with model WSMRF1 with the exception that for WSMRF3 the mode radius was set equal to 8.0 μm whereas the mode radius in WSMRF1 was 10.0 μm.

The results are graphically displayed in figure 1.6.1, where we have plotted the ratio of the extinction coefficient at chosen wavelengths to the extinction coefficient at 0.55 μm against the chosen wavelength. The disparity between models WSMRF1 and WSMRF3, which differ only by 2 μm in the mode radius and are therefore related, highlights the difficulty in attempting to find an analytic expression that would be valid for various aerosol models at sundry wavelengths. To find an analytic expression that could be used for models WSMRF1 and WSMRF2 (models that are unrelated) would be more difficult than attempting to relate associated models.

Since aerosol distributions may vary greatly in a short period of time, or may be altered by battlefield-induced contaminants, it would appear that estimates of extinction at various wavelengths derived from the extinction at .55 μm is risky at best. This work is also in general agreement with the work of Mason and Hoidale [5] who have assessed the utility of visibility as an indicator of transmittance in the infrared. Chylek [7] has investigated the dependence of the extinction coefficient against liquid water content, and finds that there is a definite wavelength (λ = 11 μm) for which these parameters are related. However at different wavelengths (e.g., 0.55 μm) Chylek has determined that there is no unique relationship between the extinction coefficient and the liquid water content; the extinction varies greatly as a function of the size distribution when the liquid water content is held constant.

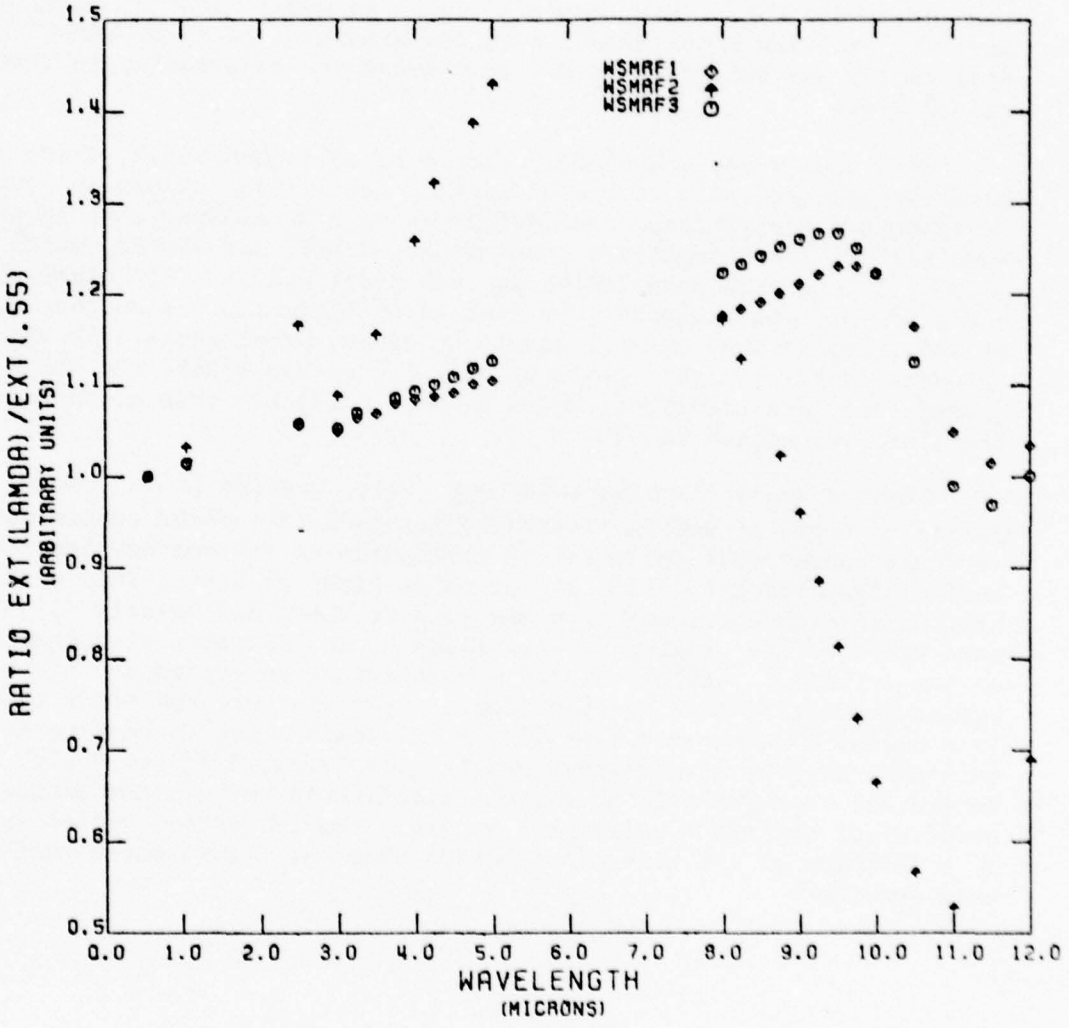

Figure 1.6.1 Ratio of extinction coefficient at various wavelengths to the extinction at 0.55 μm versus wavelength for fog models WSMRF1, WSMRF2, and WSMRF3.

Chapter 2

MULTIPLE SCATTERING INVESTIGATIONS

Introduction

Two aspects of radiative transfer problems in which multiple scattering effects are significant have been subjected to further study under this contract. The two topics are (a) approximation methods aimed at speeding up calculations with concurrent sacrifices in accuracy, and (b) further examination of the problem of treating multiple scattering effects under illumination by beams with finite cross-sectional areas. The results of these studies are presented in more detail in the following sections of this report.

2.1 APPROXIMATION METHODS

2.1.1 Introduction: An investigation of various methods for obtaining numerical solutions to the equation of radiative transfer by approximate methods has been undertaken at NMSU. There are two basic approaches, the first of which uses the complete phase function but treats the multiple scattering only approximately; this is useful for obtaining estimates of the flux and albedo. The second method uses an approximate phase function and treats the multiple scattering exactly; this is useful when the angular dependence of the intensity is desired.

We have reviewed numerous methods for elongated phase functions which occur when the particle size is greater than the wavelength under consideration that have appeared in the literature. These include: approximating the phase function by only a few terms in the Legendre expansion; calculating first order scattering exactly and approximating higher order scattering; dividing the phase function into various segments such that an exact solution may be found for angles near incidence; truncation of the phase function; approximate analytic phase functions; similarity relations (see Figure 2.1.1); and asymptotic curve fitting. None of the above methods will work well under all conditions. Additionally we have tried curve fitting to calculated intensities (see Figure 2.1.2); comparing intensity distributions within a cloud to those calculated up to a final optical depth that is the same as that of the intensity within the cloud (see Figures 2.1.3 and 2.1.4); and interpolation.

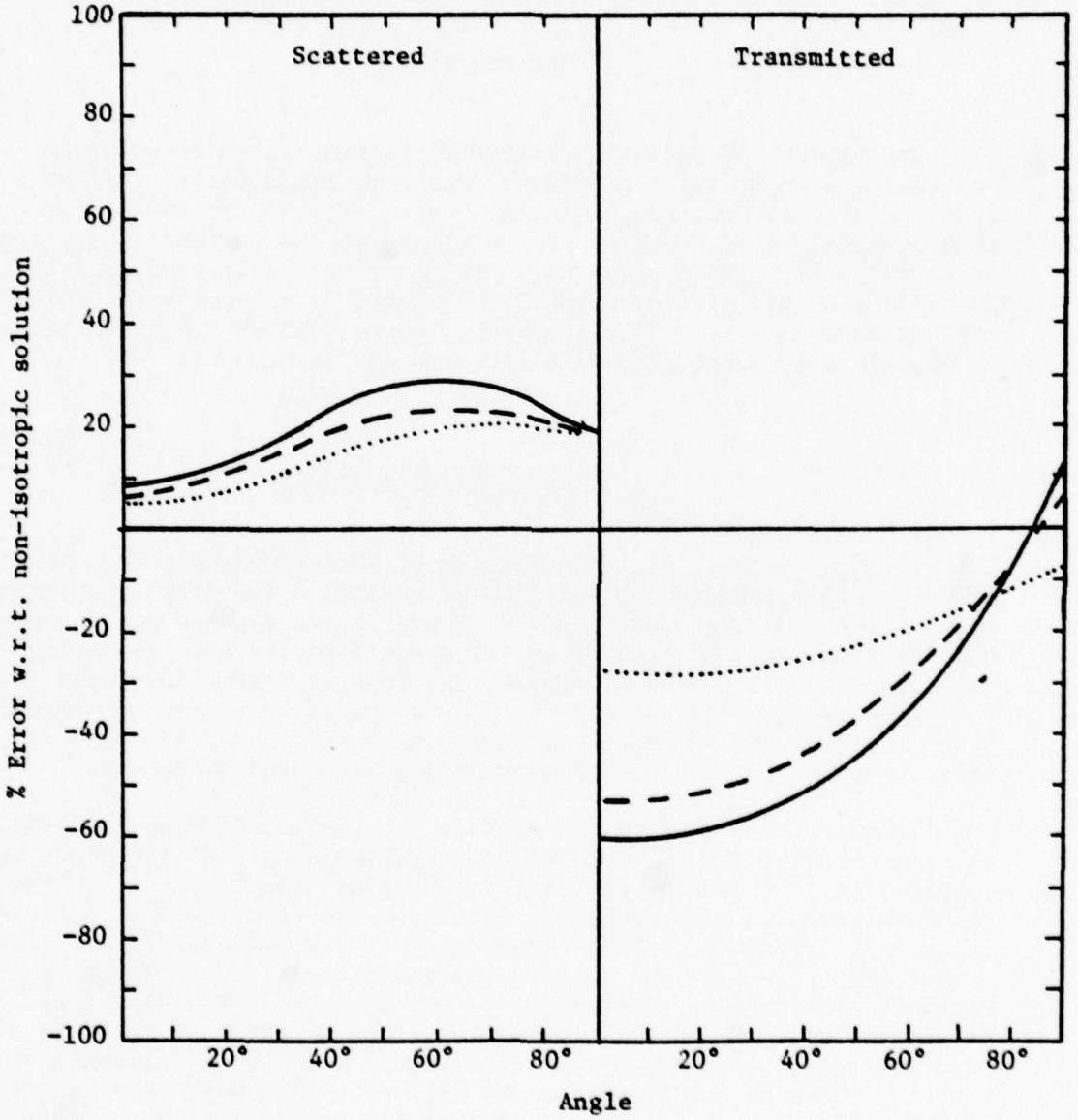

Figure 2.1.1 Comparison of similarity solution for optical depths of 0.25 (solid line), 1.0 (dashed line), and 8.0 (dotted line): $\tilde{\omega}_o = 0.6555$, $g = 0.1538$.

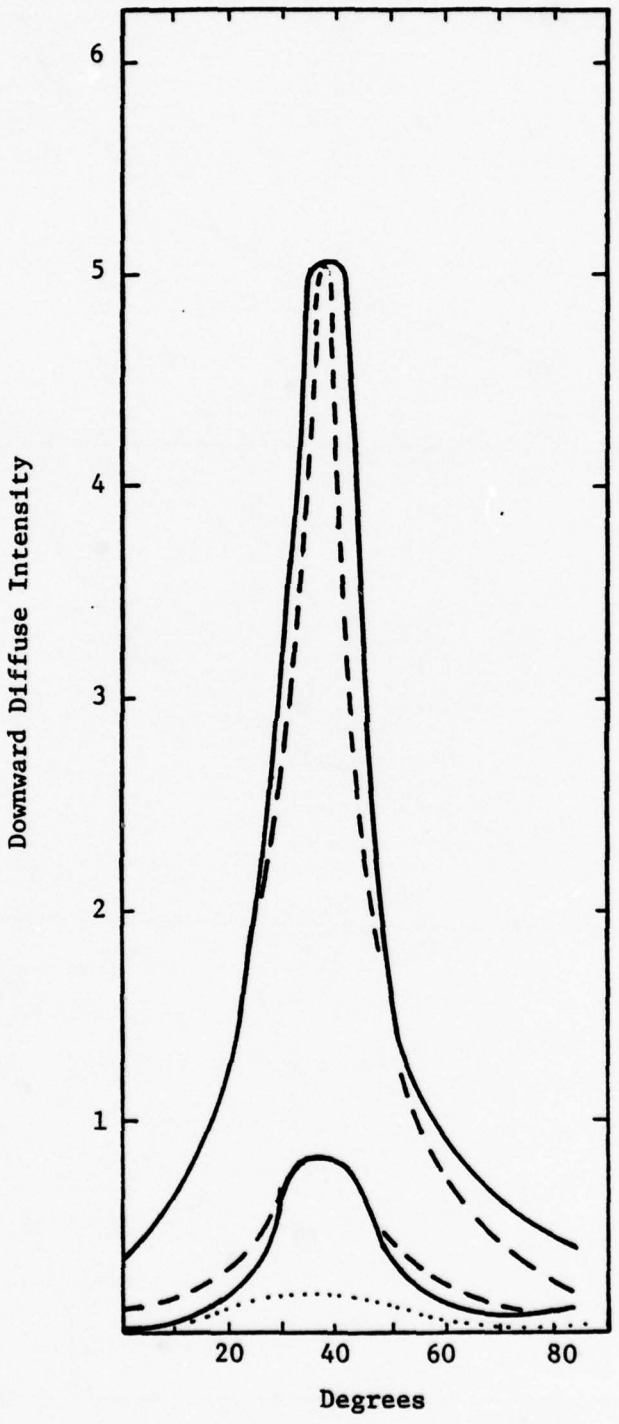

Figure 2.1.2 Comparison of Henyey-Greenstein phase function (dashed and dotted lines) normalized to various points on the true intensity curve (solid line).

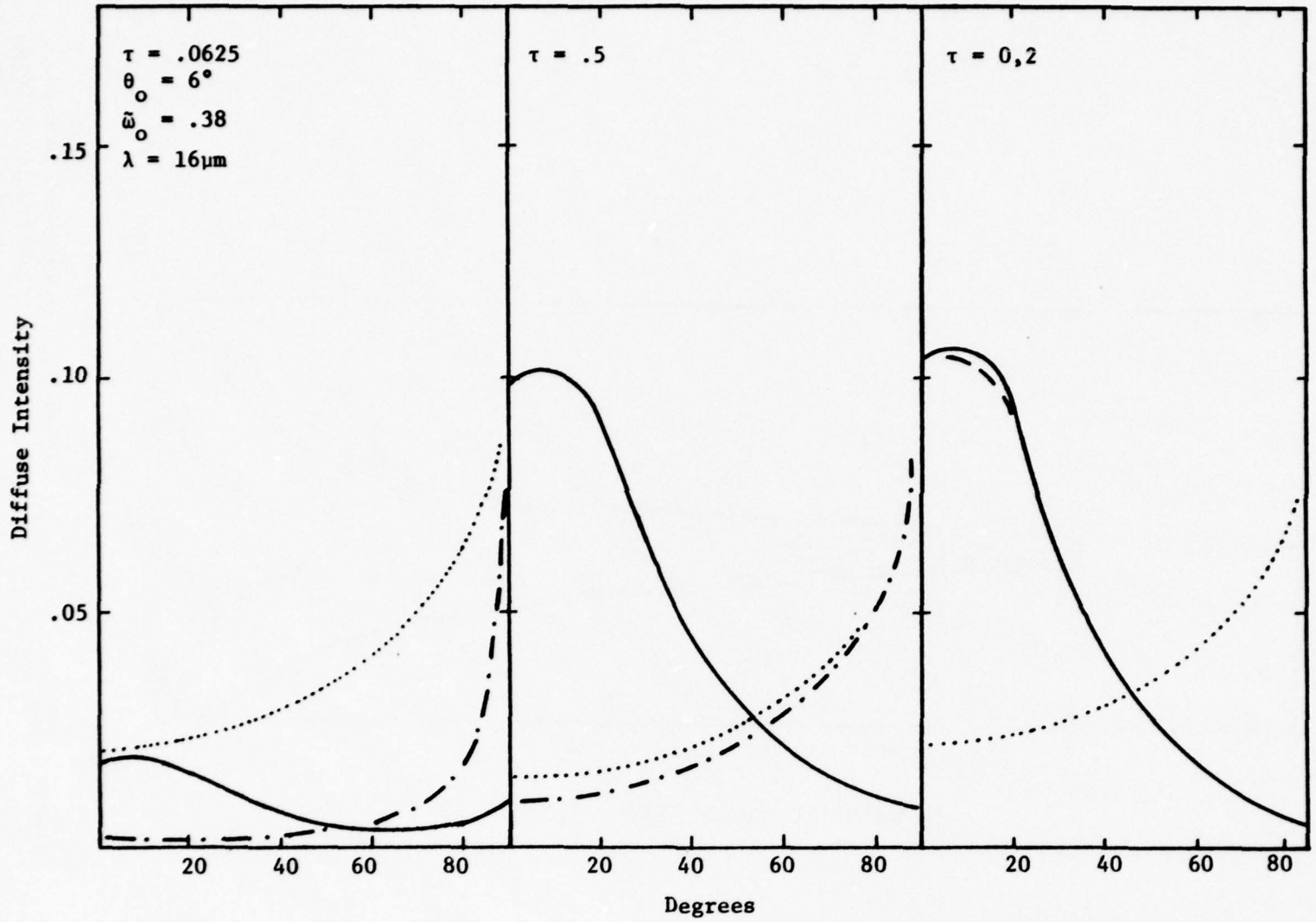

Figure 2.1.3 Comparison of internal vs 'external' intensities. The solid and dotted lines correspond to transmitted and reflected internal intensities, respectively. The dashed and dash-dot lines correspond to 'external' intensities. Where a comparison line does not appear the lines are coincident. The scale should be divided by ten for the scattered intensities.

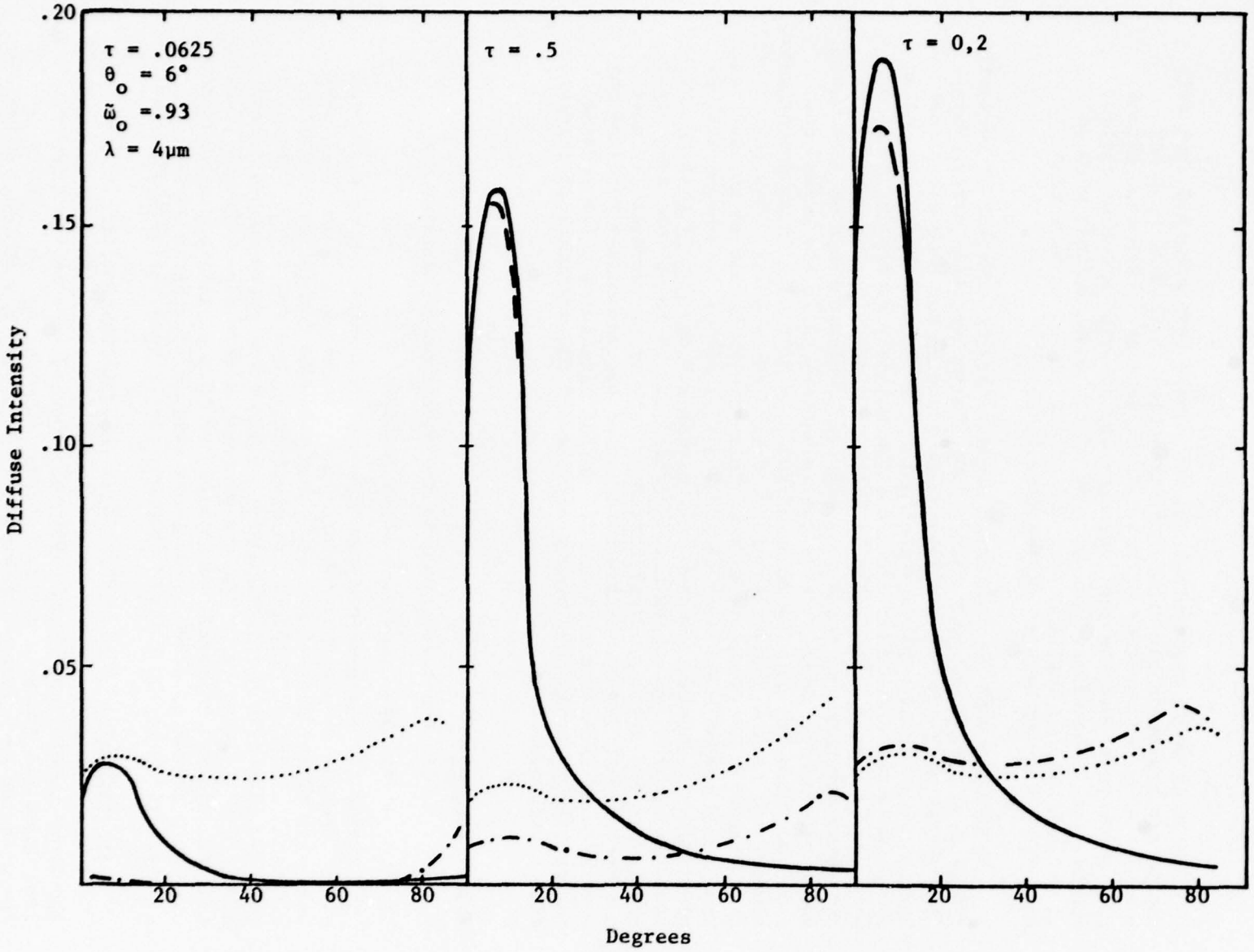

Figure 2.1.4 Comparison of internal vs 'external' intensities. The solid and dotted lines correspond to transmitted and reflected internal intensities, respectively. The dashed and dash-dot lines correspond to 'external' intensities. Where a comparison line does not appear the lines are coincident. The scale should be divided by ten for the scattered intensities.

While it would appear that one can always find a method that will adequately represent the angular distribution of intensity at any optical depth and wavelength, it would be unusual if the same method will adequately describe the intensity distribution at other optical depths, etc. Therefore, because none of the above methods work well at various optical depths and angles of incidence, we have also employed a tabular method (see section 1.4.5).

In dealing with approximation methods for the equation of radiative transfer we have found that there appear to be two basic approaches: (1) methods that use the complete phase function but only treat the multiple scattering problem approximately, and (2) methods that use an approximate phase function but treat the multiple scattering problem in an exact manner. The first of these is generally useful for obtaining estimates of the albedo and flux, which contain no information about the angular dependence of the intensity, while the second does give the intensity as a function of angle, albeit only in an approximate manner. As we are primarily concerned with the angular distribution of the intensity, the emphasis in what follows will be placed entirely on the second method. Wherever possible a full set of references will be provided. It should be borne in mind that for any <u>specific</u> radiative transfer problem, an approximate solution may be found that adequately represents the original distribution of intensity. However, it does not appear that any one approximate method can adequately describe the variation of intensity with optical depth, particularly for internal intensities, nor can they accurately predict the variation of intensity with other parameters.

2.1.2 <u>Methods</u>:

1) Exact solutions to the equations of transfer for slightly elongated phase functions.

Irvine [8] has examined the effect of approximating an elongated phase function by one that contains three terms or less in the Legendre expansion of the phase function. This was done for situations with azimuthal symmetry, conservative scattering, and for $\tau \leq 1$. Generally he finds that as the optical depth increases the approximated intensity approaches the true value but the process is very slow. Irvine finds that the diffuse reflection determined by this approximate method "may vary by a factor of 2 or 3 from those (values) for large particle scattering, while the diffuse transmission is qualitatively different".

Approximating an elongated phase function by isotropic scattering, where the scattering coefficient (effectively the optical depth under the above conditions) is appropriately reduced to some fraction of its true value (in order to simulate forward scattering) was also investigated by Irvine. Comparison of this method with exact solutions showed that this approximation method is inherently wrong, producing large errors.

2) Approximate methods based on the use of exact expressions for first-order large particle scattering

Using the Neumann solution to the equation of radiative transfer Irvine [8] has calculated successive orders of scattering under the conditions $\tau \leq 1$, $\tilde{\omega}_o = 1$, and azimuthal symmetry. He then considers the following: calculation of exact first-order scattering and approximating additional higher order scattering by simplified phase functions; i.e., isotropic and Sobolev. His conclusions based upon this method are as follows: the diffusely transmitted intensity is well represented, but the reflected intensity may be only qualitatively correct.

3) Romanova's small-angle approximation

If the phase function is highly peaked it is possible to separate that portion of the intensity that changes most rapidly with angle compared with the slowly varying component. Thus, if the phase function is highly peaked, and the single scattering is primarily in the forward direction, the following approximations are made in the equation of transfer. Writing the equation of transfer as

$$\mu \frac{\partial I}{\partial \tau} + I = \frac{1}{2} \int_{-1}^{1} I(\tau,\mu')P(\mu,\mu')d\mu', \qquad (2.1\text{-}1)$$

we replace the factor μ in the first term of the above equation on the left-hand side by μ_o and neglect backscattering in the boundary condition. Setting $\mu_o = 1$ it can be shown [9,10] that the <u>exact</u> solution to this approximate problem is:

$$I(\tau,\mu) = \frac{F}{4} \sum_{\ell=o}^{\infty} (2\ell+1)P_\ell(\mu)e^{-K_\ell \tau}, \qquad (2.1\text{-}2)$$

where F is the flux, $P_\ell(\mu)$ are the Legendre polynomials and $K_\ell = 1-\omega_\ell/(2\ell+1)$, where ω_ℓ is defined by the relation $P(\cos\theta) = \sum_{\ell=o}^{\infty} \omega_\ell P_\ell(\cos\theta)$, $P(\cos\theta)$ being the phase function. Romanova's method [11] is to now separate the intensity into two parts; that of the small angle approximation and that due to the slowly varying part of the intensity (called the correction factor by Romanova). Thus $I = I_{sa} + \tilde{I}$; substituting this into the equation of transfer and using the definition of the small angle approximation we find that

$$\mu \frac{dI}{d\tau} + \tilde{I} = \int_{-1}^{1} \tilde{I}\, P\, d\mu' + (\mu_o - \mu) \frac{dI_{sa}}{d\tau}. \qquad (2.1\text{-}3)$$

The above equation may be solved by any of the numerous numerical methods, the primary advantage being the (supposed) slow varying of $\tilde{I}$ as a function of angle. This should simplify the quadrature problem usually encountered for elongated phase functions. Irvine [12] has examined the computations of Romanova [13,14] and finds that her results agree with those computed by Irvine using the doubling method to within 5% accuracy. To the author's knowledge a computational code based on the small angle approximation has not been constructed in this country, and one must therefore rely upon Irvine's feeling that Romanova's method "may effect a very considerable saving in time over more conventional methods."

4) Truncation of Phase Function and Approximate Phase Functions

Hansen [15] has made comparisons of intensities determined by doubling with those determined by approximating the phase function in various manners. Specifically his approximations were made by 1) truncating the peak of anisotropic phase functions, 2) using the Henyey-Greenstein phase function, and 3) using the Kagiwada-Kalaba phase function, the latter two being analytic functions.

In truncating the peak of anisotropic phase functions Hansen has taken the slope of the logarithm of the phase function as being constant for $\theta < 20°$, with the slope equal to that of the untruncated phase function at 20°. Once the peak of the phase function has been truncated the optical depth and $\tilde{\omega}_o$ must be appropriately scaled. This approximation effectively replaces photons that are scattered through a few degrees by photons scattered through 0°. As would be expected this method produces errors of the order of a few percent in: a) angles near the incident angle, b) in the direct backscatter, and c) in emergent angles near grazing, as photons moving nearly parallel to the surface stand a greater chance of being scattered than do photons that are moving perpendicular to the surface. Unfortunately Hansen gives no graphs of the transmitted intensity but one can easily see that (a) above would be the largest source of error in the transmission.

In using the analytic Henyey-Greenstein (HG) and Kagiwada-Kalaba (KK) phase functions Hansen has found that neither of the above phase functions can accurately duplicate the angular distribution of intensity; the HG phase function represents the intensity distribution better than the KK function. The analytic phase function's representation of the distribution of intensity becomes better the more anisotropic the original phase function and the thicker the atmosphere becomes.

5) Similarity Relations

Irvine [16] in an excellent review paper presents a method of approximating the solution for an anisotropic phase function in terms

of a known solution for isotropic scattering. Such a transformation may be valid if the radiation field has been smoothed, which usually only occurs for large optical depths or integration over angle. The appropriate equations are:

$$\tilde{\omega}_o^* = (1-g)\tilde{\omega}_o/(1-g\ \tilde{\omega}_o), \qquad (2.1\text{-}4)$$

$$\tau_o^* = (1-g\ \tilde{\omega}_o)\tau_o, \qquad (2.1\text{-}5)$$

where the superscript * refers to isotropic values. This method was tried and the results may be seen in Figure 2.1.1. As expected the fit is not very good and improves with increasing optical depth.

6) Asymptotic Curve Fitting

van de Hulst [17] has given a method of essentially fitting a curve to the intensity at large optical depths and for $\tilde{\omega}_o \geq 0.6$. His method is presented in a way that appears to be easily programmable. In addition van de Hulst's method is set up to receive output of reflection and transmission functions that have been computed by the doubling method. In reference 16, van de Hulst implies that one needs an optical depth of about 32 to apply his formulae, but in further papers [18,19] he seems to imply that the results of the asymptotic fitting are accurate for lower values of the optical depth. Unfortunately van de Hulst only provides formulae for normal incidence, and therefore independent of azimuth.

2.1.3 Additional Methods: A number of simple methods were examined to determine their feasibility and accuracy. These consisted of: 1) curve fitting, 2) comparison of internal versus 'external' intensities, and 3) interpolation.

1) Curve Fitting

As the distribution of the intensity for single scattering follows the 'probability distribution' of the phase function, it was hoped that one might be able to adequately fit the true intensity by using the Henyey-Greenstein phase function normalized to some point on the 'true' intensity distribution. Figure 2.2.2 shows some results of this method. The results for τ=2 are rather anomalous insofar as the fit is rather good from 0° to 36°. However the results begin to deviate after this. Two fits were tried for τ = .0625, neither producing very good results. Subsequent to this the same procedure was computerized and fits were

tried for various other intensity distributions, normalizing at sundry points on the distributions. The best fit was obtained by normalizing the curves at the maximum of the intensity distribution, but the "average" error was still between 30 and 100 percent. Coupling the above error with the fact that apriori knowledge of the intensity distribution is needed, the method was given up as inadequate.

2) Comparison of internal versus 'external' intensities

Because the doubling method of numerically solving the equation of transfer is the fastest computer method a comparison of the results from doubling were made with those from the Gauss-Seidel method, which will produce internal intensities. Thus the transmitted and reflected intensities at internal optical depths of .0625, 0.5 and a final optical depth of 2.0, as computed by the Gauss-Seidel method, were compared with the intensities produced by the doubling method at final optical depths of .0625, .5 and 2.0. The results presented for two values of $\tilde{\omega}_o$, the albedo for single scattering, may be seen in Figures 2.2.3 and 2.2.4. The results are striking insofar as the transmitted intensities from both programs match exceedingly well. This is a natural consequence of the extreme directivity of the phase function; most of the light is scattered in the forward direction. Unfortunately the same cannot be said for the reflected intensities; agreement is only achieved at the boundary ($\tau=0$): as expected, the agreement is better as $\tilde{\omega}_o$ decreases.

3) Interpolation

Interpolation was tried using the intensities determined by the Gauss-Seidel method. This met with little success as there were not enough values of the intensity at various optical depths to allow accurate, or even semi-accurate, interpolation. This situation can be changed by modification of the Gauss-Seidel computer code to allow the intensities to be printed out at a few places within the atmosphere.

2.1.4 Summary: We may summarize the previous methods by stating that there is apparently no approximate method that will adequately describe the variation of intensity with angle under all conditions. The methods that have been reviewed, or tried, appear to be inadequate or else require that a computer program of some complexity be written.

2.2 MULTIPLE SCATTERING OF NARROW RADIATION BEAMS BY AEROSOLS

2.2.1 Introduction:

Steady state multiple scattering by typical homogeneous aerosols is often described by the radiative transfer (RT) equation

$$\underset{\sim}{s}\cdot\nabla_{\underset{\sim}{r}} I(\underset{\sim}{r},\underset{\sim}{s}) + \gamma\, I(\underset{\sim}{r},\underset{\sim}{s}) = (4\pi)^{-1}\gamma\int d\Omega_{s'}\, p(\underset{\sim}{s},\underset{\sim}{s}')I(\underset{\sim}{r},\underset{\sim}{s}'), \qquad (2.2\text{-}1)$$

where $r = (x,y,z)$ = spatial coordinates, s = unit vector, $I(r,s)$ = total specific intensity at point r in direction s, $\gamma \equiv$ extinction coefficient of medium, and $p(\underset{\sim}{s},\underset{\sim}{s}') \equiv$ phase function of medium. The specific intensity $I(\underset{\sim}{r},\underset{\sim}{s})$ is the radiant power at a given wavelength per unit solid angle around s that crosses unit area parallel to s, at point r. Eq. (1) is the simplest of a hierarchy of equations; strictly speaking, it applies only to situations where there is no time dependence, no source of radiation in the aerosol, and polarization may be neglected. Many actual illuminated aerosols satisfy these conditions to a good approximation.

In theoretical calculations, it is usual to treat a model aerosol composed of spherical particles, because it is only for spherical particles that the scattering properties (γ, $p(s,s')$) can be calculated exactly from Mie theory. For a homogeneous aerosol containing several components of different optical type (particles having different complex refractive indices $m_i = n_i - ik_i$) and different size distributions $f_i(a)$ and number densities N_i for each component, the quantities $(\gamma, p(\underset{\sim}{s},\underset{\sim}{s}'))$ are given by

$$\gamma = \sum_i N_i \int f_i(a) C_{ext}^{(i)}(a)\,da \Big/ \int f_i(a)\,da \equiv N\,\overline{C}_{ext},$$

$$p(\underset{\sim}{s},\underset{\sim}{s}') = (4\pi/\gamma)\sum_i N_i \int f_i(a)\; C^{(i)}(a,\, \underset{\sim}{s},\underset{\sim}{s}')\,da \Big/ \int f_i(a)\,da,$$

where $f_i(a)da$ = no. of particles of type i with radius in $(a, a+da)$, $C_{ext}^{(i)}(a)$ = Mie theory extinction cross-section of a particle of type i, radius a, $C^{(i)}(a, s, s')$ = Mie theory differential scattering cross-section, from direction s' to direction s, of a particle of type i, radius a. The last equality of Eq. (2) defines $\overline{C}_{ext}$, the average extinction cross-section, where $N = \sum_i N_i$ = total number density of particles in the aerosol.

The phase function is normalized so that $\int d\Omega_s \; p(s,s') = 4\pi \; \bar{\omega}_o$, where $\bar{\omega}_o$, the (average) single-scattering albedo, is given by

$$\bar{\omega}_o = \gamma^{-1} \sum_i N_i \int f_i(a) \; C_{sca}^{(i)}(a) da \Big/ \int f_i(a) dr \equiv \bar{C}_{sca} / \bar{C}_{ext},$$

and the last equality defines $\bar{C}_{sca}$, the average total scattering cross-section. Note well that the extinction coefficient $\gamma = NC_{ext}$ is the same quantity as the K_{ext} used in other parts of this report.

2.2.2 Incident Beams and Formal Solutions of the RT Equation:

Many problems of interest involve one or several aerosol "clouds" of finite extent, acted on by a beam of radiation from some source. Each of these clouds may have non-uniform composition; regions of different composition have different scattering properties (γ, $p(\underset{\sim}{s},\underset{\sim}{s}')$), but each region may be treated separately, and the intensities matched at interfaces. Therefore, the generic problem for calculation is that of a single homogeneous cloud of aerosol, acted on by a specified incident beam. If the incident beam intensity is given on the cloud surface, then it may be found inside the cloud as the solution of

$$\underset{\sim}{s} \cdot \underset{\sim}{\nabla}_r \; I_{in}(\underset{\sim}{r},\underset{\sim}{s}) + \gamma I_{in}(\underset{\sim}{r},\underset{\sim}{s}) = 0. \qquad (2.2\text{-}2)$$

Formally, if $I_{in}^{(\Sigma)}(\underset{\sim}{r}_\Sigma,\underset{\sim}{s})$ is given at all points $\underset{\sim}{r}_\Sigma$ on the surface Σ of the cloud, then the solution is

$$I_{in}(\underset{\sim}{r},\underset{\sim}{s}) = e^{-\gamma \ell(\underset{\sim}{r},\underset{\sim}{s})} \; I_{in}^{(\Sigma)}(\underset{\sim}{r} - \underset{\sim}{s}\ell(\underset{\sim}{r},\underset{\sim}{s}), \; \underset{\sim}{s}), \qquad (2.2\text{-}3)$$

where $\ell(r,s)$ = distance from $\underset{\sim}{r}$ back along $(-\underset{\sim}{s})$ to the surface Σ (see appendix C.)

A formal implicit solution of Eq. 2.2.1 in the presence of an incident beam is then (see appendix C).

$$I(\underset{\sim}{r},\underset{\sim}{s}) = I_{in}(\underset{\sim}{r},\underset{\sim}{s}) + (4\pi)^{-1} \gamma \int_0^{\ell(\underset{\sim}{r},\underset{\sim}{s})} d\xi \; e^{-\gamma\xi} \int d\Omega_{s'} p(\underset{\sim}{s},\underset{\sim}{s}') I(\underset{\sim}{r}-\xi\underset{\sim}{s},\underset{\sim}{s}'). \qquad (2.2\text{-}4)$$

The formal iterative (Born series) solution of this equation is

$$I^{(n+1)}(\underset{\sim}{r},\underset{\sim}{s}) = (4\pi)^{-1}\,\gamma\int_{o}^{\ell(\underset{\sim}{r},\underset{\sim}{s})} d\xi\, e^{-\gamma\xi}\int d\Omega_{s'}\, p(\underset{\sim}{s},\underset{\sim}{s}')\, I^{(n)}(\underset{\sim}{r}-\xi\underset{\sim}{s},\underset{\sim}{s}'), \quad (2.2\text{-}5)$$

$n = 0,1, \ldots$, where $I^{(o)}(\underset{\sim}{r},\underset{\sim}{s}) \equiv I_{in}(\underset{\sim}{r},\underset{\sim}{s})$, and $I(\underset{\sim}{r},\underset{\sim}{s}) = \sum_{n=o}^{\infty} I^{(n)}(\underset{\sim}{r},\underset{\sim}{s})$. Here, $I^{(n)}(\underset{\sim}{r},\underset{\sim}{s})$ is called the n^{th} order scattered intensity. This iteration solution is very useful in calculation of first order intensities for any geometry, but it becomes very hard to handle numerically if many orders of scattering must be calculated.

2.2.3 Practical Methods of Solution of Transfer Problems:

For situations involving a given aerosol cloud and a given incident beam, the computational problem is to calculate the radiant power into a given detector; the detector is characterized by its location, orientation, conical angle, and aperture area. Regardless of its location, the detector is assumed to produce a negligible perturbation of the radiation field. Therefore, the fundamental problem is to calculate the total intensities I(r,s) inside the homogeneous cloud, given the cloud shape and size, and the incident beam intensity on the cloud surface.

In the absence of any simplifying symmetries, the most practical accurate method of computation appears to be the Monte Carlo technique. This technique is extremely time-consuming if indeed a map of $I(\underset{\sim}{r},\underset{\sim}{s})$ for all $(\underset{\sim}{r},\underset{\sim}{s})$ is desired.

In the presence of symmetries, many other analytical techniques have been used to provide computer algorithms for solving the RT equation. The lower the symmetry, the slower the solution. Most of these analytical techniques require at least that the aerosol cloud be idealized to plane-parallel translation invariance. Within this geometry, only the completely plane-translation-invariant problem that results if the incident beam is infinite in extent is amenable to rapid digital computer solution. Several analytic methods have been applied to this relatively simple problem (e.g., doubling (Hansen [20]), discrete ordinate (Mudgett and Richards [21]; Gauss-Seidel (Herman and Brownling [22])). The doubling method is particularly rapid, but it yields only the transmitted and reflected intensities, not the intensities inside the cloud.

The finite incident beam (searchlight) problem is of major interest, inasmuch as modern guidance systems make use of laser radiation. Some analytic numerical techniques have been applied in the special cases of plane parallel geometry with isotropic scattering (Rybicki, [23] Beckett, [24]) and with strongly forward peaked scattering (Weinman, [25]; 1976). However, it is believed by the authors of this report that no accurate computerized analytic algorithm for the plane parallel searchlight problem with general scattering properties has yet been developed.

During the tenure of this contract, an attempt was made to validate and apply the doubling method computer program for the searchlight problem that had been developed under a previous contract [1]. In principle this program should be applicable to the plane-parallel normal incidence cylindrically symmetric searchlight problem for an aerosol with arbitrary scattering properties. However, it was found that previous estimates of the Univac 1108 CPU time and storage capacity that would be required to provide sufficient accuracy were an order of magnitude too low; a realistic time estimate is 100 hrs per calculation, rather than 10 hrs; storage requirements would be over 512K words, rather than 128K. Any attempt to treat beams at oblique incidence, or non-plane-parallel clouds, would increase the computation time by yet another order of magnitude. It became necessary to conclude that the searchlight problem is one of sufficiently great complexity that its accurate solution by analytic numerical techniques probably exceeds the storage capacity and practical time limitations of computers of the Univac 1108 generation. Indeed, this doubling algorithm would strain the capabilities of the CDC 7600 generation. Evidently, even for the searchlight problem of highest possible geometric symmetry, (normally incident cylindrically symmetric beam on a plane-parallel medium), Monte Carlo algorithms are no more time-consuming than analytic ones, if high accuracy is desired.

However, it does appear possible, by means of simple physical arguments, to predict narrow finite beam transmission and scattering approximately, once the corresponding infinite beam results are known. These arguments lead to the conclusion that, for narrow incident beams and small solid angle detectors, the Bouguer exponentially attenuated transmission is valid, and single scattering is a good approximation in many situations, even for optically thick clouds. Similar conclusions have been reached by several investigators (Anderson, [26] ; Beckett [24]; Zuev [27]), using methods different from those used here. In what follows, the simple physical arguments and their predictions are presented.

2.2.4 Searchlight Beam Transmission:

Consider the prototypical finite beam transmission problem illustrated in Fig. 2.2.1. It is sufficient to consider this case of highest possible symmetry (normally incident cylindrically symmetric searchlight beam on a plane parallel cloud).

Typically, the beam spread angle for a laser beam may be taken as the diffraction limit, $\theta_s \approx 0.6\lambda/R_\ell$, where R_ℓ = radius of laser aperture $\lesssim$ 1mm. This ranges from $\theta_s \approx .00024$ radians for visible light of $\lambda = 0.4$ μm to $\theta_s \approx .006$ radians for infrared radiation of $\lambda = 10$ μm. The cloud thickness L may range from a few meters to several kilometers, as may the detector positioning at distance D from the incident cloud face.

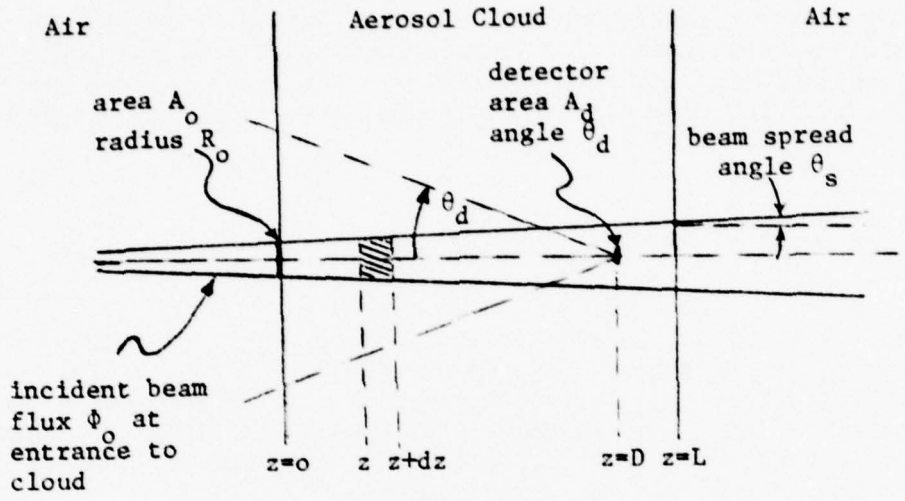

Figure 2.2.1 Finite Beam Transmission Geometry.

The cloud optical depth γL may vary from very small (≈ 0) to very large (10 or more). But multiple scattering can possibly be important only for optically thick clouds ($\gamma L \gtrsim 0.3$). Consider that an optical depth of unity corresponds to an actual thickness L between 10m (dense fog) and 10 km (light haze). Then $\gamma \lesssim L_{min}^{-1} \approx 10^{-1}$m.

The beam entrance radius R_o, area $A_o = \pi R_o^2$, and flux Φ_o are determined by how far the laser is situated behind the entrance face of the cloud. (If the laser is in the cloud, $R_o = R_\ell$, etc.) The beam radius at any point z inside the cloud is given by $R(z) = R_o + z\theta_s$, the beam area by $A(z) = \pi(R(z))^2$, and the beam flux at any point z by $\Phi(z) = \Phi_o A_o(\exp-\gamma z)A(z) = (P_o/A(z))\exp-\gamma z$, where $P_o = \Phi_o A_o$ is the incident power in the laser beam.

The detector is endowed with circular aperture A_d, and conical angle θ_d; typically, $A_d \lesssim \pi$ cm^2, and $\theta_d \approx 4° = .067$ radians. The direct beam flux into the detector is thus

$$\Phi(D) = \Phi_o(A_o/A(D))\exp - \gamma D. \qquad (2.2\text{-}6)$$

Now, note that, in the absence of the cloud, the direct beam flux into the detector is

$$\Phi^o(D) = \Phi_o(A_o/A(D)), \qquad (2.2\text{-}7)$$

so that

$$I_{direct} \equiv \Phi(D)/\Phi^o(D) = \exp-\gamma D. \qquad (2.2\text{-}8)$$

Now the multiple scattering contribution (diffuse flux) to the detector must be estimated. It will be necessary to calculate the number of incident beam photons per unit time that are scattered out of the beam during its travel. The number dn scattered between z, z+dz is given by

$$dn = (h\nu)^{-1}\,\Phi(z)\bar{C}_{sca}\,N\,A(z)dz = (h\nu)^{-1}\,\bar{\omega}_o\gamma\Phi_o A_o(\exp-\gamma z)dz, \tag{2.2-9}$$

where N = no. of scatterers per unit volume, $\bar{C}_{sca}$ = (average) total scattering cross-section per particle, $\bar{\omega}_o \equiv \bar{C}_{sca}/\bar{C}_{ext}$ = single scattering albedo, $\bar{C}_{ext}$ = (average) extinction cross-section per particle, $\gamma = N\bar{C}_{ext}$, $h\nu$ = energy of photon. Therefore, the total number of incident beam photons per unit time that are scattered out of the beam across the whole cloud is

$$n = \int_{z=o}^{L} dn = (h\nu)^{-1}\,\bar{\omega}_o\Phi_o A_o(1 - e^{-\gamma L}). \tag{2.2-10}$$

The diffuse power into the detector is proportional to this number.

Now, imagine that an infinite incident beam, with flux Φ_o, is normally incident on the same medium, with the same detector positioning and orientation. Then it is reasonable to assert that only those incident beam photons that are scattered out of a cylindrical volume of optical radius unity (actual radius γ^{-1}) centered around the symmetry axis (where the detector is situated) will contribute noticeably to the diffuse flux into the detector. Therefore, the number of such photons per unit time, n_∞, is

$$n_\infty = (h\nu)^{-1}\,\bar{\omega}_o\,\Phi_o(\pi/\gamma^2)(1 - e^{-\gamma L}). \tag{2.2-11}$$

The diffuse power into the detector is roughly proportional to this number.

Furthermore, suppose that the diffuse flux into the detector, $\Phi_\infty(D)$ has been calculated accurately for this infinite beam case. Then, for the corresponding finite beam case, the diffuse flux into the detector, $\Phi_d(D)$, should be given approximately by

$$\Phi_d(D) = (n/n_\infty)\,\Phi_\infty(D) = (\gamma R_o)^2\,T^\infty_{diff}\,\Phi_o\,, \tag{2.2-12}$$

where $\Phi_\infty(D) \equiv T^\infty_{diff}\,\Phi_o$ defines T^∞_{diff}, the infinite beam diffuse

transmission into the detector. Then, the total transmission, T, for the finite beam case is given approximately by

$$T \equiv \frac{\Phi(D) + \Phi_d(D)}{\Phi^o(D)} \approx \exp - \gamma D + (\gamma R_o)^2 \frac{T^{\infty}_{diff}\ \Phi_o}{\Phi_o(A_o/A(D))} , \qquad (2.2\text{-}13)$$

or

$$T = \exp-\gamma D + \pi^{-1}(\gamma R(D))^2\ T^{\infty}_{diff} . \qquad (2.2\text{-}14)$$

According to the ranges of numerical values determined above, $R(D) = R_o + D\theta_s < 10^{-3}m + (10^3 m)(6x10^{-3}) = 6m$, and $\gamma < 10^{-1}\ m^{-1}$, so $(\gamma R(D))^2/\pi \lesssim 0.1$. In most applications, more likely values would be $D \approx 100m$, $\gamma = 10^{-2}\ m^{-1}$, $\theta_s \approx 10^{-3}$, so $R(D) \approx 0.1$ m, $\gamma R(D) = 10^{-3}$, $(\gamma R(D))^2/\pi \lesssim 10^{-6}$. Thus it may be concluded that the diffuse part of the transmission for the finite beam case is usually much less than one-tenth of the diffuse part for the infinite beam case.

Since T^{∞}_{diff} is almost always smaller than T_{direct} for small-angle detectors, up to large optical depths, the diffuse transmission is therefore negligible in most cases of interest, and the total finite beam transmission is insignificantly different from the Bouguer law $T_{direct} = \exp - \gamma D$, even for large D (at least $\gamma D \approx 20$).

2.2.5 Searchlight Beam Scattering:

Consider the finite beam scattering problem illustrated in Fig. 2.2.2. The detector is located at coordinates (x,o,z), and receives radiation at angles (ϕ=0,θ).

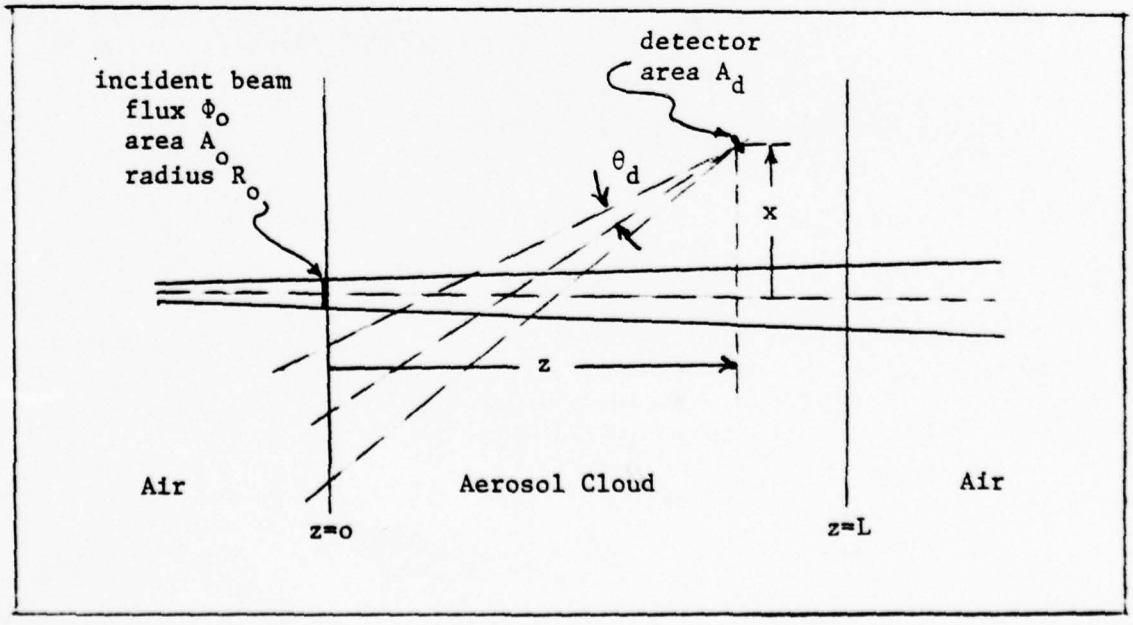

Figure 2.2.2 Finite Beam Scattering Geometry.

The first-order scattered intensity $I^{(1)}(x,o,z,\theta,o)$ at the detector is fairly easy to calculate from equation (2.2-5), given a simple form of incident beam. For this first order scattering, the incident beam spread is obviously unimportant, so it is convenient to choose the following solution of Eq. (2.2-5),

$$I_{in}(x,y,z,\mu,\phi) = \Phi_o \frac{\delta(\mu-1)}{2\pi} \Theta(R_o-r)e^{-\gamma z}, \qquad (2.2\text{-}15)$$

where $\mu = \cos\theta$, $r = (x^2+y^2)^{1/2}$, Θ is the unit step function, and (R_o, Φ_o) are the beam (radius, flux) at entry. Then, from Eq. (2.2-5) for $\tan^{-1}(x/z) \leq \theta \leq \pi/2$,

$$I^{(1)}(x,o,z,\mu,o) = \frac{p(\mu)}{4\pi} \Phi_o \gamma \int_o^{z/\mu} e^{-\gamma\ell} e^{-\gamma(z-\ell\mu)} \Theta[R_o-|x-\ell \sin\theta|]d\ell. \qquad (2.2\text{-}16)$$

Now, the step function is zero unless $(x-R_o)/\sin\theta \leq \ell \leq (x+R_o)/\sin\theta$, so

$$I^{(1)}(x,o,z,\mu,o) \approx \frac{\gamma R_o \Phi_o p(\mu)}{4\pi \sin\theta} \exp(-\gamma z-\gamma x(1-\mu)/\sin\theta), \qquad (2.2\text{-}17)$$

valid for $\gamma R_o << 1$, which is almost always true for a laser beam incident on a physical aerosol.

Now, from Eq. (2.2-3) the corresponding infinite incident beam is

$$I^{\infty}_{in}(z,\mu) = (2\pi)^{-1} \Phi_o \delta(\mu-1)\exp(-\gamma z). \qquad (2.2\text{-}18)$$

Then, from Eq. (5), the first order intensity is

$$I^{(1)}_{\infty}(z,\mu) = (4\pi)^{-1} \Phi_o p(\mu) [\exp(-\gamma z) - \exp(-\gamma z/\mu)]/(1-\mu), \qquad (2.2\text{-}19)$$

valid for $\mu \geq 0$.

The first order flux into the detector is equal to the first order intensity times the detector solid angle, $\pi\theta_d^2$, for $\theta_d << 1$. Therefore, the ratio of the finite beam to the infinite beam first order fluxes is given by the ratio of Eq. (2.2-17) to Eq. (2.2-19)

$$\frac{\Phi^{(1)}}{\Phi^{(1)}_{\infty}} = \frac{\gamma R_o(1-\mu)}{\sin\theta} \cdot \frac{\exp(-\gamma x(1-\mu)/\sin\theta)}{1-\exp(-\gamma z(1-\mu)/\mu)}, \qquad (2.2\text{-}20)$$

valid for $\tan^{-1}(x/z) \leq \theta \leq \pi/2$. For estimation purposes, consider $\mu = 0$; then

$$\Phi^{(1)}/\Phi_{\infty}^{(1)} = \gamma R_o \exp(-\gamma x). \qquad (2.2\text{-}21)$$

Now, the ratio of the finite to infinite beam multiply scattered fluxes into the detector should be similar to the diffuse flux ratio in the transmission case, because these multiply scattered fluxes are determined primarily by the number of scattered incident beam photons in each case. However, the relevant scattering volume that contributes appreciably to the multiply scattered flux in the infinite beam case is now a cylinder of radius γ^{-1} centered at the off-axis detector position. Therefore, photons scattered from the incident finite beam must travel an extra distance x, on the average, to get to the detector, compared to photons scattered from the corresponding infinite incident beam. So when the detector is located a distance x from the finite beam axis, the ratio of finite to infinite beam multiply scattered fluxes should be approximately

$$\Phi^{(mult)}/\Phi_{\infty}^{(mult)} = (n/n_{\infty})\exp-\gamma x, \qquad (2.2\text{-}22)$$

where (n,n_{∞}) are the relevant numbers of photons per unit time scattered out of the incident beams, given by Eqs. (2.2-10) and (2.2-11). So it is estimated that the total flux scattered from a finite beam into a detector located and oriented as in Fig. 2.2.2 is

$$\Phi^{(1)} + \Phi^{(mult)} \approx (e^{-\gamma x})\gamma R_o \, \Phi_{\infty}^{(1)}[1+\gamma R_o(\Phi_{\infty}^{(mult)}/\Phi_{\infty}^{(1)})]. \qquad (2.2\text{-}23)$$

Since $e^{-\gamma x} \gamma R_o \, \Phi_{\infty}^{(1)}$ is supposed to equal $\Phi^{(1)}$, an approximate expression for the total diffuse flux into the detector in the finite beam case is

$$\Phi = \Phi^{(1)}[1+\gamma R_o(\Phi_{\infty}^{(mult)}/\Phi_{\infty}^{(1)})], \qquad (2.2\text{-}24)$$

which means that multiple scattering is less important in the finite beam case than in the infinite beam case, as long as $\gamma R_o < 1$. If γR_o is very small, the higher order scattered radiation into an off-axis detector whose cone of view contains a segment of the incident beam may be neglected, unless the ratio $\Phi_{\infty}^{(mult)}/\Phi_{\infty}^{(1)}$ of the infinite beam fluxes is correspondingly large. But this ratio is commonly of order unity or smaller.

2.2.6 Summary: The foregoing analysis indicates that, for a narrow incident

beam, multiple scattering effects are considerably less important than for a very broad incident beam, in most cases. For a narrow incident beam, the multiple scattering correction to the transmission given by the Bouguer law is almost always negligible. The multiple scattering correction to the single scattering prediction of the flux into an off-axis detector is also negligible in many cases of interest. The magnitude of the multiple scattering corrections can be estimated easily from Eqs. (14),(24) once the infinite beam results are known. These latter results can be obtained rapidly by analytic numerical techniques for many realistic model aerosol clouds.

2.2.7 Discussion:

It is important to point out that the direct plus first order diffuse transmission into an on-axis detector aligned with a narrow incident beam represents undistorted transmission, while (almost) all higher order transmission contributes to distortion of a modulated incident beam. This follows because multiply scattered photons travel a longer path. Similarly, the multiply scattered flux into an off-axis detector represents a distortion of a signal. For example, suppose the incident beam to be pulsed, and a reflecting target to be in the cloud, on the beam axis. Then, photons single scattered from the aerosol particles into the off-axis detector arrive at the detector coincidentally with photons scattered by the target only; but multiply scattered photons that enter the medium at the same time arrive later. Now, the detector receives singly scattered photons as long as its cone of view intersects the beam, but it receives photons scattered just by the target only if its cone of view also intersects the target. Therefore, for such a scenario, for cases where multiply scattered photons contribute negligibly, the signal-to-noise ratio (ratio of flux from target to flux from aerosol single scattering into the off-axis detector) should always increase noticeably as the detector orients toward the target, unless the target itself is a strong absorber and/or a weak emitter at the wavelengths used.

It is also worth pointing out that the approximate physical arguments given here can probably be refined to compensate for idiosyncracies of particular model aerosols. In particular, a sharply forward peaked phase function strongly augments the infinite beam total transmission, and reduces the scattering, but does not much affect the arguments given above that relate the finite to the infinite beam fluxes. Such considerations remain to be studied in future work.

Chapter 3

UPDATES IN PROGRAM ATRANX

Program ATRANX, an NMSU/ASL atmospheric transmittance prediction code developed under previous contracts, has been extended and improved as a small part of the current research program.

1. The Van Vleck-Weisskopf line profile has been added (case IPRO = 5) to provide a line shape which is more appropriate to millimeter wavelengths than those originally coded into ATRANX.

2. The aerosol extinction subroutines have been modified to include the changes in sizes of hygroscopic aerosol particles which occurs with changes in relative humidity. The size adjustment formula used is that of J. Fitzgerald (Naval Research Laboratory), and has the form:

$$\frac{r}{r_o} = \left[1 + \frac{0.061}{\gamma(1-f)}\right]^{1/3} ,$$

in which

f is the fractional humidity ($0.2 \leq f \leq 0.97$),

r_o is a particle radius for $f = 0$,

and γ is Fitzgerald's "air mass characteristic".

The quantity f is calculated within the programs from data on water vapor densities. The parameter, γ, however, must be supplied by program users. Its value is entered in the position (and with the same format) that was used for the quantity EMM in previous ATRAN versions. EMM is no longer an input parameter.*

Because the same accretion of liquid water which causes size increases also brings about changes in indices of refraction, it has also been necessary to add information about the optical constants of liquid water. Rather than using additional input data cards, a new subroutine (WATER) has been added to provide table look-ups for the wavelength range of 0.2 to 200 μm. The optical parameters m (real part of index of refraction) and k (imaginary part) are adjusted according to:

* EMM is taken to be 1.0 in the latest version of ATRAN.

$$m = m_w + (m_a - m_w)(r/r_o)^3,$$

and,

$$k = k_w + (k_a - k_w)(r/r_o)^3.$$

In the two preceding expressions, the subscript "w" represents pure liquid water, and "a" represents the dry aerosol.

The above changes require the substitution of new routines (GASUB4, NMSME9, NMSA9, NMSB9 and NMSC9) for some older routines (GASUB3, NMSMIE, NMSA, NMSB, NMSC), as well as the addition of subroutine WATER.

Suggested general choices for the parameter γ (called GAMMAF in the program listings) are given on "comment cards" in the source deck for subroutine NMSB9.

3. Floyd Herbert's [28] Galatry profile codes (XTV, XTS, XKGSER, XKASSY, VOIGTX and XKCFRA) have been substituted for NMSU routines LINE01 and LINE02 used in generalized Voigt profile runs (IPRO = 2).

4. The tape reading routine TTCOR8 has been replaced by routine TTCORE, which contains a new "compression option" ICMPR = 2. The new option permits line strength comparisons before deletion of molecular types.

5. Some portions of the main program and subroutine HTRN10 have been restructured to provide somewhat faster execution. The main program (ATRAN10) has been replaced by ATRAN14, and HTRN10 by HTRN13.

6. The entire code has been edited to improve readability by ordering statement labels and formats consecutively within each routine. Complete listings and a source deck for the revised code will be provided to ASL.

References

1. A Miller, R.C. Shirkey, E. Gemoets and G.H. Goedecke: Investigations on the Prediction of Infrared Transmission and Emission by Clear and Aerosol Laden Atmospheres, NMSU Department of Physics, January 1978; Final Report for Contract DAEA18-77-C-00003.

2. H.C. van de Hulst, Light Scattering by Small Particles, John Wiley & Sons, Inc., New York, 1957.

3. D. Deirmendjian, Electromagnetic Scattering on Spherical Polydispersions, American Elsevier Publishing Co., Inc., New York, 1969.

4. C.M. Chu, and S.W. Churchill, Representation of the Angular Distribution of Radiation Scattered by a Spherical Particle, J.O.S.A., 45, 958 (1955).

5. J. Mason, and G.B. Hoidale, Visibility as an Estimator of Infrared Transmittance, ECOM report 5598, 1976.

6. G. Hanel, The Properties of Atmospheric Aerosol Particles as Functions of the Relative Humidity at Thermodynamic Equilibrium with the Surrounding Moist Air, in Advances in Geophysics, eds. H.E. Landsberg and J. van Mieghem, Academic Press, New York, 1976.

7. P. Chylek, Extinction and Liquid Water Content of Fogs and Clouds, J. Atmos. Science, 35, 296 (1978).

8. W.M. Irvine, Multiple Scattering by Large Particles, Ap. J., 142, 1563 (1965).

9. M.C. Wang, and E. Guth, On the Theory of Multiple Scattering, Particularly of Charged Particles, Phys. Rev., 84, 1092 (1951).

10. S. Goudsmit, and J.L. Saunderson, Multiple Scattering of Electrons, Phys. Rev. 57, 24 (1940).

11. L.M. Romanova, The Solution of the Radiation-Transfer Equation for the Case when the Indicatrix of Scattering Greatly Differs from the Spherical One. I., Opt. Spek., 13, 429 (Eng. Trans. 238), (1962).

12. W.M. Irvine, in The Atmospheres of Venus and Mars, ed. J.C. Brandt and M.B. McElroy (New York: Gordon and Breach), 1968a.

13. L.M. Romanova, Solution of the Radiative Transfer Equation for the Case of a Highly Nonspherical Scattering Index. II., 13, 819 (Eng. Trans. 463), (1962a).

14. L.M. Romanova, Radiation Field in Plane Layers of a Turbid Medium with Highly Anisotropic Scattering, Opt. Spek., 14, 262 (Eng. Trans. 135), (1963).

15. J.E. Hansen, Exact and Approximate Solutions for Multiple Scattering by Cloudy and Hazy Planetary Atmospheres, J. Atmos. Sci., 26, 478 (1969).

16. W.M. Irvine, Multiple Scattering in Planetary Atmospheres, Icarus, 25, 175 (1975).

17. H.C. van de Hulst, Asymptotic Fitting, A Method for Solving Anisotropic Transfer Problems in Thick Layers, J. Computational Phys., 3, 291 (1968).

18. H.C. van de Hulst, in Planetary Atmospheres, ed. C. Sagan, T.C. Owen and H.J. Smith (Springer-Verlag: New York), 1971.

19. H.C. van de Hulst, and K. Grossman, in The Atmospheres of Venus and Mars, ed. J.C. Brandt and M.B. McElroy (New York: Gordon & Breach), 1968.

20. J.E. Hansen, Radiative Transfer by Doubling Very Thin Layers, Astrophys. J. 155, 565-573 (1969).

21. P.E. Mudgett, and L.W. Richards, Multiple Scattering Calculations for Technology, Appl. Opt. 10, 1485-1502 (1971).

22. B.M. Herman, and S.R. Brownling, "A Numerical Solution to the Equation of Radiative Transfer, J. Atmos. Sci. 22, 559-566 (1965).

23. G.B. Rybicki, The Searchlight Problem with Isotropic Scattering, J. Quant. Spectros. Radiat. Transfer, 11, 827-849 (1971).

24. P. Beckett, P.J. Foster, V. Hutson, and R.L. Moss, Radiative transfer for a Cylindrical Beam Scattered Isotropically, J. Quant. Spectros. Radiat. Transfer, 14, 1115-1125 (1974).

25. J.A. Weinman, Effects of Multiple Scattering on Light Pulses Reflected by Turbid Atmospheres, J. Atmos. Sci. 33, 1763-1771 (1976).

26. C. Anderson, and E.V. Browell, First- and Second-Order Backscattering from Clouds Illuminated by Finite Beams, Appl. Optics 11, 1345-1351 (1972).

27. V.E. Zuev, M.V. Kabonov, and B.A. Savelev, Propagation of Laser Beams in Scattering Media, Appl. Optics 8, 137-141 (1969).

28. F. Herbert, J. Quant. Spectrosc. Radiat. Transfer 14, 943 (1974).

29. G. Mie, Ann. Phys. 25 (1908).

30. P. Davis and P. Rabinowitz, J. Res. Natl, Bur. Stds. 56, 35 (1956).

31. W.M Irvine and J.B. Pollack, Icarus 8, 324 (1968).

32. S. Chandresekar, Radiative Transfer, Dover Publications, New York, 1960.

Appendix A

PROGRAMS AGAUS9 AND AGAUS10

A.1 MIE THEORY*

Mie theory [29] predicts the scattering by and the absorption in an isolated, discrete, homogeneous, isotropic sphere of diameter D with a known complex refractive index $n = m-ik$ relative to the surrounding medium and illuminated by monochromatic radiant energy with wavelength λ in the surrounding medium. The theory is given in detail in standard texts and need not be repeated here. Instead, those elements of theory needed for an understanding of the numerical algorithms used in the ASL model are included.

Scatterers attenuate beams of radiant energy by scattering some of the energy into directions other than the incident or forward direction and by absorbing some of the incident energy within the body of the particle. The combined effect of pure scattering by the particle and true absorption within the particle is termed extinction. The amount of extinction, scattering, and absorption by a single particle is given in terms of corresponding equivalent blocking areas or cross sections, C_{ext}, C_{sca}, and C_{abs}, respectively. These cross sections depend only on the refractive index of the particle $n = m-ik$ and the size parameter $\alpha = 2\pi r/\lambda$, where r is the particle radius, and λ is the wavelength.

The transmission, T, of a cloud of particles of geometric depth, d, and number density, N, is given by

$$T = e^{-\tau}, \tag{A-1}$$

with the optical depth, τ, given by

$$\tau = K_{ext} \cdot d, \tag{A-2}$$

where

$$K_{ext} = NC_{ext}. \tag{A-3}$$

The balance between loss by scattering and loss by absorption is frequently characterized by the albedo of single scattering $\tilde{\omega}_o$, given by

*This section is partially based on material taken from ECOM report ECOM-5558 by R.B. Gomez, C. Petracca, C. Querfeld and G.B. Hoidale, March 1975.

$$\tilde{\omega}_o = \frac{C_{sca}}{C_{sca} + C_{abs}} = \frac{C_{sca}}{C_{ext}} . \qquad (A-4)$$

A scatterer with $\tilde{\omega}_o = 1$ has no absorption and is termed a conservative scatterer. The albedo $\tilde{\omega}_o$ gives the probability that a photon encountering the scatterer will be scattered into some direction including the incident direction.

Although the extinction by a cloud of particles is correctly given by Eqs. (A-1) and (A-2), two implicit assumptions may lead to improper use of the equations. The optical depth τ in Eq. (A-2) does not include losses caused by absorption in the medium surrounding the particles.

This assumption obviously breaks down at wavelengths for which atmospheric gases absorb appreciably. The second assumption is that scattered photons never return to the incident direction, i.e., that there is no multiple scattering. This effect becomes increasingly important as optical depths exceed $\tau = 0.1$.

A final caution should be noted in regard to absorption within the particle. Although absorption within the particle is correctly determined by the wavelength-dependent imaginary part k of the refractive index m, the explicit mechanism which causes the absorption is usually not specified. Usually the absorption is joule heating, and it is sometimes necessary to account for the isotropic black body radiation emitted by the scatterer when its temperature rises above that of its surroundings. There may also be circumstances when quantum transitions occur in the scatterer followed by emission at or near the same wavelengths. It is incumbent on the user of the numerical algorithms presented here to properly include these effects since they are not automatically accounted for in these algorithms.

All scattering properties of spheres are computed from m and k, and through the use of the induced electric and magnetic multipole moments of the sphere a_n and b_n, respectively. The moments are given by†

$$a_n = \frac{\Psi_n'(n\alpha)\ \Psi_n(\alpha) - n\ \Psi_n(n\alpha)\ \Psi_n'(\alpha)}{\Psi_n'(n\alpha)\ \xi_n(\alpha) - n\ \Psi_n(n\alpha)\ \xi_n'(\alpha)} , \qquad (A-5)$$

and

$$b_n = \frac{n\ \Psi_n'(n\alpha)\ \Psi_n(\alpha) - \Psi_n(n\alpha)\ \Psi_n'(\alpha)}{n\ \Psi_n'(n\alpha)\ \xi_n(\alpha) - \Psi_n(n\alpha)\ \xi_n'(\alpha)} . \qquad (A-6)$$

The prime denotes differentiation with respect to the argument. The $\Psi_n(z)$ and $\xi_n(z)$ functions are Ricatti-Bessel functions of the first and third kind, respectively, and are related to spherical Bessel functions $j_n(z)$ and $n_n(z)$ by

†Note that n is used as a subscript, an integer index and a complex index of refraction when it is not a subscript.

$$\Psi_n(z) = z\, j_n(z), \tag{A-7}$$

and

$$\xi_n(z) = zj_n(z) - i\, zn_n(z) = \Psi_n(z) + i\chi_n(z), \tag{A-8}$$

where

$$j_n(z) = \left(\frac{\pi}{2z}\right)^{1/2} J_{n+1/2}(z), \tag{A-9}$$

and

$$n_n(z) = \left(\frac{\pi}{2z}\right)^{1/2} N_{n+1/2}(z)\ . \tag{A-10}$$

The function $J_{n+1/2}(z)$ is the half integral order Bessel function; the function $N_{n+1/2}(z)$ is the half integral order Neuman function.

The extinction cross section is computed from

$$C_{ext} = \frac{\lambda^2}{2\pi} \sum_{n=1}^{\infty} (2n+1)\ \mathrm{Re}\ (a_n + b_n), \tag{A-11}$$

and the scattering cross section from

$$C_{sca} = \frac{\lambda^2}{2\pi} \sum_{n=1}^{\infty} (2n+1)\ [|a_n|^2 + |b_n|^2]\ . \tag{A-12}$$

The various cross sections are the basic quantities used in scattering problems, but they are not the quantities usually computed directly from Mie algorithms. Instead, it is more convenient to compute dimensionless efficiency factors Q_{ext} and Q_{sca}, which depend on n, k, and α, and which are multiplied by the geometrical sphere cross section to obtain the true cross section $C_i = \pi r^2 Q_i$. Thus,

$$Q_{ext} = \frac{2}{\alpha^2} \sum_{n=1}^{\infty} (2n+1)\ \mathrm{Re}(a_n + b_n), \tag{A-13}$$

and

$$Q_{sca} = \frac{2}{\alpha^2} \sum_{n=1}^{\infty} (2n+1)[|a_n|^2 + |b_n|^2]\ . \tag{A-14}$$

Although the cross sections account for the energy removed from the forward beam, they do not give any information about where the scattered photons go. This information is contained in scattering amplitudes and intensity factors which relate the flux density scattered through an angle θ relative to the incident flux density. There are two amplitudes, $S_1(\theta)$ and $S_2(\theta)$, and intensity factors $i_1(\theta)$ and $i_2(\theta)$,

which correspond to light respectively polarized perpendicular and parallel to the plane of scattering defined by the direction of incidence and the direction of scattering.

The intensity factors are related to the scattering amplitudes by

$$i_1(\theta) = |S_1(\theta)|^2 , \tag{A-15}$$

and

$$i_2(\theta) = |S_2(\theta)|^2 . \tag{A-16}$$

The amplitudes come from the multipole moments through

$$S_1(\theta) = \sum_{n=1}^{\infty} \frac{2n+1}{n(n+1)} [a_n \pi_n(\theta) + b_n \tau_n(\theta)], \tag{A-17}$$

and

$$S_2(\theta) = \sum_{n=1}^{\infty} \frac{2n+1}{n(n+1)} [b_n \pi_n(\theta) + a_n \tau_n(\theta)], \tag{A-18}$$

and angular factors $\pi_n(\theta)$ and $\tau_n(\theta)$ defined in terms of associated Legendre functions:

$$\pi_n(\theta) = P_n^1(\cos\theta)/\sin\theta; \tag{A-19}$$

$$\tau_n(\theta) = \frac{dP_n^1(\cos\theta)}{d\theta} . \tag{A-20}$$

The amplitudes have relative phase $\delta = \arg S_1 - \arg S_2$.

Alternative expressions frequently used are

$$\pi_n(\theta) = \frac{dP_n(\cos\theta)}{d(\cos\theta)} , \tag{A-21}$$

and

$$\pi_n(\theta) = \cos\theta \cdot \pi_n(\theta) - \sin^2\theta \cdot \frac{d\pi_n(\theta)}{d(\cos\theta)} , \tag{A-22}$$

where

$$P_n(\cos\theta) = \frac{1}{2^n n!} \frac{d^n}{d\cos^n\theta} (\cos^2\theta - 1)^n . \tag{A-23}$$

These functions satisfy the following recurrence relations:

$$\pi_n(\theta) = \cos\theta \frac{(2n-1)}{(n-1)} \pi_{n-1}(\theta) - \frac{n}{n-1} \pi_{n-2}(\theta), \quad \text{(A-24)}$$

and

$$\tau_n(\theta) = \cos\theta\,[\pi_n(\theta)-\pi_{n-2}(\theta)]-(2n-1)\sin^2\theta\pi_{n-1}(\theta)+\tau_{n-2}(\theta). \quad \text{(A-25)}$$

The scattering cross section measures the ability of a particle to scatter light, and it is to be expected that C_{sca} is obtained from an integral over the scattering intensity factors. Equation (A-12) follows from

$$C_{sca} = \frac{\lambda^2}{4\pi} \int_{-1}^{1} (i_1(\theta) + i_2(\theta))\, d\cos\theta. \quad \text{(A-26)}$$

Although the intensity factors themselves may be used in scattering calculations, they are primarily suited for computing flux densities, and it is frequently more convenient to measure and compute scattered light in terms of radiances. Radiances do not have the $1/r^2$ dependence, and it is therefore unnecessary to know the distance from the scatterer to the detector if the detector field of view is small and is filled by the scattering cloud. The phase function $p(\theta)$ gives a radiance I scattered into the θ direction in terms of the radiance I_o incident on the particle.

The phase function is dimensionless and is defined here as

$$p(\theta) = \frac{\lambda^2}{2\pi C_{ext}} [i_1(\theta) + i_2(\theta)] . \quad \text{(A-27)}$$

The normalized phase function $p(\theta)d\Omega/4\pi$ gives the probability of a photon being scattered through an angle θ into an element of solid angle $d\Omega = d\phi d\cos\theta$. The integral of the normalized phase function is the single scattering albedo $\tilde{\omega}_o$, which gives the probability that the photon is scattered:

$$\tilde{\omega}_o = \frac{1}{4\pi} \int_0^{2\pi} \int_{-1}^{1} p(\theta) d\phi d\cos\theta = \frac{\lambda^2}{4\pi C_{ext}} \int_{-1}^{1} [i_1(\theta)+i_2(\theta)]d\cos\theta \quad \text{(A-28)}$$

or

$$\tilde{\omega}_o = C_{sca}/C_{ext} . \quad \text{(A-29)}$$

The phase function contains a sum over the polarization states implicit in the i_1 and i_2 intensity factors, and is thus unsuitable for describing the polarization of the scattered light.

The phase functions can also be represented by a Legendre series:

$$p(\theta) = \sum_{\ell=o}^{n-1} \tilde{\omega}_\ell P_\ell(\cos\theta), \tag{A-30}$$

where the Legendre expansion coefficients $\tilde{\omega}_\ell$ are given by

$$\tilde{\omega}_\ell = \frac{(2\ell+1)}{2} \int_{-1}^{1} p(\theta)\ P_\ell(\cos\theta)\ d(\cos\theta) \tag{A-31}$$

and $P_\ell(\cos\theta)$ are the usual Legendre polynomials.

A.2 DETAILED DESCRIPTION OF PROGRAM AGAUS9

Introduction

Program AGAUS9 is designed to calculate various scattering functions like phase functions (Mie theory), scattering fractions (ASLSOM code), extinction cross-section, attenuation coefficient, etc., for diverse natural and artifically created polydisperse atmospheric aerosols. The program consists of subroutines ANGLE, GUSET, AG9PT1, AG9PT2, AG9PT3, AG9PRT, MIEGS, GAUS, VERFY, and WATER. The organization and operation of these subroutines is controlled by the MAIN program AGAUS9.

A.2.1 General Description of the Operation of AGAUS9

The first input card contains the parameters IDSTP, NRADI, IDUMMY, NWAVE, NINDX, MQRTE, NCRDS, NUNIT, IT, IANG, and ISCAT. The various modes of operations of AGAUS9 that are possible, are controlled by some of these parameters. If IANG = 0, the subroutine GUSET is called to choose 'IT' scattering angles between 0° and 180° for use in numerical integrations using Gauss-Legendre (GL) quadrature. GUSET returns two arrays of numbers to MAIN. The array C(I) corresponds to the cosine of scattering angles and the array H(I) corresponds to what are called quadrature weights. Using the array C(I), MAIN constructs Legendre polynomials, PL which will be used later.

If IANG=1, all the calculations of the previous paragraph are skipped. Instead, subroutine ANGLE is called. It also returns arrays C(I) and H(I) to MAIN. In this case, however, H(I) corresponds to 'IT' equally spaced angles between 0° and 180°, and C(I) corresponds to the cosine of these angles.

Next, subroutine AG9PT1 is called. One or more input parameters are read at this point depending on the value of IDSTP. AG9PT1 calculates and returns two arrays R(I) and F(I) which describe the normalized size distribution, and VOL, the average 'dry' volume per particle. The array R(I) contains values of 'NRADI' particle radii, and the array F(I) contains values of the distribution for the corresponding R(I). For IDSTP=3, or 7,8,9,10,11,12 AG9PT1 also returns DENS, the particle number density (per cm^3). To find what is done for other distribution types see the definition of DENS below.

Before entering, in MAIN, the do-loop indexed by NWAVE, the parameters WAVE, DWAVE, RELHUM, DENSH, and TEMP are read. This do-loop allows computations at several wavelengths during a single run. Additional looping options are available, however. For example, by assigning DWAVE any value less than 10^{-4}, one could use the same do-loop to handle several values of relative humidity (RELHUM) in a run.

A switch parameter LLLL is assigned a value 0 or 1, in a manner dependent upon the value of IDSTP and DENSH. Later, through the assigned value of LLLL the value of particle number density is chosen from three different values for it that may be available. (See the discussion of the parameter "DENS", below).

In subroutine AG9PT2 optical and physical data (index of refraction and mass density) for the aerosol material are read. For the user's convenience, subroutine WATER has been added to provide the relevant data for water (see subroutine WATER). If RELHUM and growth factor (EMUA) are non-zero, AG9PT2 takes into account the particle growth and the change in density and indices of refraction of the aerosol material due to the absorption of water.

In AG9PT2, subroutine MIEGX is called for each 'adjusted' radius. MIEGX returns to AG9PT2 the values of extinction, scattering and back-scattering efficiency factors, and the average intensity factors $(I_1+i_2)/2$, for 'IT' scattering angles chosen earlier. These scattering functions are weighted and integrated over the size distribution.

If the aerosol is a mixture of components having different physical and/or optical properties, the above calculation is repeated for each component and various functions are summed over NINDX (the number of components). In the end AG9PT2 returns to MAIN, for each wavelength, the average (sum/total particle number density) extinction, scattering, and back-scattering cross-sections (*CTSUM*, *CSSUM*, CRSUM), the average intensities (P(J)), and the total mass concentration (TMASS, in gm/cc, which includes the mass of any liquid water absorbed by hygroscopic aerosols).

Next, subroutine AG9PT3 is called. It uses the numbers received from AG9PT2 and returns to MAIN the total extinction, scattering, and back-scattering coefficients, scattering fractions and phase functions. AG9PT3 also calculates the albedo for single scattering "ALBDO" = $\tilde{\omega}_o = C_{sca}/C_{ext}$. It prints out all the single wavelength results. Later in AG9PT3, if IANG = 0, subroutine GAUS is called. Using the quadrature weights H(I) calculated earlier, GAUS generates the Legendre expansion coefficients $\tilde{\omega}_\ell$ for the phase functions, and places them in array OL(I). $\tilde{\omega}_\ell$'s are then used to reconstruct phase functions, PC(I) and the routine computes the rms (root mean square) deviation between the original phase functions and the reconstructed phase functions. See the section on subroutine GAUS for further details. If IANG = 1, the above calculation is skipped.

If NWAVE > 1, all the calculations of AG9PT2 and AG9PT3 are repeated (NWAVE-1) additional times. In MAIN, various scattering functions are summed and divided by NWAVE. Then, subroutine AG9PRT is called to print out all the averaged results. It also calls GAUS once more (if IANG = 0) to generate the coefficients $\tilde{\omega}_\ell$ for the averaged phase functions.

There are many other options available which the user will find mentioned in this report. One which is of importance relates to control parameter ISCAT. If ISCAT = 0, scattering fractions are printed;

if ISCAT = 1, they are punched (or written on NUNIT) as well as printed. If IANG = 0, scattering fractions are neither printed nor punched.

Explanation of Symbols used in AGAUS9 (MAIN)

SYMBOL	Explanation or Definition
AMAX	the largest Mie size found in the aerosol distribution.
CATTN	the average (sum/NWAVE) attenuation coefficient in square meters per milligram of aerosol material.
CRSUM	the back-scattering cross-section in sq. micrometers for each wavelength and integrated over size distribution. AG9PT3 returns 'coefficients'.
CSSUM	the scattering cross-section in sq. micrometers for each wavelength and integrated over size distribution. AG9PT3 returns 'coefficients'.
CTSUM	the extinction cross-section in sq. micrometers for each wavelength and integrated over size distribution. AG9PT3 returns 'coefficients'.
DENS	the particle number density (number per cubic centimeter). The value of DENS may be supplied by the user as an input parameter, DENSH. However, it will be ignored when IDSTP = 0 or greater than 6, because these distribution type carry pre-determined values of DENS. In the case of IDSTP = 1,2,4,5 the user supplied value of number density will be ignored only if it is less than 10^{-4}. In such cases DENS is calculated from mass density and concentration, and average volume per particle, and is represented by DENSC.
DENSH	the user-supplied particle number density; units are particles per cubic centimeter. See discussion of DENS (above).
DRYVOL	the average volume per particle of dry aerosol in cubic micrometers.
DWAVE	the wavelength increment in micrometers. See NWAVE.
ELWC	the liquid water content in gm/cm^3 (used only for cases IDSTP=6 and 12).
EMM	the refractive index of the surrounding medium, taken to be a vacuum in this program.
ENWAV	DFLOAT (NWAVE).

AD-A069 449 NEW MEXICO STATE UNIV LAS CRUCES DEPT OF PHYSICS F/G 4/1
STUDIES ON THE DEVELOPMENT OF ALGORITHMS FOR THE PREDICTION OF --ETC(U)
DEC 78 A MILLER, G H GOEDECKE, R C SHIRKEY DAAD07-78-C-0063
UNCLASSIFIED NMSU-PHYS-586-78-1 NL

2 OF 2
AD
A069449

END
DATE
FILMED
7-79
DDC

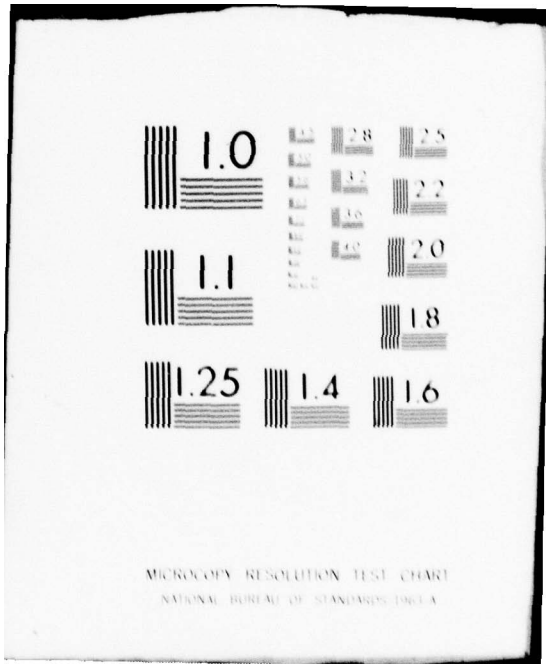
1.0
1.1
1.25
1.4
1.6
2.8
2.5
3.2
2.2
3.6
2.0
4.0
1.8
MICROCOPY RESOLUTION TEST CHART
NATIONAL BUREAU OF STANDARDS 1963-A

SYMBOL	Explanation or Definition
FSUM	the numerical result for the integral over the size distribution function with respect to radius; it is used to normalize the distribution function to one (equivalent) particle per cubic centimeter.
GNU	wave number in cm^{-1}.
IANG	= 0, for the computation of phase functions at 'IT' Gauss-Legendre quadrature angles. = 1, for the computation of phase functions and scattering fractions at 'IT' equally spaced angles between 0° and 180°.
IDSTP	identifies the type of aerosol size distribution to be used. It can only take values between 0 and 12. See AG9PT1 for more details.
IDUMMY	a spare input parameter.
ISCAT	= 0, for scattering fractions to be printed. = 1, for the scattering fractions to be printed as well as punched or written on NUNIT format.
IT	the order of Legendre expansion for phase functions when IANG = 0, or the number of equally spaced angles between 0° and 180° when IANG = 1.
KBAKT	the average (sum/NWAVE) back-scattering coefficient per km, integrated over the size distribution.
KEXTT	the average (sum/NWAVE) extinction coefficient per km, integrated over the size distribution.
KSCAT	the average (sum/NWAVE) scattering coefficient per km, integrated over the size distribution.
LLLL	a switching parameter used to control whether or not particle number density is to be calculated from DRYVOL and mass concentration.
LMAX	=3*IFIX (AMAX). Integer estimate of the optimal order for Gauss-Legendre quadrature; used only for diagnostic message print.
MCRTE	is not used in AGAUS9 (or AGAUS10).
MQRTE	= 12345, will cause subroutine AG9PT2 to print efficiency factors QT, QS, and QR, and the normalized distribution function for every value of radius used.
NCRDS	= 1, for punch (or write on NUNIT) of Legendre expansion coefficients of phase functions. = 2, for storing input and/or output data, to be used later in a program attached to AGAUS9, on a device identified by NUNIT.

SYMBOL	Explanation or Definition
NINDX	the number of aerosol components which will have different optical constants, mass density or mass concentration.
NRADI	the number of values of particle radius to be used in the calculations. (In effect, points on the radius vs size distribution function plot.)
NUNIT	defines the device on which output data may be stored in lieu of actual card punching; may be used to place nominal card output into data files on tape, etc. The default value (NUNIT=0) is 4 (card punch) for UNIVAC and 7 for IBM.
NWAVE	the number of wavelengths or relative humidity values to be treated in a given run. DWAVE has to be less than 10^{-4} for the latter.
OL(I)	the average Legendre expansion coefficients. OLT(I)/ENWAVE.
OLT(I)	the total Legendre expansion coefficients (summed over all values of 'WAVE').
OUT( )	an array used for storing some of the numbers to be printed later.
PI	= 3.1415926535898
PL(I,J)	the Legendre polynomials of order (I-1) and argument C(J). C(I) are cosines of the scattering angles.
PSUM(I)	the average phase functions integrated over the size distribution.
PSUMT(I)	the total phase functions integrated over size distribution and summed over wavelength.
QATTN	the attenuation coefficient in sq. meters per milligram of aerosol material for each wavelength.
R(NRADI)	the radius of the largest particle encountered.
RELHUM	the relative humidity in percent.
SCAT(I)	the scattering fractions as defined in ASL-SOM for each wavelength. 'IT' elements in the array.
SCATT(I)	the average (sum/NWAVE) scattering fractions (ASLSOM).
TEMP	the temperature of the atmosphere in degrees C.

SYMBOL	Explanation or Definition
TMASS	the total mass of aerosol in gm/cm^3 in the atmosphere.
VOL	the average volume per particle in cubic micrometers.
WAVE	the first wavelength, in micrometers, at which calculations are to be done.

AGAUS9 (MAIN program) - Simplified Flowchart

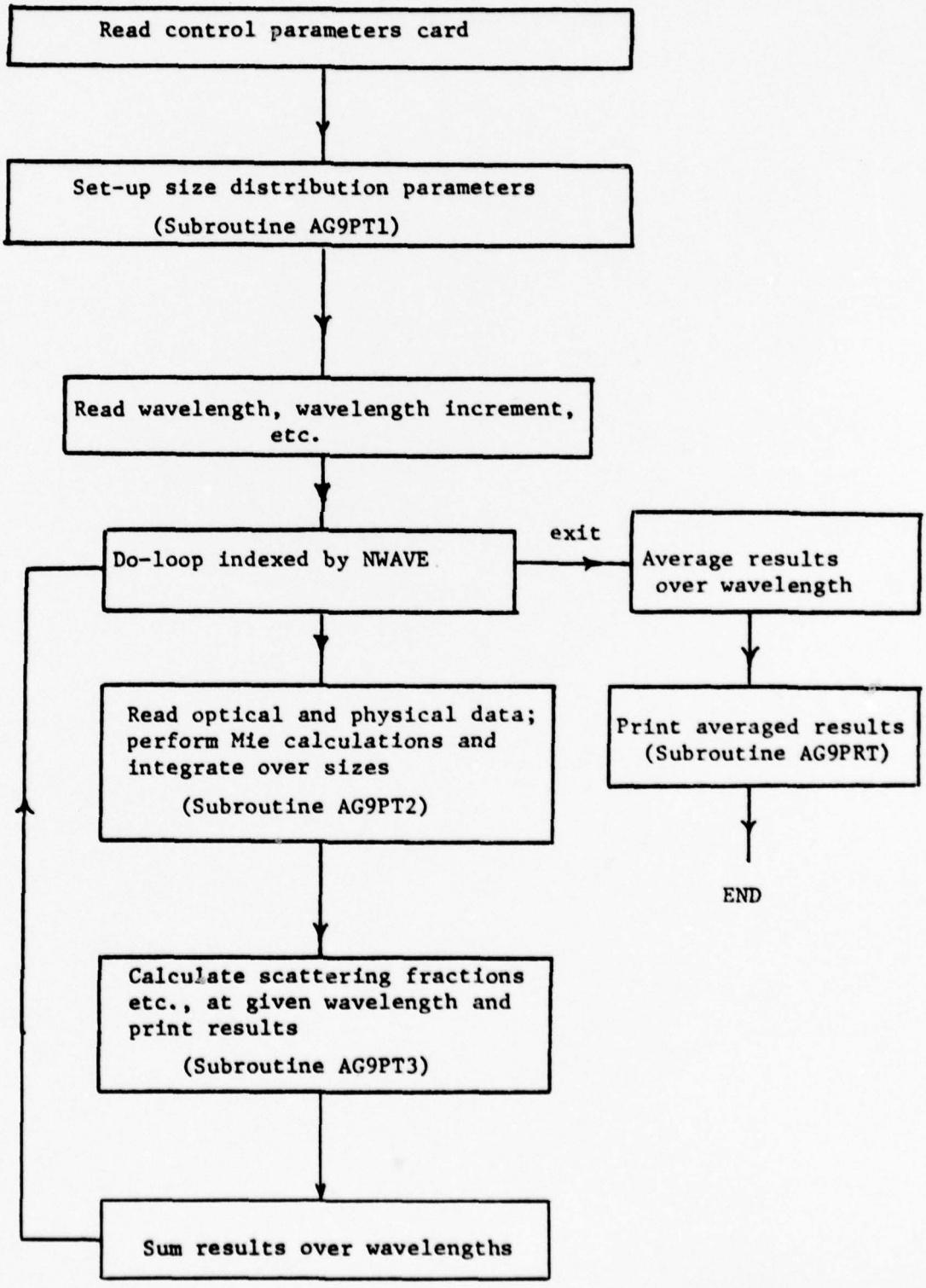

A.2.2 Subroutine Angle

Subroutine ANGLE is called when IANG = 1. It is used to compute the values of 'IT' equally spaced scattering angles between 0° and 180°. It places these angle values in the array, H(I). It also computes the cosines of those angles and places them in the array, C(I).

SYMBOLS	Explanation
C(I)	the array containing the cosines of scattering angles in the array H(I).
H(I)	the array containing 'IT' scattering angles (in degrees).
IT	is the number of scattering angles chosen between 0°and 180°.
PI	= 3.1415926535898
RAD	RADS*H(I); scattering angles in radians.
RADS	= PI/180.

A.2.3 Subroutine GUSET

Subroutine GUSET uses the Davis and Rabinowitz algorithm [30] to choose n values of $\cos\theta_{kn}$ $(k = 1,2,\ldots n)$ between the interval $-1 \leq \cos\theta \leq 1$ and the corresponding values of quadrature weights a_{kn}. The abcissas, $\cos\theta_{kn}$ are n zeros of Legendre polynomial $P_n(\cos\theta_{kn})$ while the weights a_{kn} are given by

$$a_{kn} = 2(1 - x_{kn}^2)/[nP_{n-1}(x_{kn})]^2 \ . \qquad \text{(A-32)}$$

Initial estimates of the zeros are obtained from the n successive zeros of the Bessel function $(J_o(j_k) = 0)$ via

$$x_{kn} = \cos[j_k/((n + \tfrac{1}{2})^2+(1-(\tfrac{2}{\pi})^2)/4)^{1/2}]. \qquad \text{(A-33)}$$

Final values of the x_{kn} are found by Newton-Raphson iteration. The tolerance of Legendre polynomial zeros is set at 10^{-14}.

SYMBOL	Explanation
AKN(K)	a_{kn} (Eq. (A-32)). 'IT' elements in the array.
IT	n; it is the order of Legendre expansion for phase functions.
P(N)	Legendre polynomials, $P_n(x)$.
PI	3.1415926535898
X	x_{kn} (Eq.(A-33)).
XKN(K)	$\cos\theta_{kn}$; $P_n(\cos\theta_{kn}) = 0$ within 10^{-14}.
TOL	the tolerance of zeros of Legendre polynomials.
Z(I)	j_k (Eq.(A-33)). I,k = 1,2,... IT.

A.2.4 Subroutine AG9PT1

The main purpose of subroutine AG9PT1 is to generate two arrays R(J) and F(J); R(J) contains 'NRADI' values of radius (particle size) in micrometers (μm) and F(J) contains the corresponding values of the distribution function. The units of unnormalized F(J) are cm^{-3} μm^{-1} and that of normalized F(J) are μm^{-1}.

The other quantities that are calculated are the normalization factor, FSUM and the average volume per particle, VOL (in μm^{-3}). AG9PT1 also calculates some other quantities which vary from one distribution type to another, as indicated in the flowchart.

Two parameters IDSTP and NRADI read on the very first input card in MAIN are of relevance to AG9PT1. IDSTP identifies the type of size distribution function to be used in a given run, and NRADI fixes the number of radii that will be used to describe the size distribution function. The details of each distribution type are given later. First we give the explanation of symbol which have the same explanation for all distribution types.

SYMBOL	Explanation or Definition
AVOL	the average volume per particle in cubic microns obtained via analytical integration over the limits RLO=0 and RHI=∞. That has only been done for IDSTP = 5,6,8,9,10,11,12.
DENS	the particle number density in cm^{-3}.
DELRD	= (RHI-RLO)/RADS; increment between successive values of R.
DELLR	increment in radius for the case IDSTP = 0.
F(J)	the array containing 'NRADI' values of the size distribution function. See the description of AG9PT1 for more details.
FSUM	the numerical integral over the size distribution function with respect to radius between the limits RHI and RLO; used to normalize the distribution function.
IDSTP	identifies the type of aerosol size distribution to be used. See below for more details.
IDUMMY	not used in AGAUS9.
NCRDS	not used in this subroutine.
NRADI	the number of radius values to be used in describing the size distribution function.
NRADII	is same as NRADI except for IDSTP = 7,8,9,10,11. For IDSTP=7, the input value of NRADI is ignored, for IDSTP=8,9,10,11 it is doubled.

SYMBOL	Explanation or Definition
NUNIT	is not used in this subroutine.
PI	= 3.1415926535898.
R(J)	the array containing 'NRADI' values of radius (particle size) in micrometers.
RADS	= DFLOAT (NRADI-1).
RHI	the largest value of radius used (in μm).
RLO	the smallest value of radius used (in μm).
VOL	the average 'dry' volume per particle (in μm^3) calculated numerically.

Description of Types of Distributions

IDSTP	DESCRIPTION
0	This is arbitrary user-supplied distribution. 'NRADI' + 1 cards have to be read; the first card contains RLO and DELLR (μm). The rest of the cards carry the values of F(J) and must be in order of increasing radius value.
1	This zero-order log-normal distribution and the distribution function is given by $$F(R) = \frac{1}{\sqrt{2\pi}\ \ell og_e(\sigma) R} \exp\left\{-\frac{1}{2}\left[\frac{\ell og_e(R/\bar{R})}{\ell og_e(\sigma)}\right]^{1/2}\right\}.$$ $\bar{R} \equiv$ RBAR; $\sigma \equiv$ SIGMA, is the standard deviation. This distribution type requires one input data card to read in the values of $\bar{R}$, σ, RLO, and RHI.
2	This is called double exponential distribution and its distribution function is given by $$F(R) = QA \exp(-AR) + (1-Q)B \exp(-BR).$$ Q ≡ CUE. This distribution type requires one input data card to read in the values of RLO, RHI, Q, A, and B. Q is dimensionless while A and B have units of μm^{-1}.
3	This model (Deirmendjian's "Model C") does not require any input data card. It carries fixed value of DENS, RLO, and DELRD. RHI is determined by the input parameter NRADI. $$F(R) = 450.2 \quad R \leq .08$$ $$= 2.251*DELRD*R^{-4} \quad R > .08$$

IDSTP	DESCRIPTION

4 The distribution function of this model (Junge distribution) is given by

$$F(R) = QR^{-A},$$

Q ≡ CUE. This distribution type requires one input data card to read in RLO, RHI, Q, A.

5 The distribution function for the Modified Gamma/Generalized Khirgian-Mazin distribution is

$$F(R) = R^{\alpha} \exp\left[-\left(\frac{R}{R_c}\right)^{\gamma} \cdot \frac{\alpha}{\gamma}\right],$$

$\alpha \equiv$ ALF, $\gamma \equiv$ GAM, and $R_c \equiv$ RC. One input card is needed to read in RLO, RHI, RC, ALF, GAM, and ELWC. ELWC is not needed for type 5 distribution and, therefore can be left blank.

6 This size-distribution model (NMSU Fog or Cloud Model) is very similar to type 5, except in that the user must supply one additional input parameter--namely, the liquid water content (ELWC) in gm/cc. This model can be used for treating situations involving liquid water aerosols like clouds or fogs. For type 6 runs one does not need to read in the values of EMA, CAYA, RHOA, CONC.

7 This distribution is essentially same as Junge's distribution (type 4) except that it has fixed parameters. The input value of NRADI read in initially, is ignored. One input card is needed to read in VIS (visibility in km); VIS is used in calculating DENS.

8 This is a fixed parameter Continental Bi-modal Model. It does not require an input data card of type 2 (see sec. A.3.3).

9 This is a fixed parameter Maritime Bi-modal Model. It does not require an input data card of type 2 (see sec. A.3.3).

10 This is a fixed parameter Urban Bi-modal Model. It does not require an input data card of type 2 (see sec. A.3.3).

11 This is a user-supplied Bi-modal Model. This requires one input card to read in FOA, FOC, SGA, SGC, RBARA, RBARC. Types 8,9,10, and 11 use the sum of two log-normal distributions:

$$F(R) = \sum_{i=1}^{2} \frac{N_i}{\sqrt{2\pi}\, \log_e(\sigma_i) R} \exp\left\{-\frac{1}{2}\left(\frac{\log_e(R/\bar{R}_i)}{\log_e(\sigma_i)}\right)^2\right\}$$

$N_1 \equiv$ FOA, $\bar{R}_1 \equiv$ RBARA, $\sigma_1 \equiv$ SGA with similar meaning for

IDSTP	DESCRIPTION

N_2, $\bar{R}_2$, and σ_2. Note that in Type 8, 9, 10 the values of SGA and SGC are $\log_e(\sigma)$. For type 8,9,10, and 11 the total number of radii used will be twice as large as the input value of NRADI.

12 This model (Marshall-Palmer Rain Model) is a simple exponential model which assumes an empirical relationship between rain rate and droplet size distribution parameters:

$$F(D) = N_o \exp(-\Lambda D).$$

$N_o = 0.08\ cm^{-4}$, and $\Lambda = 41\ (RN)^{-0.21}$ in which RN = RAIN is the rain rate in mm/hour. Diameter D is in cm. The corresponding size distribution function as a function of radius R is given by

$$F(R) = 2N_o \exp(-2\Lambda R).$$

This distribution requires one input data card to read in RAIN. The values of RLO and RHI are fixed at 0 and 0.5 cm respectively. Due to the limitations on the range of Mie-sizes (subroutine MIEGX) type 12 usage is limited to wavelengths of the order of 1 mm or larger. Since subroutine WATER does not contain optical data for wavelengths longer than 0.2 mm, type 12 runs require the user to supply the values of EMA, CAYA, and RHOA as if rain were a non-aqueous aerosol.

Subroutine AG9PT1 - Simplified Flowchart

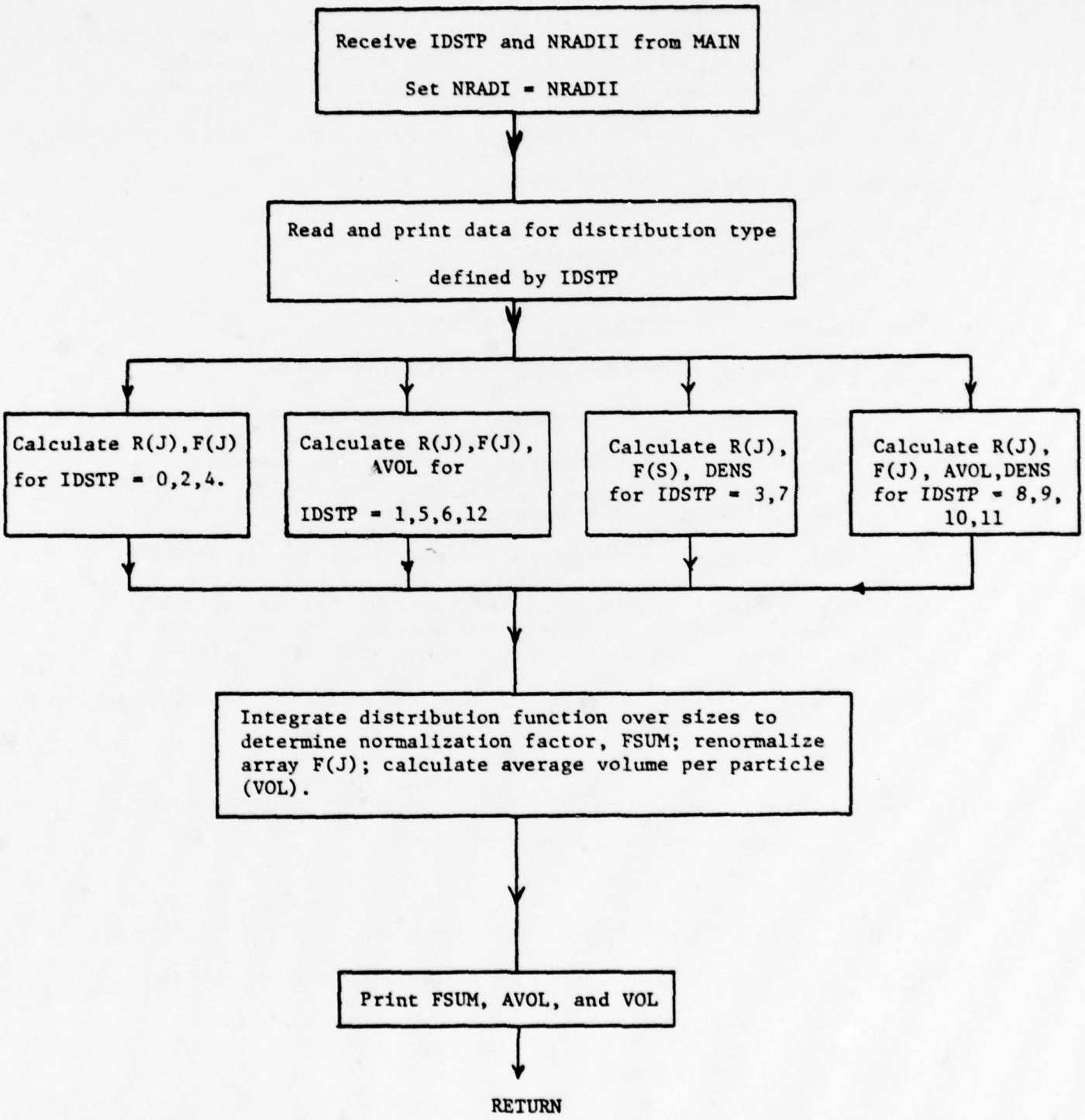

A.2.5 Subroutine AG9PT2

Subroutine AG9PT2 deals with the most important computational aspects of AGAUS9. If RELHUM and the growth factor (EMUA) are non-zero, AG9PT2 makes adjustment in particle radii, density and refractive index of aerosol material to account for the absorption of water by aerosol particles. These adjustments are made through following equations:

Radius: RT = AC*R(L) - BC/AC,

Index of Refraction:

i) Real part:EM = EMW + (EMA-EMW)/A,

ii) Imaginary:part CAY = CAYW + (CAYA-CAYW)/A,

Density: RHO = RHOW + (RHOA - RHOW)/A,

All the symbols used above are explained in detail below.

Now, subroutine MIEGX is called to compute single particle scattering functions QR, QS, QT, and P(J) for each adjusted radius. These scattering functions are weighted and integrated over the size distribution by the trapezoidal method. The convergence of integration for volume and the extinction cross-section is checked, and warnings are printed if the final one or two contributions exceed 5% of the previous total values. If there is more than one component (NINDX>1) in the aerosol with different refractive index and density, the above calculation is carried out NINDX times, and results are summed and divided by the total particle number density. In the end, the attenuation coefficients in square meters per milligram of 'dry' aerosol material, and in square meters per milligram of 'wet' aerosol material are calculated. The same value of the extinction coefficient is used for calculating both attenuation coefficients.

SYMBOL	Definition
A	= 1 + (RHOA/RHOW) * EMUA * CH; used in making adjustments due to water absorption by aerosol.
AC	= $A^{1/3}$.
ALPHA	= 2*PI*EMM*RT/WAVE. Mie size parameter for adjusted radii.
BC	= BHT*CH; used in making adjustments in size growth.
BH	= $1.056*10^{-3}$.
BHT	= BH*(298/TEMK).

SYMBOL	Definition
CATTN	the total attenuation coefficient in square meters per milligram of 'dry' aerosol material for each WAVE. However, CTSUM corresponds to 'wet' aerosol.
CATTNW	the total attenuation coefficient in square meter per milligram of 'wet' aerosol material.
CAY	the imaginary part of 'effective' refractive index of 'wet' aerosol. When RELHUM and growth factor are non-zero particles absorb water vapors. CAY = (CAYW + (CAYA - CAYW)/A). CAY = CAY/EM.
CAYA	the imaginary part of refractive index of dry aerosol. (Assumed to be negative; do not enter a value with a negative sign on the data card(s)).
CAYW	the imaginary part of refractive index of pure water at a given TEMP(DEG C) and WAVE.
CH	= FH/(1-FH).
CONC	the mass concentration in gm/cc of a component of dry aerosol. It is the number of grams of dry aerosol per cubic centimeter of "cloud" or "fog", etc.
CONCT	the total mass concentration in mg/cc of dry aerosol.
CRNEW	= FACT1*QR; both FACT1 and QR correspond to the current radius in the do-loop indexed over NRADI, except when L=1; CRNEW does not exist for L=1.
CROLD	= FACT1*QR; both FACT1 and QR correspond to the previous radius in the do-loop indexed over NRADI except when L=1; when L=1, they correspond to the current radius.
CRSUM	the average (sum/DENST) back-scattering cross-section in square micrometers, integrated over the size distribution, for each WAVE.
CSNEW, CSOLD	= FACT1*QS. See CRNEW, CROLD.
CSSUM	the average (sum/DENST) scattering cross-section in square micrometers, integrated over the size distribution, for each WAVE.
CTNEW, CTOLD	= FACT1*QT. See CRNEW, CROLD

SYMBOL	Definition
CTNK	the extinction cross-section in square micrometers, integrated over the size distribution, for each WAVE and each component of the aerosol.
CTSUM	the average (sum/DENST) extinction cross-section in square micrometers, integrated over the size distribution, for each WAVE.
CTSUMT	the total extinction cross-section in square micrometers, integrated over the size distribution, for each WAVE.
DENS	the particle number density per cubic centimeter. See DENSC also.
DENSC	the particle number density per cc for each component of aerosol. It is calculated from mass density and concentration, and average volume per particle. If LLLL=1, the calculated value of DENSC is replaced by DENS, the value of which has been determined or supplied elsewhere. (Also see description of the MAIN program.)
DENST	the total particle number density per cc. See also DENSC.
DQT	a term in the numerical integration over the size distribution of the extinction cross-section (CTSUM) by the trapezoidal method.
DRYVOL	the average volume per particle in cc.
DVOL	a term in the numerical integration over the size distribution of the volume of a sphere by the trapezoidal method.
ELWC	the liquid water content in gm/cc.
EM	the real part of the effective refractive index of 'wet' aerosol. See CAY. EM = (EMW + (EMA - EMW)/A).
EMA	the real part of refractive index of the dry aerosol.
EMASS	is 'wet' mass concentration in gm/cc of a component of an aerosol when RELHUM and growth factor are non-zero. EMASS and CONC should have same value if growth factor is zero.
EMM	the refractive index of the surrounding medium, set equal to 1 here implying no surrounding medium.
EMUA	Hanel's mass accretion coefficient $\bar{\mu}$. Values must be supplied by the user and depend on the type or composition of the aerosol being modeled as well as upon the value of the relative humidity.

SYMBOL	Definition
EMW	the real part of refractive index of water at a given TEMR (DEG C) and WAVE.
F(I)	the normalized size distribution function (in micrometers^{-1}).
FACT1	= $\frac{\pi}{2}$ * F(L)*RT**2, or $\frac{\pi}{2}$ * F(L-1)*RT1**2.
FH	the fractional relative humidity (saturation ratio).
FQT(I)	= DQT/CTSUM. In this formula CTSUM = $\sum_{i=1}^{N} DQT_i$ and DQT = DQT_N; N = NRADI-2, NRADI-1, or NRADI.
FR	= F(L)*DENSC. DENSC is in cm^{-3}.
FVOLD(I)	= DVOL/VOL. See FQT(I).
IDSTP	identifies the type of aerosol size distribution being used in the run.
IERROR	a flag which is set to unity if the number of terms reaches the maximum value allowed in the dimensions of the Mie-coefficients a_n and b_n.
KEXOLD	the extinction coefficient per km summed over the number of components one less than the current value of the running loop index NK.
KEXT	the extinction coefficient per km for each component of the aerosol.
KEXTT	the total extinction coefficient per km for each WAVE.
LLLL	a switch parameter. If LLLL=0, the particle number density (DENSC) is calculated using mass density and concentration, and the average volume per particle (DRYVOL). If LLLL=1, a pre-calculated or pre-supplied value of DENS is used.
MERROR	an error counter: If MERROR exceeds 10, execution is terminated.
MCRTE	is not used in this version of the routine.
MQRTE	= 12345, QT, QS, QR and FR are printed for each radius.
NCRDS	not used in this subroutine, but appears in a common block.
NINDX	the number of aerosol components which will have different optical constants, mass density or mass concentration.

SYMBOL	Definition
NRADI	the number of points on the radius vs. size distribution function plot.
NUNIT	defines the device on which the input and/or output data may be stored in lieu of actual card punching; may be used to place nominal card output into data files on tape etc. The default value (NUNIT=0) is 4 (card punch) for UNIVAC and 7 for IBM.
OLSTAR	not used in AGAUS9.
P(J)	an array containing 'IT' average intensity factors $(i_1+i_2)/2$ for each radius RT.
PI	= π = #.
PSNEW(J)	= P(J)*F(L), where P(J) corresponds to L^{th} radius; $L \geq 2$.
PSOLD(J)	= P(J)*F(L), where P(J) corresponds to $(L-1)^{th}$ radius except when L=1; in that case PSOLD(J) = P(J)*F(1), and P(J) corresponds to the 1^{st} radius.
PSUM(J)	average intensity factors integrated over the size distribution. They are then summed over NINDX components and divided by DENST.
QR	the back-scattering efficiency factor for each radius.
QS	the scattering efficiency factor for each radius.
QT	the extinction efficiency factor for each radius.
R(L)	the array containing 'NRADI' values of radius in micrometers.
RELHUM	the relative humidity in percent.
RFACT	= (R(L)-R(L-1)) * DENSC.
RHO	the specific density (in gm/cc) of 'wet' aerosol.
RHOA	the specific density (in gm/cc) of dry aerosol.
RHOW	the specific density (in gm/cc) of water at the temperature TEMP (in DEG C).
RT	the radius of a particle after taking into account its growth due to absorption of water. RT = AC*R(L) - BC/AC.
RT1	= AC*R(L-1) - BC/AC. See RT. For L=1, RT1 = RT.
TEMK	the temperature of the surrounding in degrees Kelvin.
TEMP	the temperature of the surrounding in degrees Centigrade.

SYMBOL	Definition
TMASS	the total mass concentration in gm/cc of wet aerosol.
TVOL	is used to pass the value of DRYVOL from MAIN to the subroutine.
WAVE	the wavelength in micrometers at which all the scattering functions are computed.

Subroutine AG9PT2 - Simplified Flowchart

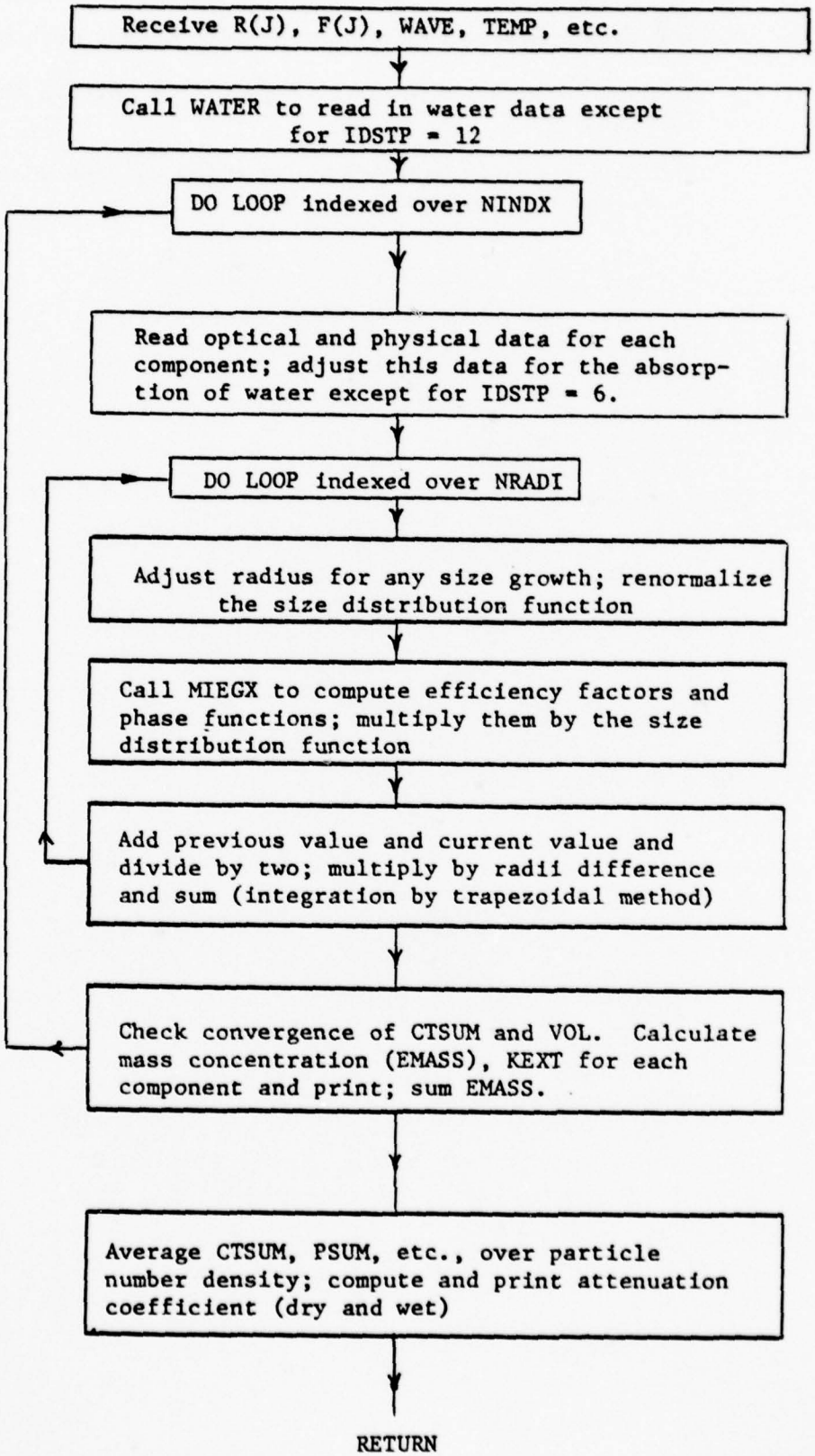

A.2.6 Subroutine WATER

The purpose of subroutine WATER is to relieve the user of programs AGAUS9 or AGAUS10 of the task of looking up and keypunching data on the index of refraction and mass density of liquid water. This routine receives the wavelength (μm) and temperature (°K) from the calling program as variables WVD and TEMPD. It returns the mass density through variable DENSD, and the real and imaginary parts of the refractive index of liquid water through the variables EMD and CAYD, respectively.

The data on optical constants coded into routine WATER were taken from the tabulation by Irvine and Pollock [31], and the water densities were taken from a copy of the C.R.C. Handbook of Chemistry and Physics.

The optical data cover only the wavelength range 0.20 μm to 200 μm and are not entered at uniform wavelength increments. Values of the real (m) and imaginary (k) parts of the refractive index at wavelengths lying between values for which data are entered in the tables are estimated through straight-line interpolation. Linear interpolation is also used between tabulated temperatures in calculating the mass density (ρ_w = DENSD).

Methods Used

Subroutine WATER conducts separate binary searches of the wavelength table [LAMBDA( )] and temperature table [TEMP( )] to find the indices L and L+1 which bracket** the received wavelength (WVD) and temperature (TEMPD). It then uses linear interpolation to get estimated values of EMT(m) CAYT(k) and RHODEN(ρ_w).

The interpolation formula used can be written as

$$y(x) = y(x_\ell) + \left[\frac{y_{\ell+1}-y_\ell}{x_{\ell+1}-x_\ell}\right](x-x_\ell) \ ,$$

with $y = m, k$ or ρ_w and

x = wavelength or temperature.

**"bracket" means, for example: LAMBA(L) < WAVE < LAMBDA (L+1)

SYMBOL	Explanation or Definition
CAYD	imaginary part of refractive index k [double precision format].
CAYT	the interpolated value of k in single precision form; used intermediately to hold summed quantities.
DENSD	interpolated result for the mass density of liquid water - ρ_w [double precision form].
EMD	real part of index of refraction - m [double precision form].
EMT	the interpolated result for the real part of the refractive index (single precision form).
H	an indexing (integer) parameter.
L	an integer indexing parameter.
LAMBDA( )	Array of wavelengths at which data are entered for m and k; [typed as "real"].
NSUBI( )	array of values for k (or, $n_{imaginary}$); [typed as "real"].
NSUBR( )	array of data entries for m (or, n_{real}) [typed as "real"].
P	an (integer) indexing parameter.
POINT	an (integer) indexing parameter.
TEMP( )	array of temperature values (°K) at which entries for ρ_w exist [single precision form].
TEMPD	temperature at which ρ_w is to be found [double precision form].
TMCHUR	temperature at which value of ρ_w is desired [single precision form].
RHODEN	interpolated result for ρ_w [single precision form]
WAVE	single precision version of wavelength at which values of n and k are desired.

A.2.7 Subroutine MIEGX

Subroutine MIEGX computes various efficiency factors, and intensity factors i_1 and i_2 for each complex refractive index m and size parameter α. The Ricatti-Bessel functions and their derivatives in Eqs. (A-5) and (A-6) are computed by the forward recursion method. The initial values used in forward recursion are

$$\psi_o(z) = \sin z \ ,$$

$$\psi_1(z) = \frac{\sin z}{z} - \cos z,$$

$$\chi_o(z) = \cos z, \quad \text{and}$$

$$\chi_1 = \frac{\cos z}{z} + \sin z.$$

[Note: $\xi_n(z) = \psi_n(z) + i\chi_n(z)$]

The angular functions π_n and τ_n are also computed by forward recursions from Eqs. (A-24) and (A-25). The initial values used are $\pi_o(\theta) = 0$, $\pi_1(\theta) = 1$, $\tau_o(\theta) = 0$, and $\tau_1(\theta) = \cos\theta$.

The Mie series is terminated either when two successive terms have $(|\mathrm{Re}(a_n)| + |\mathrm{Im}(a_n)| + |\mathrm{Re}(b_n)| + |\mathrm{Im}(b_n)|) < 10^{-5}$, or when the number of terms exceeds $(8+F\alpha)$. F is 1.2 for $\alpha \leq 51$ and is $1+2.26\alpha^{-0.613}$ for $\alpha > 51$. The tolerance value of 10^{-5} could be decreased for higher precision, if the user so desires.

The subroutine computes and stores arrays of a_n and b_n until convergence is reached and then generates necessary π_n and τ_n functions. Finally it computes values of Q_{ext}, Q_{sca}, Q_{abs} (absorption), i_1, i_2, Q_{rad} (back scatter), $p(\theta)$, and radiation pressure Q_{pr}. For AGAUS9, only the values of Q_{ext}, Q_{sca}, Q_{rad}, and $p(\theta)$ are returned.

SYMBOL	Explanation or Definition
ALPHA	Mie size parameter, $\alpha = 2\pi r/\lambda$.
C(K)	the array of cosine of the scattering angles. There are 'IT' elements in the array.
CAY	the ratio of the imaginary part to the real part of adjusted refractive index. See AG9PT2.
EM	the real part of adjusted refractive index.
EN	Floating point representation of N
EYE1(K)	i_1 (Eq. A-15) at angles = Arc cos[C(K)]. 'IT' elements in the array.
EYE2(K)	i_2 (Eq. A-16) at angles = Arc cos[C(K)]. 'IT' elements in the array.
FACT	determines the cutoff criterion to terminate the Mie series. It is equal to 1.2 if $\alpha \leq 51$ and is $1+2.26\alpha^{-0.613}$ for $\alpha > 51$. See Mie theory text.
FAN(N)	= Im (a_n); Eq. (A-5).
FBN(N)	= Im(b_n); Eq. (A-6).
GAMMA	the true imaginary part of adjusted refractive index.
IERROR	a flag which is set to unity if the number of terms (N) reaches the maximum value allowed in the dimensions of a_n and b_n.
ISW1	a switch parameter used in applying cutoff criterion.
MCRTE	is not used in this subroutine.
O1STAR	= $\tilde{\omega}_1^*$; first order coefficient for Legendre expansion of the average intensity P(K).
P(K)	= $(i_1+i_2)/2$, the average intensity at angles, Arc cos (C(K)). There are 'IT' elements in the array.
PIE	= π = 3.1415926535898.
PIN	= $\pi_n(\theta)$; Eq. (A-17).
REAN	= Re(a_n); Eq. (A-5).
REBN	= Re(b_n); Eq. (A-6).

SYMBOL	Explanation or Definition
RN	= $Re(\psi_n(n\alpha))$; Eq. (A-7).
RNL1	= $Re(\psi_o(n\alpha))$; Eq. (A-7).
RPN	= $Re(\psi'_n(n\alpha))$. Prime indicates differentiation with respect to the argument.
SGA	the absorption efficiency factor.
SGMAS	the average value of $Cos(\theta)$, where θ is the scattering angle; not used by AGAUS9.
SGMP	the radiation pressure factor Q_{pr}-not used by AGAUS9.
SGR	the back-scattering efficiency factor.
SGS	the scattering efficiency factor.
SGT	the extinction efficiency factor.
SN	= $Im(\psi_n(n\alpha))$; Eq. (A-7).
SNL1	= $Im(\psi_o(n\alpha))$; Eq. (A-7).
SPN	= $Im(\psi'_n(n\alpha))$. Prime indicates differentiation with respect to the argument.
SUMI1I	the imaginary part of the scattering amplitude $S_1(\theta)$; $$Im\ S_1(\theta) = \sum \frac{(2n+1)}{n(n+1)}[Im(a_n)\pi_n(\theta)+Im(b_n)\tau_n(\theta)].$$
SUMI2I	the imaginary part of the scattering amplitude $S_2(\theta)$; $$Im\ S_1(\theta) = \sum \frac{(2n+1)}{n(n+1)}[Im(b_n)\pi_n(\theta)+Im(a_n)\tau_n(\theta)].$$
SUMI1R	the real part of the scattering amplitude $S_1(\theta)$; $$Re\ S_1(\theta) = \sum \frac{(2n+1)}{n(n+1)}\ [Re(a_n)\pi_n(\theta)+Re(b_n)\tau_n(\theta)].$$
SUMI2R	the real part of the scattering amplitude $S_2(\theta)$; $$ReS_2(\theta) = \sum \frac{(2n+1)}{n(n+1)}[Re(b_n)\pi_n(\theta)+Re(a_n)\tau_n(\theta)].$$

SYMBOL	Explanation or Definition
SUMRI	$= \sum_{n=1}^{N} (-1)^n (2n+1)\,\mathrm{Im}(a_n - b_n)$.
SUMRR	$= \sum_{n=1}^{N} (-1)^n (2n+1)\,\mathrm{Re}(a_n - b_n)$.
SUMS	$= \sum (2n+1)(\lvert a_n \rvert^2 + \lvert b_n \rvert^2)$.
SUMS1	$= \sum_{n=2}^{N} \frac{(n-1)(n+1)}{n}[\mathrm{Re}(a_n)\mathrm{Re}(a_{n+1}) + \mathrm{Re}(b_n)\mathrm{Re}(b_{n+1}) + \mathrm{Im}(a_n)\mathrm{Im}(a_{n+1}) + \mathrm{Im}(b_n)\mathrm{Im}(b_{n+1})]$.
SUMS2	$= \sum_{n=2}^{N} \frac{(2n-1)}{n(n-1)}[\mathrm{Re}(a_n)\mathrm{Re}(b_n) + \mathrm{Im}(a_n)\mathrm{Im}(b_n)]$.
SUMT	$= \sum (2n+1)\,\mathrm{Re}(a_n + b_n)$.
TAUN	$= \tau_n(\theta)$; Eq. (A-17).
TERMN	$= \lvert \mathrm{Re}(a_n) \rvert + \lvert \mathrm{Im}(a_n) \rvert + \lvert \mathrm{Re}(b_n) \rvert + \lvert \mathrm{Im}(b_n) \rvert$. TERMN determines the cutoff criterion for terminating Mie series.
TN	$= \psi_n(\alpha)$; Eq. (A-7).
TNL1	$= \psi_o(\alpha)$; Eq. (A-7).
TPN	$= \psi_n'(\alpha)$; prime indicates differentiation with respect to the argument.
UN	$= \chi_n(\alpha)$; Eq. (A-8).
UNL1	$= \chi_o(\alpha)$; Eq. (A-8).
UPN	$= \chi_n'(\alpha)$; prime indicates differentiation with respect to the argument.

Subroutine MIEGX - Simplified Flowchart

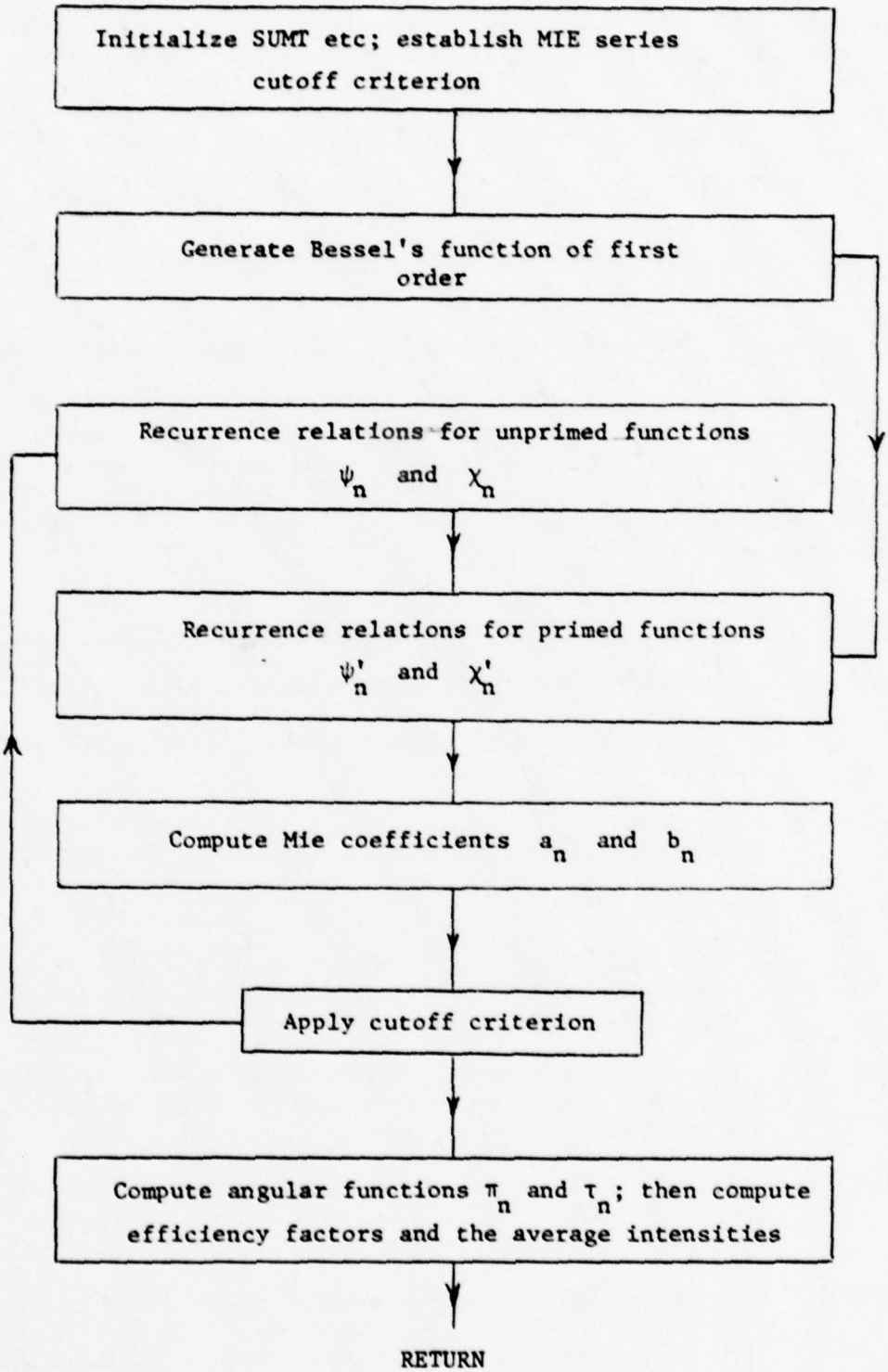

A.2.8 Subroutine AG9PT3

Subroutine AG9PT3 receives the values of various cross-sections and the integrated average intensity factors from AG9PT2 and converts them into more directly useful quantities:

$$\text{Coefficient (per km)} = 10^{-3}*\text{DENS}*\text{cross-section},$$

$$\text{Scattering fractions} = \frac{\lambda^2}{4\pi^2}*\text{DENS}*\text{intensity factors},$$

and

$$\text{Phase function} = \frac{\lambda^2}{\pi C_{ext}} *\text{intensity factors}.$$

λ is in μm. It then prints out all the single wavelength results.

It also computes albedo for single scattering using Eq. (A-4). It then calls on subroutine GAUS which, among other things (see GAUS for details), also returns a value for albedo calculated differently. The two values are compared, and if they differ by more than 0.01 percent the user is advised to rerun the program using a larger value of IT.

SYMBOL	Explanation or Definition
ALBDO	= CSSUM/CTSUM; albedo for single scattering. See Mie theory.
C(I)	the cosines of scattering angles. 'IT' elements in the array.
CAY	the ratio of the imaginary part to the real part of adjusted refractive index of the last component. See AG9PT2.
CAYNG	= - CAY.
CRSUM	the average back-scattering cross-section when it is received by AG9PT3 but it returns to MAIN the value of the average back-scattering coefficient per km.
CSSUM	the average scattering cross-section when it is received by AG9PT3 but it returns to MAIN the value of the average scattering coefficient per km.
CTSUM	the average extinction cross-section when it is received by AG9PT3 but it returns to MAIN the value of the average extinction coefficient per km.
DENS	the total particle number density in cm^{-3}.
EM	the real part of the adjusted refractive index of the last aerosol component.

SYMBOL	Explanation or Definition
EMM	the refractive index of the surrounding medium. It is set equal to 1 in AGAUS9.
GNU	the wave number in cm^{-1}.
H(I)	the array containing 'IT' scattering angles (in degrees).
IANG	= 0, for the computation of phase functions at 'IT' Gauss-Legendre quadrature angles. =1, for the computation of phase functions and scattering functions at 'IT' equally spaced angles between 0° and 180°.
IDSTP	identifies the type of aerosol size distribution to be used. See AG9PT1 for more details.
IT	the order of expansion for phase functions when IANG=0, or the number of equally spaced angles between 0° and 180° when IANG=1.
KRSUM	the back-scattering coefficient per km integrated over the size distribution, for each WAVE.
KSSUM	the scattering coefficient per km integrated over the size distribution, for each WAVE.
KTSUM	the extinction coefficient per km integrated over the size distribution, for each WAVE.
NCRDS	= 1, for punch of Legendre expansion coefficients of phase functions. =2, for storing input and/or output data, to be used later in a program attached to AGAUS9, on a device identified by NUNIT.
NINDX	the number of aerosol components which will have different optical constants, mass density or mass concentration.
NUNIT	defines the device on which the input and/or output data may be stored in lieu of actual card punching; may be used to place nominal card output into data files on tape, etc. The default value (NUNIT=0) is 4 (card punch) for UNIVAC and 7 for IBM.
OL(1)	the first coefficient in the Legendre expansion of phase functions. When OL(1) disagrees with ALBEDO by more than 0.01 percent program AGAUS9 should be rerun using a larger value of IT.
PFACT	= WAVE*WAVE/(PI*CTSUM*EMM*EMM). When PSUM(J) is multiplied by PFACT we get the original phase functions.

SYMBOL	Explanation or Definition
PI	= π = 3.1415926535898.
PSUM(J)	the average intensity factors integrated over the size distribution when received by AG9PT3, but they are the original phase functions for each WAVE when returned to MAIN.
SCAT(J)	contains 'IT' values of scattering fractions for each WAVE.
SFACT	= WAVE*WAVE*DENS*10^{-6}/4*PI*PI. When PSUM(J) is multiplied by SFACT, one gets the scattering fractions of ASLSOM code.
WAVE	the wavelength in microns.

Subroutine AG9PT3 - Simplified Flowchart

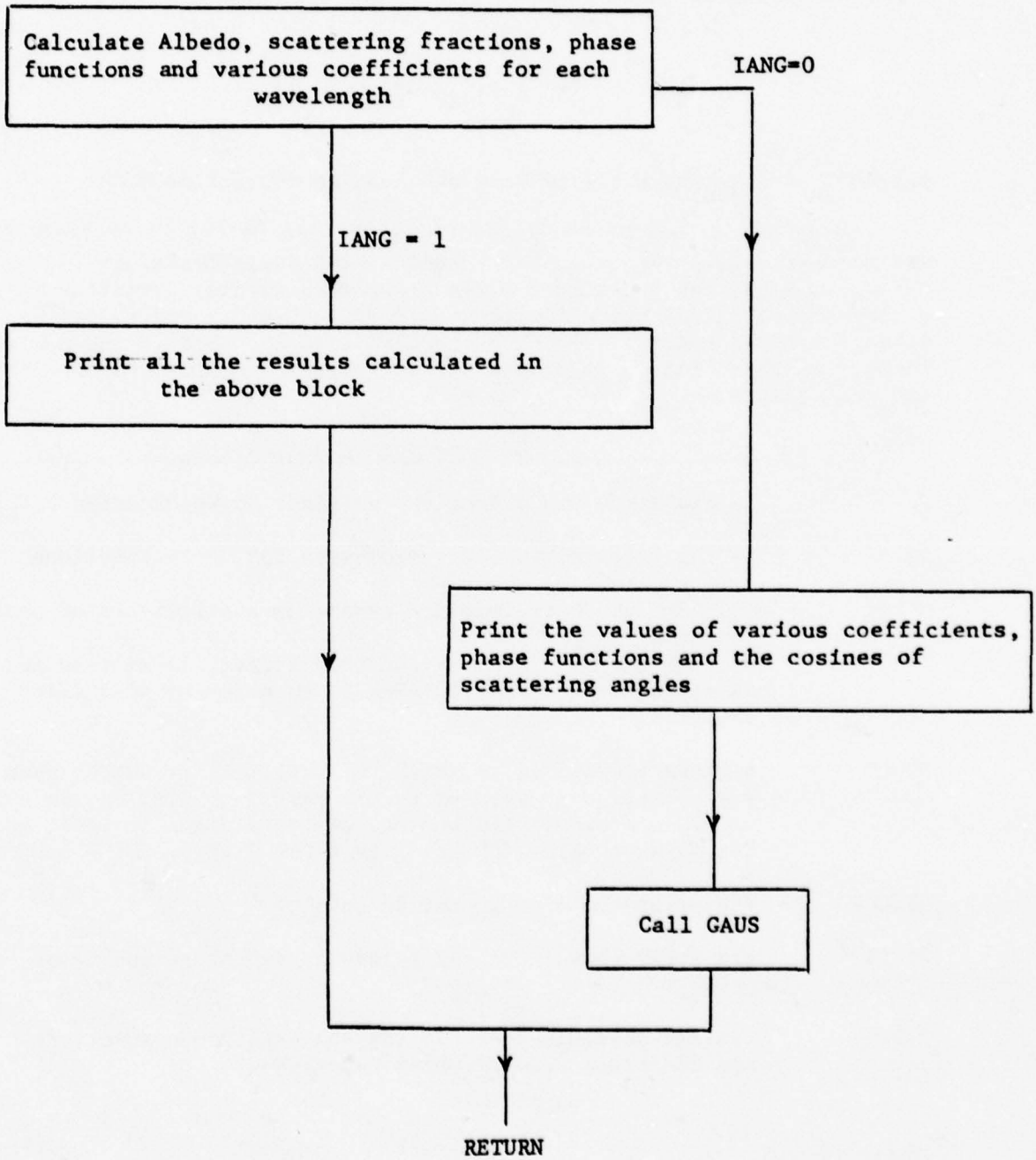

A.2.9 Subroutine GAUS

Subroutine GAUS computes Legendre expansion coefficients given by Eq. (A-31) numerically. To do that the integral in Eq. (A-31) is replaced by summation as follows:

$$\tilde{\omega}_\ell = \frac{(2\ell+1)}{2} \sum_{k=1}^{n} p(\theta_{kn}) P_\ell(\cos\theta_{kn}) a_{kn} ,$$

where θ_{kn} and a_{kn} have the meaning as given in subroutine GUSET.

Using the values of coefficients $\tilde{\omega}_\ell$ and Eq. (A-30) phase functions are reconstructed. We call them reconstructed phase functions, $p_c(\theta_{kn})$. GAUS then computes the rms (root mean square) deviation between the original phase functions $p(\theta_{kn})$ and the reconstructed phase functions $p_c(\theta_{kn})$ as each successive term is added to the series in Eq. (A-30). Finally it prints out the values of coefficients and rms deviations.

SYMBOL	Explanation or Definition
F	is the array containing the original phase function $p(\theta_{kn})$.
IT	is the order of Legendre expansion for phase functions.
NCRDS	= 1, for punch of Legendre expansion coefficients of phase functions =2, for storing input and/or output data, to be used later in a program attached to AGAUS9, on a device identified by NUNIT.
NUNIT	defines the device on which the input and/or output data may be stored in lieu of actual card punching; may be used to place nominal card output into data files on tape, etc. The default value (NUNIT=0) is 4 for UNIVAC, and 7 for IBM.
OL(LL)	the array containing coefficients $\tilde{\omega}_\ell$.
PC(I)	the array containing the reconstructed phase functions $p_c(\theta_{kn})$.
RMS(J)	the rms deviation between the original phase functions and the reconstructed phase functions.

A.2.10 Subroutine AG9PRT

Subroutine AG9PRT prints out all the averaged (sum/NWAVE) results essentially in the same way as AG9PT3 does for each wavelength. If IANG=0, subroutine GAUS is called to generate Legendre expansion coefficients which are used to reconstruct the averaged phase functions. GAUS also computes the rms deviation between the original phase function and the reconstructed phase functions. See the section on subroutine GAUS for more details. If IANG=1, the above calculation is skipped.

If ISCAT=0, the averaged scattering fractions are printed; if ISCAT=1, they are punched (or written on NUNIT) as well as printed. If IANG=0, scattering are neither printed nor punched.

SYMBOL	Explanation or Definition
C(I)	the cosines of scattering angles. 'IT' elements in the array.
CATTN	the average (sum/NWAVE) attenuation coefficient in square meters per milligram of aerosol material.
H(I)	the array containing 'IT' scattering angles (in degrees).
IANG	= 0, for the computation of phase functions at 'IT' Gauss-Legendre quadrature angles. = 1, for the computation of phase functions and scattering fractions at 'IT' equally spaced angles between 0° and 180°.
ISCAT	= 0, for scattering fractions to be printed. = 1, for scattering fractions to be printed as well as punched or written on NUNIT.
IT	the order of Legendre expansion for phase functions when IANG=0, or the number of equally spaced angles between 0° and 180° when IANG=1.
KBAKT	the average (sum/NWAVE) back-scattering coefficient per km, integrated over the size distribution.
KEXTT	the average (sum/NWAVE) extinction coefficient per km, integrated over the size distribution.
KSCAT	the average (sum/NWAVE) scattering coefficient per km, integrated over the size distribution.
NUNIT	defines the device on which the input and/or output data may be stored in lieu of actual card punching; may be used to place nominal card output into data files on tape, etc. The default value (NUNIT=0) is 4 (card punch) for UNIVAC, and 7 for IBM.

SYMBOL	Explanation or Definition
NWAVE	the number of wavelengths or relative humidity values to be treated in a given run.
PSUM(J)	the array containing the values of average (sum/NWAVE) phase functions integrated over the size distribution.
SCATT(J)	the array containing the values of average (sum/NWAVE) scattering fractions.

Subroutine AG9PRT - Simplified Flowchart

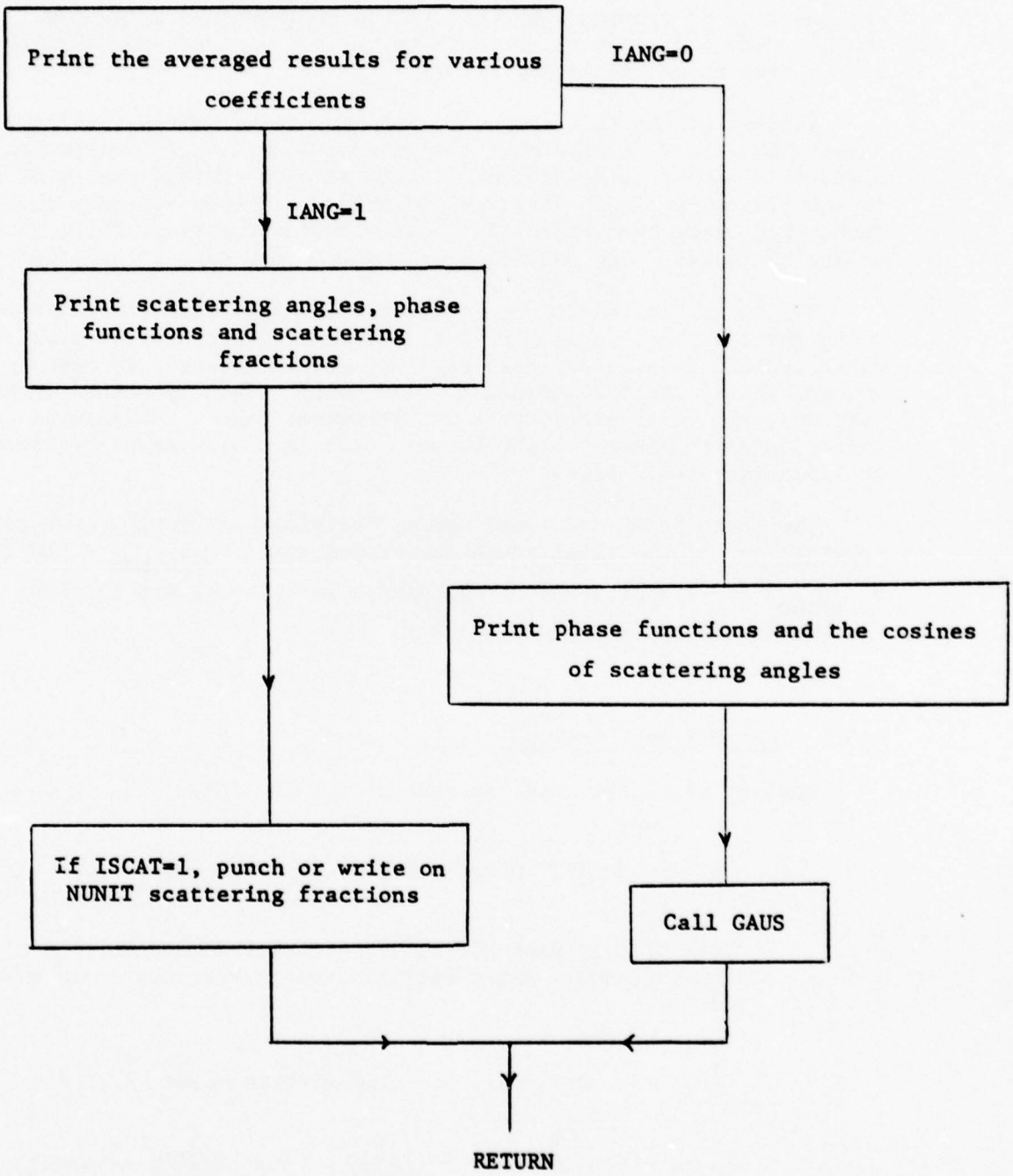

A.3 PROGRAM AGAUS10

This appendix contains a presentation of the details of the mathematical procedures used for the "halving" procedures of AGAUS10, explanations of program symbols found in the routines unique to AGAUS10, and a summary of the ways in which input data for AGAUS10 differ from those of AGAUS9.

Readers of the following descriptions of the mathematical procedures should bear in mind that the general AGAUS single scattering code computes a number of quantities associated with the Mie theory of the interaction of a single spherical scatterer and then averages those quantities using the aerosol size distribution function, f(r), as a weighting factor. The following definitions may also be helpful:

The terms "component" or "aerosol component" apply to cases in which the overall aerosol may be a mixture of different materials whose optical properties, mass density, growth factors, or mass concentrations are not identical. The number of "components" to be used in a run is specified by input parameter NINDX. An example of a multi-component aerosol might be one which is a mixture of hygroscopic and non-hygroscopic particles.

The terms "size-interval" and/or "original interval" refer to subdivisions of the total range of aerosol radii ($R_{minimum}$ = RLO to $R_{maximum}$ = RHI) within which the halving and convergence testing procedures are applied independently.

A.3.1 The "Halving" Method

Most averages that must be done are of the form

$$(1) \qquad G \equiv \int_{RLO}^{RHI} dr\ f(r)\ G(r)/FSUM,$$

where G(r) is some Mie theory quantity for a particle of radius r, and a given optical type (refractive index m = m-ik), and

$$FSUM = \int_{RLO}^{RHI} dr\ f(r).$$

The size distributions f(r), RLO≤r≤RHI, may be given in analytic form, or numerically on a set {R(J)} of values of r. They may or may not be normalized

to unity (FSUM may equal 1.0, or not). The relevant Mie theory quantities include $C_{ext}(r)$, $C_{sca}(r)$, $p(r,\mu)$ for each Gauss-Legendre μ, etc. Other averages that must be done have somewhat different form, e.g.,

$$(2) \quad \tilde{\omega}_n = \frac{1}{C_{ext}} \int dr\ f(r)\tilde{\omega}_n(r)C_{ext}(r)/FSUM,$$

for the coefficients $\tilde{\omega}_n$ of the phase function expression

$p(\mu) = \sum_{n=o}^{\infty} \tilde{\omega}_n P_n(\mu)$, in terms of the coefficients $\tilde{\omega}_n(r)$ of the phase function $p(r,\mu) = \sum_{n=o}^{\infty} \tilde{\omega}_n(r) P_n(\mu)$.

The above integrals over r must be done numerically. In order to minimize computation time, the number of points in the numerical integration should be chosen as small as possible, consistent with adequate accuracy. Each value of r that is used requires the full Mie calculation for the quantities $C_{ext}(r)$, $C_{sca}(r)$, $p(r,\mu)$ for each μ, etc., these calculations absorb a large part of the total computation time. It has been found in this work that, instead of fixing the number of values of r to be, say, 500, adequate accuracy results, in many cases, for as few as 50 to 100 values of r; this reduction allows a reduction in total computation time by roughly a factor of 4 to 8.

The numerical integration method which was developed makes use of successive halving of intervals until a preset convergence criterion is met. This halving method allows an initial set of unequal intervals to be chosen. For example, suppose that the distribution function f(r) is sharply peaked around some value of r, and also has a long tail, as in Fig. A.3.1.

Then it makes sense to choose unequal initial intervals, perhaps as shown. The numerical integration then proceeds by halving each of the original intervals, until the convergence criterion is met. The convergence criterion that was used is the requirement that $|G^{(n+1)} - G^{(n)}|/|G^{(n)}| < \Delta$, where Δ is some small preset number. Here, $G^{(n)}$ is the value of the integral G after the n^{th} halving, separately in each initial interval. The trapezoidal rule was used throughout. The value of the integrand at any given point r is calculated just once; it does not have to be recalculated on that point after halving.

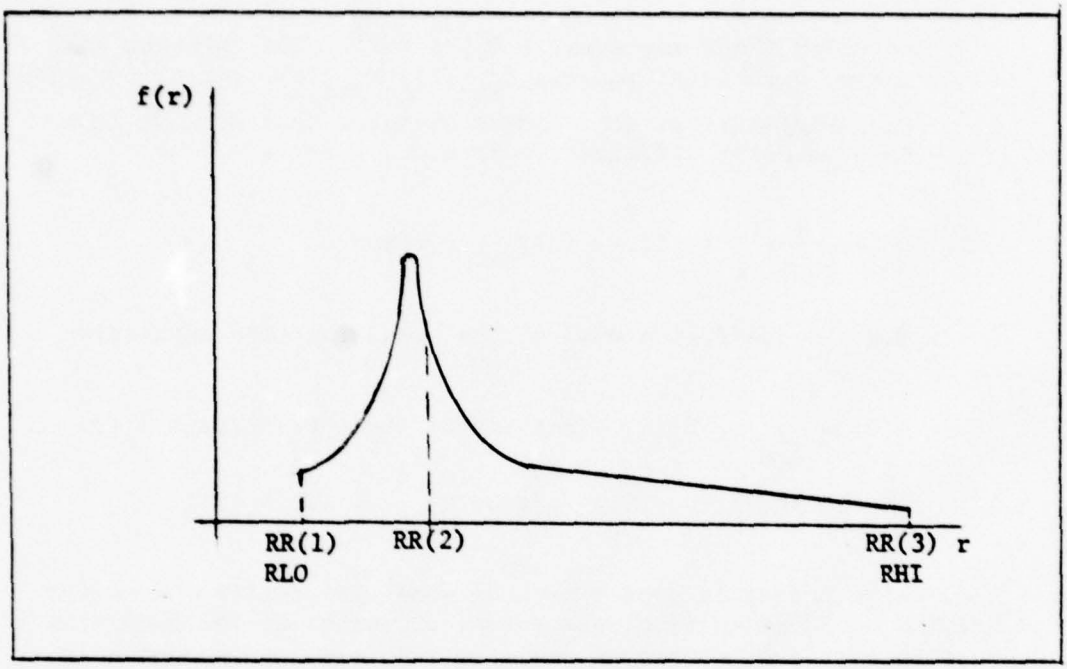

Figure A.3.1 Sketch of a hypothetical size-distribution

The logical flow through the halving integration code is as follows:

1) Given RLO, RHI, and f(r), RLO $\leq$ r $\leq$ RHI, in analytic form; or f(r) numerically on the equally spaced set r = R(J), J = 1, NRADI.

2) For the given f(r), RLO, RHI, choose the number and size of the original intervals. That is, choose RR(I), I=1, NLAST = 2**MIN + 1, with RR(1) = RLO, RR(NLAST) = RHI. Note that NI = no. of initial intervals = 2*MIN = 1,2,4,8,16,... . Then set NHALV = no. of halvings in each interval = MAX-MIN, and NK = maximum no. of points in each interval = 2**NHALV.

3) The maximum number of points allowed is NMAX = 1+2**MAX. In this work, MAX = 9 was used, so NMAX = 513. Calculate R(KK), F(KK) = f(R(KK)), KK = 1, NMAX, on all the points R(KK) which might be used if the halving goes all the way to NMAX points. For f(r) given numerically, this is done by linear interpolation.

4) Calculate $C_{ext}(I) = \int_{RR(I)}^{RR(I+1)} dr\ f(r)C_{ext}(r)$ in each interval

no. I, I=1, NI, by halving of that interval and the trapezoidal rule, until the convergence criterion is met in that interval, or until the halving has progressed all the way to NK points, the maximum number allowed in any interval.

At the same time, calculate $FSUMG(I) = \int_{RR(I)}^{RR(I+1)} dr\ f(r)$, and

all other needed averages

$G(I) = \int_{RR(I)}^{RR(I+1)} dr\ f(r)G(r)$, on the same set of points used for

$C_{ext}(I)$. (This means that the convergence criterion is applied only to $C_{ext}(I)$). Then $C_{ext} = \sum_{I=1}^{NI} C_{ext}(I)$,

$FSUM = \sum_{I=1}^{NI} FSUM(I)$, etc.; and then $C_{ext} = C_{ext}/FSUMG$,

$G = G/FSUMG$. This last step is equivalent to making $\int_{RLO}^{RHI} dr\ f(r) = 1.0$.

A.3.2 Glossary for Subroutines AGXPT1 and AGXPT2

SYMBOL		Explanation
RLO	=	min. value of particle radius in any size distribution
RHI	=	max. value of particle radius in any size distribution
DELLR	=	increment of radius in arbitrary (user-supplied) distribution
NRADI	=	no. of radii at which arbitrary distribution is given
RP	=	a value of particle radius
FF(J)	=	value of arbitrary distribution function at radius RP = RLO + (J-1)*DELLR, J=1, NRADI
MIN	=	integer
MAX	=	integer $\geq$ MIN
NI	=	2**MIN = number of initial intervals in halving method of integration
NLAST	=	NI+1 = number of radii RR(I) defining the NI basic size intervals
RR(I)	=	lower radius of I^{th} initial interval. I=1, NLAST RR(1) = RLO, RR(NLAST) = RHI
NMAX	=	2**MAX+1 = maximum number of points which may be used in halving method
NHALV	=	MAX-MIN = maximum number of interval halvings allowed for each initial interval
NKG	=	2**NHALV = maximum number of points which may be used in each initial interval.
RBAR	=	mean radius in log-normal distribution
SIGMA	=	Std. deviation in log-normal distribution (as input data); used later as ln(SIGMA)
CUE	=	parameter in double exponential distrib., and in exponential distributions
A	=	parameter in several distributions and in exponential distributions
B	=	parameter in several distributions and in exponential distributions

SYMBOL		Explanation
DENS	=	particle number density
DELRD	=	increment of radius for Type 5 and 6 distributions.
VIS	=	visibility in km
RC	=	parameter in modified gamma distribution
ALF	=	parameter in modified gamma distribution
GAM	=	parameter in modified gamma distribution
FOA	=	parameter in bimodal log normal distribution (number density for mode "A")
FOC	=	parameter in bimodal log normal distribution (number density for mode "C")
SGA	=	standard deviation* user supplied bimodal log normal distribution
SGC	=	standard deviation* user supplied bimodal log normal distribution
RBARA	=	mean radius of "accumulation" mode for bimodal distributions
RBARC	=	mean radius of "coarse" mode for bimodal distributions
DR(I)	=	RR(I+1) - RR(I) = initial interval size, I=1, NI
R(KK)	=	all possible values of radius, KK=1, NMAX
F(KK)	=	value of distribution function at each R(KK), KK=1, NMAX
DELR	=	increment of radius for arbitrary distribution
DEN	=	temporary storage
GNUM	=	temporary storage
DENA	=	temporary storage
DENC	=	temporary storage
GNUMA	=	temporary storage
GNUMC	=	temporary storage
NRADII	=	NMAX
VOL	=	particle volume
VOLA	=	particle volume
VOLC	=	particle volume
AVOL	=	analytically evaluated average particle volume
OLSTAR	=	value of expansion coefficient $\tilde{\omega}_1$ for total aerosol
OM2	=	value of expansion coefficient $\tilde{\omega}_2$ for total aerosol
CTSUMT	=	value of extinction cross-section for total aerosol
CSSUMT	=	value of total scattering cross-section for total aerosol
DENST	=	value of particle number density for total aerosol
CRSUMT	=	value of radar cross-section for total aerosol
EMM	=	refractive index of medium in which scattering particles are deployed
BH	=	a factor used in size adjustment at non-zero relative humidity
FH	=	fractional relative humidity (saturation ratio)
CH	=	temporary storage
KEXT	=	extinction coefficient for a single aerosol component (per km)
KEXTT	=	total extinction ceofficient summed over all components(per km)
DRYVOL	=	total dry aerosol particle volume in (μm^3)
PSUMT(J)	=	final average phase function at Jth Gauss-Legendre value of μ

*The pre-coded (IDSTP = 8,9,10) values of SGA and SGC are the natural logarithms of the standard deviations

SYMBOL		Explanation
PC(J) RMS(J)	=	common block arrays not used explicitly in subroutine AGXPT2
TEMK	=	absolute temperature in °K
EMW	=	real part of refractive index of water at temperature TEMK
CAYW	=	imaginary part of refractive index of water at temperature TEMK
RHOW	=	mass density (gm/cm^3) of water at temperature TEMK
EMA	=	real part of refractive index of dry aerosol particle
CAYA	=	imaginary part of refractive index of dry aerosol particle
EMUA	=	(Hanel) growth factor index of dry aerosol particle
RHOA	=	mass density (gm/cm^3) of dry aerosol particle
CONC	=	mass concentration (gm/cm^3) of a dry aerosol component
DELTA	=	convergence level for halving method of integration
VOL	=	total volume occupied by aerosol material distributed in 1 cm^3 of space
EM	=	real part of refractive index of actual aerosol particle
CAY	=	imaginary part of refractive index of actual aerosol particle. Also, CAY = CAY/EM
FSUMG	=	integral of particle size distribution for one component of an aerosol
CTSUM	=	extinction cross-section for one component of an aerosol
CSSUM	=	total scattering cross-section for one component of an aerosol
CRSUM	=	radar cross-section for one component of an aerosol
OL1SUM	=	value of $\tilde{\omega}_1$ for one component of an aerosol
OL2SUM	=	value of $\tilde{\omega}_2$ for one component of an aerosol
PSUM(J)	=	weighted average intensity $[(i_1+i_2)/2]$ at J^{th} Gauss-Legendre value of μ_J; J=1, IT.
D	=	an initial interval of radius
RIT	=	adjusted radius, according to relative humidity
AC	=	parameter in formula for RIT
BC	=	parameter in formula for RIT
ALPHA	=	size parameter = (2π)(radius)/(wavelength)
QT	=	extinction efficiency factor for a given size parameter
QS	=	scattering efficiency factor for a given size parameter
QR	=	radar efficiency factor for a given size parameter
P(J)	=	phase function factor for a given size parameter, at J^{th} value of
PC(J)	=	(phase function)(distribution function) for a given size parameter, at Jth value of μ
O1STAR	=	value of $\tilde{\omega}_1$ for a given size parameter
O2STAR	=	value of $\tilde{\omega}_2$ for a given size parameter
FKK	=	value of distribution function at radius R(KK)
FKKA	=	(FKK)(geometrical cross-section of particle)
OLGG,VOLHH	=	partial contributions to volume of average particle, for one component of aerosol
OL1GG,OL1HH	=	partial contributions to average $\tilde{\omega}_1$ average particle, for one component of aerosol
OL2GG, OL2HH	=	partial contributions to average $\tilde{\omega}_2$ average particle, for one component of aerosol
CTGG,CTHH	=	partial contributions to average extinction cross-section for one component of aerosol
CSGG,CSHH	=	partial contributions to average scattering cross-section, for one component of aerosol

SYMBOL		Explanation
CRGG, CRHH	=	partial contributions to average radar cross-section, for one component of aerosol
DEL	=	fractional change in contribution to volume from n^{th} to $n+1^{st}$ halving, for one initial interval
FT	=	partial contribution to integral of distribution function
VOLHHT	=	contribution to volume of average particle from one original interval
OL1HHT	=	contribution to $\tilde{\omega}_1$ of average particle from one original interval
OL2HHT	=	contribution to $\tilde{\omega}_2$ of average particle from one original interval
CTHHT	=	contribution to average extinction cross-section from one original interval
CRHHT	=	contribution to average radar cross-section from one original interval
CSHHT	=	contribution to average scattering cross-section from one original interval
FFT	=	contribution to integral of distribution function from one original interval
DENSC	=	particle number density for a given aerosol component
DENST	=	particle number density for total aerosol
PGG(J) PHH(J)	=	partial contributions to average intensity $(i_1+i_2)/2$ for one aerosol component at abscissa value μ_J
PHHT(J)	=	average intensity at μ_J for one original interval
CONCT	=	total aerosol mass concentration (mg/m^3), summed over all components
CATTN	=	total attenuation coefficient in m^2 per mg of dry aerosol material
CATTNW	=	total attenuation coefficient in m^2 per mg of dry aerosol + accreted water

AGAUS10 (Main Program) - Simplified Flow Chart

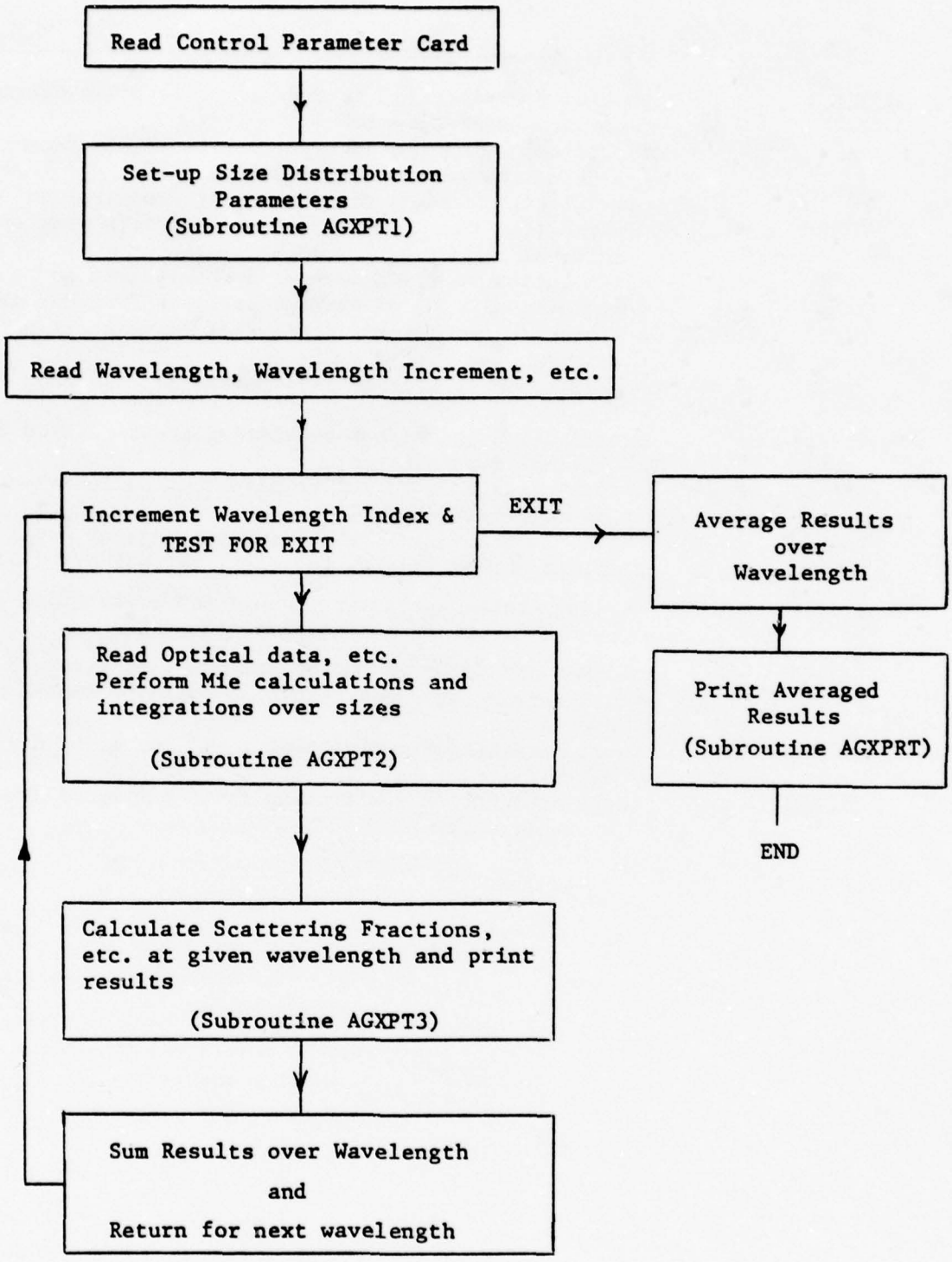

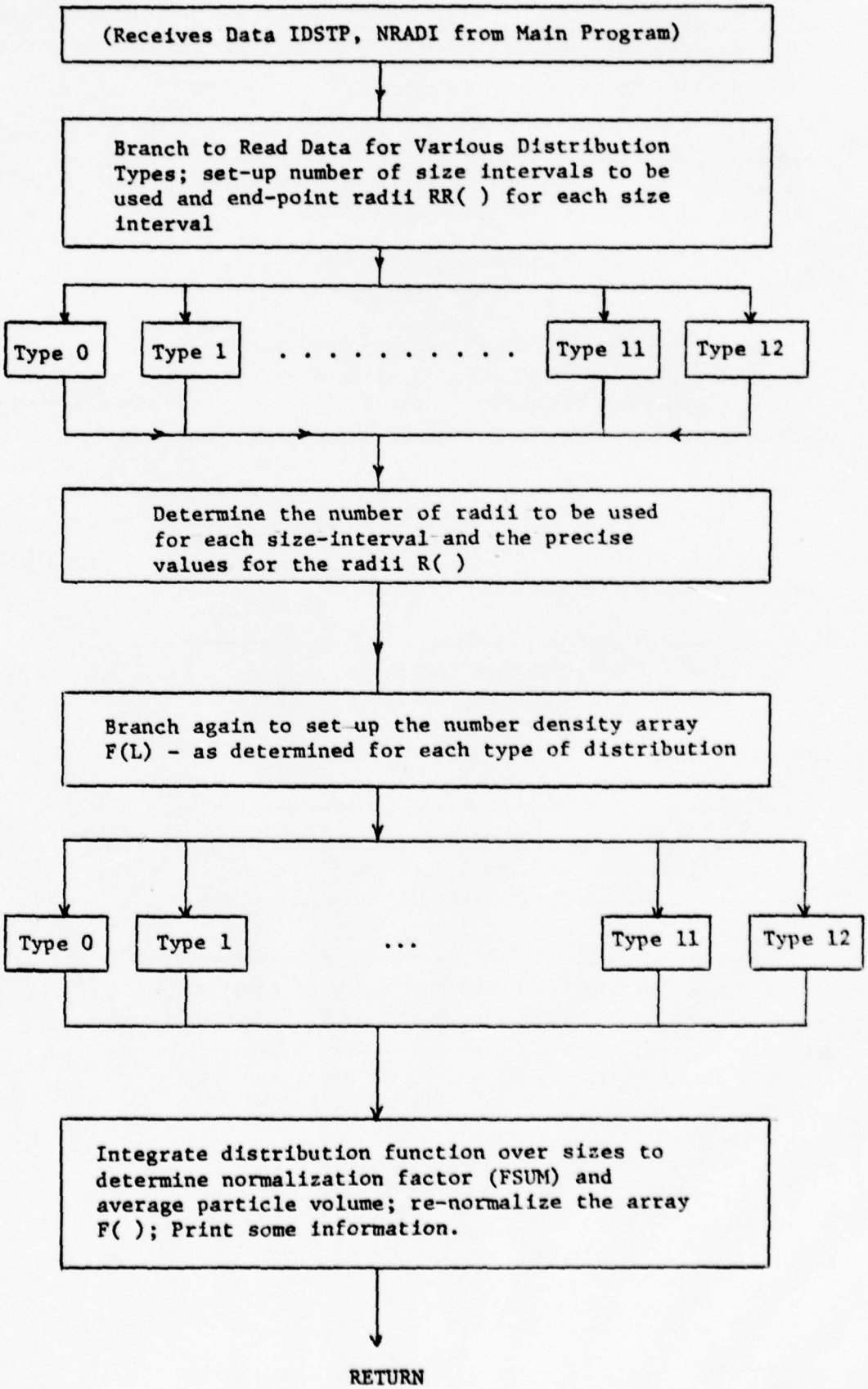
(Receives Data IDSTP, NRADI from Main Program)
Branch to Read Data for Various Distribution Types; set-up number of size intervals to be used and end-point radii RR( ) for each size interval
Type 0
Type 1
. . . . . .
Type 11
Type 12
Determine the number of radii to be used for each size-interval and the precise values for the radii R( )
Branch again to set up the number density array F(L) - as determined for each type of distribution
Type 0
Type 1
...
Type 11
Type 12
Integrate distribution function over sizes to determine normalization factor (FSUM) and average particle volume; re-normalize the array F( ); Print some information.
RETURN

Subroutine AGXPT2 - Simplified Flowchart

(Receives control data and size distribution data from main program)

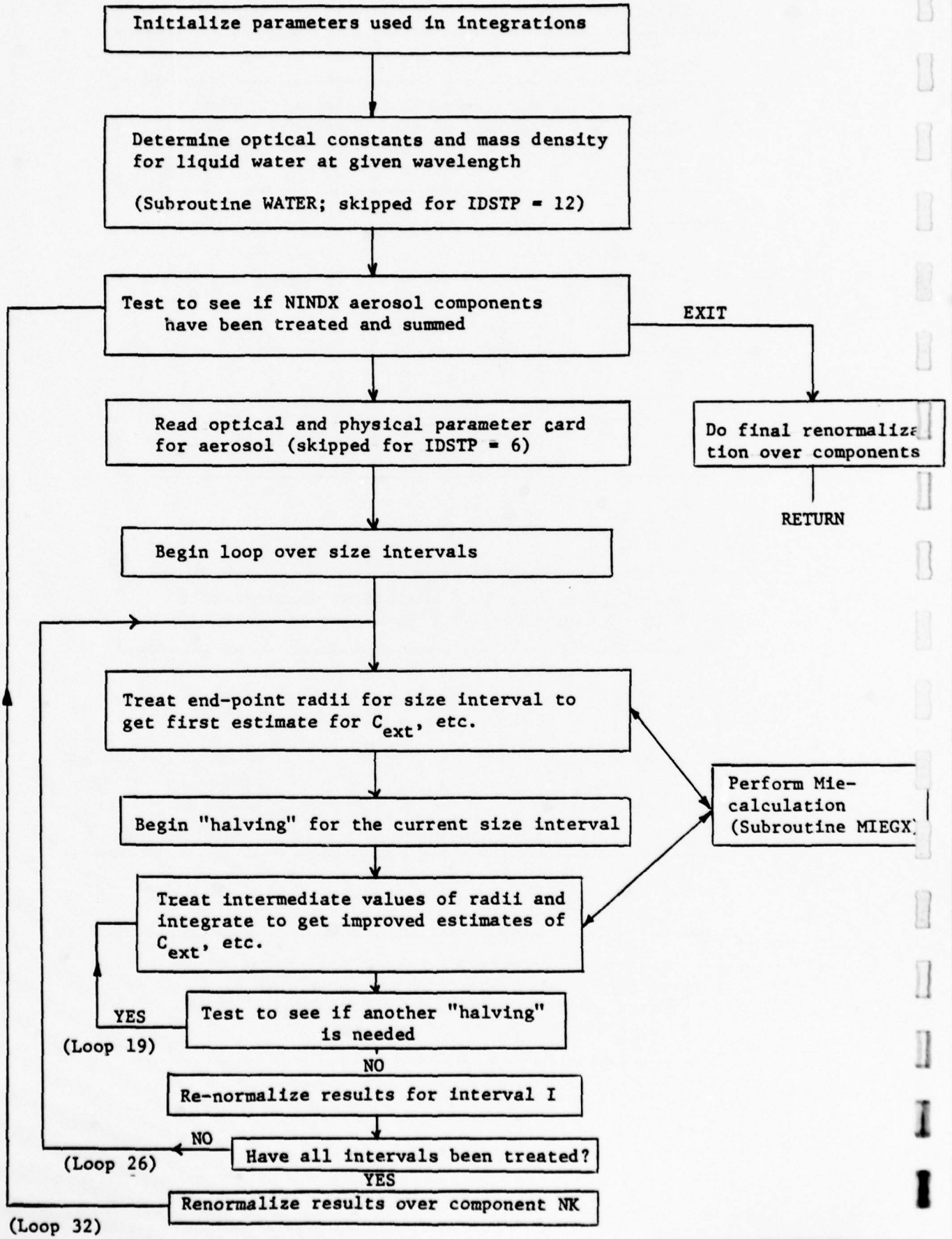

A.3.3 Input Data for AGAUS9 and/or AGAUS10

The data and control cards required for running these programs are of four basic types.

TYPE	General Description
1	A set of integers which select certain options available within the program.
2	A set of data describing the parameters of the particular size distribution function to be used. For cases other than the user-supplied "arbitrary" distribution (IDSTP=0), only one card of this type is needed.
3	A set of data describing the initial wavelength (μm) to be used, its increment, aerosol number density, relative humidity, atmospheric temperature (and, for AGAUS10, IDSTP=6, the desired convergence testing level).
4	A set of data describing the optical and physical properties of the aerosol material. If the aerosol is a mixture of materials of unlike properties, more than one card of this type is needed for each card of type 3. No card of this type is used, however, for runs with parameter IDSTP (on card type 1) is equal to 6.

Remarks:

1. The simplest type of run (IDSTP=6, water cloud or fog model) requires one card each of types 1, 2, and 3. For other IDSTP choices, at least one card of type 4 is also needed.

2. If the run is to use several wavelengths, then at least one card of type 4 is required for each wavelength (more than one type 4 card will be needed at each wavelength if the aerosol is a multicomponent mixture).

3. Two special "looping" modes of AGAUS9 and AGAUS10 affect the number of cards of type 3 which are needed:

A) For runs at constant relative humidity and several wavelengths, only one type 3 card is needed or permitted. To activate this mode, the wavelength increment DWAVE on card type 3 must be larger than 10^{-4}.

B) Runs at constant wavelength and a set of differing values of relative humidity require one <u>set</u> of cards of types 3 and 4 for each value of relative humidity. This option is invoked by setting the parameter "DWAVE" equal to zero on the first and all subsequent cards of type 3.

Summary of Data Card Requirements

CARD TYPE	Input Symbols
1	IDSTP, NRADI, IDUMMY, NWAVE, NINDX, MQRTE, NCRDS, NUNIT, IANG, ISCAT [FORMAT (11I5)] Explanations: All parameters on this card have been defined in Section A.2.1, with the exception of NRADI. NRADI is used by AGAUS10 only for the case IDSTP; its value for other IDSTP choices is ignored
2	Aerosol size distribution data; parameters vary with IDSTP value; see Section A.2.4.
3	WAVE, DWAVE, RELHUM, DENSH, TEMP, DELTAF [Format (6D12.6)] Explanations: See Sec. A.2.1 for the explanation of all quantities other than DELTAF. Parameter DELTAF is the "convergence level" to be used for IDSTP=6 runs; it's value is ignored for other IDSTP choices Cards of Type 3 may be repeated (NWAVE-1) times if and only if DWAVE < 1.0D-4
4	EMA, CAYA, EMUA, RHOA, CONC, DELTA [Format(4F10.6, 2D15.7)] Explanations: With the exception of DELTA, all parameters are defined in Section A.2.5. DELTA is the desired (fractional) convergence level (Δ); it should be positive. Remarks: A. Card Type #4 is not required and is never read-in if IDSTP=6 (water cloud/fog model) since the relevant data are obtained from subroutine WATER. Since card #4 is not used for that case, the desired value of DELTA must be inserted on card type #3 as DELTAF. B. In the case IDSTP=12, the rain model, card type #4 must carry the optical data for liquid water as EMA and CAYA. The reason for that inconsistency is that the rain model will most likely be usable at wavelengths for which no data appear in subroutine WATER (restricted to $\lambda \leq 0.2$ mm). [The large droplet sizes to be found in the rain model will usually cause premature failure of the Mie routine at small wavelengths].

C. Card Type #4, with appropriately adjusted data values, must be repeated (NWAVE-1) times.

A.3.4 Incidental Remarks Regarding AGAUS10

1) In AGAUS10, the average "dry volume per particle" is found using all available values for particle radii. It may differ from that printed in routine AGXPT2 since that routine might not proceed to the use of all available values.

2) The "volume" convergence tests in AGXPT2 use the volume inferred after any growth arising from non-zero saturation ratios has been included.

3) It should be noted that the convergence tests used in AGAUS10 do not really provide tests of the absolute accuracies achieved for the tested quantity. It is possible for "exit" to occur ($\delta<\Delta$) even though the use of "another" halving might lead to $\delta>\Delta$ again. If runs using some choice of Δ should lead to what appear to be "unusual" or unexpected results, it is advised that, as a test, the case be re-run using a smaller value of Δ

4) Some users may wish to explore possible increases in computation efficiency which might result from changes in the number (NI) of size-intervals, or, the ways in which they have been chosen (in AGXPT1).

Comments on Usage of AGAUS9 and AGAUS10 in the IANG=0 Mode

AGAUS9 and AGAUS10 have been coded to preserve the option of creating the expansion coefficients, $\tilde{\omega}_\ell$, which are needed by the ASL multiple scattering code STAR04, its NMSU version AGSCAT, and the NMSU/ASL thermal emission code CLEM70. Usage of the $\tilde{\omega}_\ell$ coefficients for the above purposes, however, requires some caution on the part of the user. In particular, users must not assume that the absence of abnormal termination of runs of *AGAUS9 or AGAUS10 guarantees* that "all is well". Past experience has shown that "warnings" of possible problems printed by those programs may not be noticed or taken very seriously. In an attempt to overcome those oversights, additional tests and warnings have been incorporated in AGAUS9 and *AGAUS10. If those* warnings are to be meaningful, users should examine printed outputs carefully for such warnings before using the results of runs as inputs to subsequent codes.

One particular point which should be checked is to see that the quantity printed under the heading ALBDO agrees reasonably well with the zeroth coefficient ($\tilde{\omega}_o$) of the expansion coefficients. Substantial disagreement between those two quantities usually means that the parameter "IT" used in a run was "too small" to acheive a really accurate reconstruction of the phase function from only "IT" Legendre expansion terms.

A.4 SAMPLES OF DATA DECKS FOR AGAUS9 AND AGAUS10

Example 1: IDSTP = 0 (User supplied distribution data)

Column 1

```
 0  011    1    7    112345    0    0   05   01
0.10000D-00 0.02000D+00
0.00000D-00
0.20000D-00
0.40000D-00
0.60000D-00
0.80000D-00
1.00000D-00
0.80000D-00
0.60000D-00
0.40000D-00
0.20000D-00
0.00000D-00
10.6000D+00 0.10000D-05 00.0000D+00 0.00000D-05 25.0000D+00
   1.9530   .468000   0.00000   1.87000   1.000000D-09  1.0000000D-02
10.6000D+00 0.10000D-05 75.0000D+00 0.00000D-05 25.0000D+00
   1.9520   .468000   0.15900   1.87000   1.000000D-09  1.0000000D-02
10.6000D+00 0.10000D-05 80.0000D+00 0.00000D-05 25.0000D+00
   1.9530   .468000   0.15600   1.87000   1.000000D-09  1.0000000D-02
10.6000D+00 0.10000D-05 85.0000D+00 0.00000D-05 25.0000D+00
   1.9530   .468000   0.15200   1.87000   1.000000D-09  1.0000000D-02
10.6000D+00 0.10000D-05 90.0000D+00 0.00000D-05 25.0000D-00
   1.9530   .468000   0.14600   1.87000   1.000000D-09  1.0000000D-02
10.6000D+00 0.10000D-05 95.0000D+00 0.00000D-05 25.0000D+00
   1.9530   .468000   0.14000   1.87000   1.000000D-09  1.0000000D-02
10.6000D+00 0.10000D-05 99.0000D+00 0.00000D-05 25.0000D+00
   1.9530   .468000   0.15800   1.87000   1.000000D-09  1.0000000D-02
```

This example is set up to read 11 distribution data cards, and to run for seven values of relative humidity at λ = 10.6 μM. Since MQRTE = 12345, detailed Mie results for each of the 11 radii will be printed. Parameter "IT" is 5, and IANG = 1. Note that the second data card contains RLO (=0.1 μM) and DELLR (=0.02). The next eleven cards contain F(RLO), F(RLO+DELLR, etc.) The remaining cards consist of seven pairs of cards, two for each of the seven values of NWAVE. In all cases, DENSH is zero which means that particle number densities will be calculated from RHOA (1.87, above), CONC (10^{-9} gm/cc, above) and the average particle volume computed within the program.

Example 2: IDSTP = 1 (Log normal distribution)

Column 5

```
    1  100     1     7     1 2345     0     0    05    00
 3.70000D-01 1.54000D+00 0.00500D-00 1.00000D-00
 10.6000D+00 0.10000D-05 00.0000D+00 0.00000D-05 25.0000D+00
    1.9530    .468000    0.00000    1.87000    1.000000D-09  1.0000000D-02
 10.6000D+00 0.10000D-05 75.0000D+00 0.00000D-05 25.0000D+00
    1.9530    .468000    0.15900    1.87000    1.000000D-09  1.0000000D-02
 10.6000D+00 0.10000D-05 80.0000D+00 0.00000D-05 25.0000D+00
    1.9530    .468000    0.15600    1.87000    1.000000D-09  1.0000000D-02
 10.6000D+00 0.10000D-05 85.0000D+00 0.00000D-05 25.0000D+00
    1.9530    .468000    0.15200    1.87000    1.000000D-09  1.0000000D-02
 10.6000D+00 0.10000D-05 90.0000D+00 0.00000D-05 25.0000D+00
    1.9530    .468000    0.14600    1.87000    1.000000D-09  1.0000000D-02
 10.6000D+00 0.10000D-05 95.0000D+00 0.00000D-05 25.0000D+00
    1.9530    .468000    0.14000    1.87000    1.000000D-09  1.0000000D-02
 10.6000D+00 0.10000D-05 99.0000D+00 0.00000D-05 25.0000D+00
    1.9530    .468000    0.15800    1.87000    1.000000D-09  1.0000000D-02
```

Remarks: This run also uses seven values of relative humidity. The second card carries RBAR, SIGMA, RLO and RHI. If RLO and RHI are set to zero, the program itself will choose RLO and RHI.

Example 3: IDSTP = 5 (Modified gamma distribution)

Column 5

```
    5  040     1     1     3 2345     0     0    01    00     0
.027852D+00 1.22549D+01 4.00000D+00 .600000D+01 .100000D+01
.700000D+00 .000000D-04 .000000D+00 1.00000D+02  5.0000D+00
    1.3300    .000000    0.00000    1.00000    1.000000D+00  1.0000000D-02
    1.4300    .000000    0.00000    1.00000    1.000000D-01  1.0000000D-02
    1.5300    .050000    0.00000    1.00000    1.000000D-03  1.0000000D-02
```

Remark: This example sets NINDX = 3, and treats a mixture of three aerosol components having different refractive indices and mass concentrations.

Example 4: IDSTP = 6 (NMSU water cloud/fog distribution)

Column 5

```
    6  000    1    5    1 2345    0    0   05   01    0
 .027852D+00 1.22549D+01 4.00000D+00 .600000D+01 .100000D+01 1.00000D-06
8.000000D+00 1.00000D+00 .000000D+00 0.00000D+00  5.0000D+00 1.00000D-02
```

Remark: This example uses the same distribution parameters as example 3, but also carries ELWC = 10^{-6} gm/cm^3 on the second data card. The setup is for runs at 5 wavelengths, beginning at 8.0 μM, with increments of 1.0 μM.

Example 5: IDSTP = 10 (Bimodal distribution)

Column 5

```
   10  050    1    7    1 2345    0    0   09   00
 10.6000D+00 .000000D-04 .000000D+00 .100000D-04 25.0000D+00
    1.9530   .468000   0.00000   1.87000   1.000000D-09  1.0000000D-02
 10.6000D+00 0.10000D-05 75.0000D+00 0.00000D-05 25.0000D+00
    1.9530   .468000   0.15900   1.87000   1.000000D-09  1.0000000D-02
 10.6000D+00 0.10000D-05 80.0000D+00 0.00000D-05 25.0000D+00
    1.9530   .468000   0.15600   1.87000   1.000000D-09  1.0000000D-02
 10.6000D+00 0.10000D-05 85.0000D+00 0.00000D-05 25.0000D+00
    1.9530   .468000   0.15200   1.87000   1.000000D-09  1.0000000D-02
 10.6000D+00 0.10000D-05 90.0000D+00 0.00000D-05 25.0000D+00
    1.9530   .468000   0.14600   1.87000   1.000000D-09  1.0000000D-02
 10.6000D+00 0.10000D-05 95.0000D+00 0.00000D-05 25.0000D+00
    1.9530   .468000   0.14000   1.87000   1.000000D-09  1.0000000D-02
 10.6000D+00 0.10000D-05 99.0000D+00 0.00000D-05 25.0000D+00
    1.9530   .468000   0.15800   1.87000   1.000000D-09  1.0000000D-02
```

Remarks: This run set up is similar to example 2, except that it is for IDSTP = 10.

Example 6 IDSTP = 12 (Marshall-Palmer rain model)

Column 5

```
    12  000    1    2    1 2345    0    0   05   01    0
  1.00000D+00
 1.000000D+03 1.00000D+03 .000000D+00 0.00000D+00  5.0000D+00 1.00000D-02
     1.3300   .000000   0.00000   1.00000   1.000000D-06  1.0000000D-02
     1.3300   .000000   0.00000   1.00000   1.000000D-06  1.0000000D-02
```

Remarks: The second card carries a rain rate of 1 mm per hour. Two wavelengths are to be used (1mm and 2mm). The optical data (last two cards) are merely examples; those data are not really correct for λ = 1mm and 2mm.

Appendix B

B.1 PREPARATION OF TABLES

Program AGAUS10 has been used to determine the scattering fractions necessary for construction of tables. Within program AGAUSX the following parameters should be set (additional parameter input is explained in program AGAUSX): NCRDS = 0, IANG = 1, ISCAT = 1, IT = 91. The output, comprised of the scattering fractions, will either be punched on cards or written on NUNIT, which is an input parameter in AGAUSX. Once the punched deck is obtained the following cards must precede the punched output:

Card 1:	HEADER,	FORMAT (20A4),
Card 2:	DWAVE,	FORMAT (D12.6),
Card 3:	CATTN,	FORMAT (25x,D25.14),

where HEADER is for informative purposes, DWAVE is the wavelength in microns and CATTN is the attenuation coefficient in m^2 mg^{-1}. Additionally, a sentinel card must be inserted at the end of the deck if more scattering fractions (additional wavelengths) are to be read in. The sentinel card is (starting in column 1) 999 (no decimal point), and should not follow the physically last data card. Program CNTRL, which is reproduced below, will then create a direct access (indexed) file which may be used with program FIND. A sample run stream for program CNTRL is provided on the following page. Three input wavelengths are assumed in the example.

B.2 DOCUMENTATION FOR PROGRAM FIND

Program FIND is a stand-alone program or may easily be incorporated into program ASLSOM. The purpose of program FIND is to read a given table and interpolate over wavelength, if necessary, to find precalculated values of the scattering fraction and attenuation coefficient (in m^2/mg). The given table is for one aerosol model; different aerosols require a different table. Program FIND operates by using a direct access (indexed) file to reduce 'look up' time. The control procedure is as follows: the wavelengths within the table are listed in increasing order and are seventeen records long, one record is eighty characters. The physical setup of one 'wavelength block', the complete information pertaining to the wavelength under consideration, contains the following information:

Record 1: RLO, RHI, RC, ALPHA, GAMMA, DENSITY
Record 2: WAVE1, CATTN1, FIRST
Records 3-17: SCAT1(I)

Sample Runstream for Program CNTRL

```
@ FOR, I          .CNTRL
    CNTRL DECK
        :
@ MAP, IN          CNTL
IN                .CNTRL
END
@ CAT, P           FILE.
@ ASG, A           FILE.
@ USE 23., FILE.
@ XQT              CNTL
    DATA DECK 1
        :
999
    DATA DECK 2
        :
999
    DATA DECK 3
        :
@ FIN
```

```
01NMSU*APX(1).CNTRL
   1      C  PGM FOR REWRITING THE OUTPUT FROM AGAUSX INTO ASLSOM FORMAT
   2      C  FOR TABLE PREPARATION TO BE USED WITH PROGRAM FIND
   3            REAL*8 SCAT (91),CATTN,DWAVE
   4            DIMENSION SSCAT (91),HEADER (20)
   5            N=0
   6      C  CHANGE THE FIRST PARAMETER IN THE DEFINE FILE 23 STMT TO BE
   7      C  17 TIMES THE NUMBER OF INPUT WAVELENGTHS (in this case, 5 wavelengths)
   8            DEFINE FILE 23(425,80,L,IFIND)
   9      6     CONTINUE
  10            READ (5,100,END=5) (HEADER(I),I=1,20)
  11            WRITE (23'IFIND,100) (HEADER(I),I=1,20)
  12            READ (5,102) DWAVE
  13            WAVE=SNGL (DWAVE)
  14            READ (5,101) CATTN
  15            CATN=SNGL(CATTN)
  16            READ (5,102) SCAT(1)
  17            SSCAT(1)=SNGL(SCAT(1))
  18            WRITE (23'IFIND,103) WAVE,CATN,SSCAT(1)
  19            DO 2 I=2,91
  20            READ (5,102) SCAT(I)
  21      2     SSCAT(1)=SNGL(SCAT(I))
  22            DO 3 I=2,86,6
  23            K=I+5
  24      3     WRITE (23'IFIND,103) (SSCAT(J),J=I,K)
  25            READ (5,104,END=5) NTEST
  26            N=N+1
  27            IF (NTEST.EQ.999) GO TO 6
  28      5     PRINT 104,N
  29      100   FORMAT (20A4)
  30      101   FORMAT (25X,D25.14)
  31      102   FORMAT (D12.6)
  32      103   FORMAT (6(E12.6,1X))
  33      104   FORMAT (1X, 'END PGM CHANGE',2X,13,
  34           + 'FILES HAVE BEEN CONCATENATED')
  35            END
```

where

RLO = minimum aerosol radius (μm)
RHI = maximum aerosol radius (μm)
RC = mode aerosol radius (μm)
ALPHA = parameter in the modified gamma distribution
GAMMA = parameter in the modified gamma distribution
DENSITY = aerosol density ($\#cm^{-3}$)
WAVE1 = wavelength under consideration (μm)
CATTN1 = attenuation coefficient ($m^2\ mg^{-1}$)
FIRST = scattering fraction at zero degrees
SCAT1(I) = scattering fraction at 2° to 180° in 2° increments.

The formats are as follows:

Record 1*: 6E12.6
Record 2 : 3(E12.6,1x)
Records 3-17 : 6(E12.6,1x)

*record 1 is read as Header [Format (A4)] and is not currently used.

Thus given the proper input, to be subsequently explained, program FIND will either; 1) find the input wavelength to ± 2% or 2) find the next largest wavelength than the input wavelength and then interpolate over the internal wavelength range. In either case the output is either punched or written as an auxillary unit under the following format (ASLSOM format):

Records 1-91: scattering fractions, FORMAT (E12.6)
Record 92 : attenuation coefficient, FORMAT (10x,E10.4)

Room has been left on the 92nd record to insert additional (needed) parameters in their proper format without having to relocate the physical position of the attenuation coefficient.

The input for program FIND is as follows:

one card: WAVE, NUNIT: FORMAT (F7.3,I2)
where WAVE = wavelength (μm) for which scattering fractions and attenuation coefficient are desired
NUNIT = auxillary unit for scattering fractions and attenuation coefficient to be written upon; the default value of NUNIT (zero or blank) is the card punch (unit 4 on Univac 1100 series).

In order to run program FIND two additional commands are needed. One must assign one of the two existing fog model files, 8201NMSU*WSMRF01 or 8201NMSU*WSMRF02 (see previous explanation for the difference in fog models) and then attach a use assigned name of 23 to the particular file under consideration. Therefore a typical run stream might appear as follows:

```
@ASG, A   8201NMSU*WSMRF01.

@USE 23., 8201NMSU*WSMRF01.

@FOR, I   .FIND

 CARD DECK

     :

@MAP, IN   FND

IN         .FIND

END

@XQT FND

+01.06022
@FIN
```

This would assign fog model WSMRF01 and write the scattering fractions and attenuation coefficient for 1.06 μm on unit 22. If the input card had read +01.060 the output would have been punched on cards.

Appendix C

FORMAL SOLUTION OF THE RADIATIVE TRANSFER EQUATION

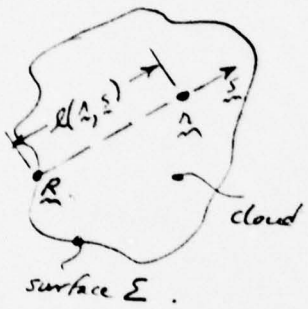

It is desired to show that Eqs. (3), (4) are solutions of Eqs. (2), (1), respectively. In order to do this, it is first necessary to show that

$$\underset{\sim}{s}\cdot\nabla_{\underset{\sim}{r}}\,\ell(\underset{\sim}{r},\underset{\sim}{s}) = 1, \qquad \text{(C-1)}$$

where $\ell(r,s)$ is the distance from the point r in the cloud back along $(-s)$ to the point R on the bounding surface Σ, as illustrated in Fig. B1. Note that

$$\underset{\sim}{R} = \underset{\sim}{r} - \underset{\sim}{s}\,\ell(\underset{\sim}{r},\underset{\sim}{s}). \qquad \text{(C-2)}$$

Let the surface Σ be given by $f(\underset{\sim}{R}) = 0 = f(\underset{\sim}{r}-\ell\underset{\sim}{s})$, $f(\underset{\sim}{R}+d\underset{\sim}{R}) = 0 = f(\underset{\sim}{R}) + dR_i(\partial f/\partial R_i)$, so

$$0 = dr_k(\partial R_i/\partial r_k)(\partial f/\partial R_i) = dr_k(\delta_{ki}-\partial_k\ell\, s_i)(\partial f/\partial R_i), \qquad \text{(C-3)}$$

where summation rotation is used (repeated indices summed over). Since the dr_k are arbitrary, it must be true that $(\delta_{ki}-(\partial_k\ell)s_i)(\partial f/\partial R_i) = 0$. But the $\partial f/\partial R_i$ are not zero; therefore the determinant of the matrix $A_{ki} = \delta_{ki}-\partial_k\ell\, s_i$ must vanish. But

$$\det A = 1 - s_i\partial_i\ell = 1 - \underset{\sim}{s}\cdot\nabla_{\underset{\sim}{r}}\ell = 0, \qquad \text{(C-4)}$$

which completes the desired proof. As an example of the relation $\underset{\sim}{s}\cdot\nabla_{\underset{\sim}{r}}\ell = 1$, consider a plane parallel cloud, as in Fig. B2. Then

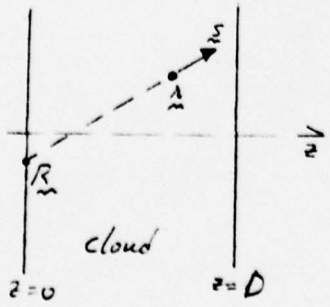

$$\ell(\underset{\sim}{r},\underset{\sim}{s}) = z/\cos\theta = z/\mu$$

$$\underset{\sim}{s} = \underset{\sim}{i}\sin\theta\cos\phi + \underset{\sim}{j}\sin\theta\sin\phi + \underset{\sim}{k}\mu$$

$$\nabla_{\underset{\sim}{r}}\ell = \underset{\sim}{k}\,\partial\ell/\partial z = \underset{\sim}{k}\mu^{-1}.$$

$$\underset{\sim}{s}\cdot\nabla_{\underset{\sim}{r}}\ell = \underset{\sim}{k}\mu\cdot\underset{\sim}{k}\mu^{-1} = 1.$$

Here, (i,j,k) are the usual orthogonal triplet of cartesian basis vectors.

Now, consider the expression for the incident beam intensity in the cloud, given by Eq. (3): $I_{in}(\underset{\sim}{r},\underset{\sim}{s}) = \exp - \gamma\ell(\underset{\sim}{r},\underset{\sim}{s}) I_{in}^{(\Sigma)}(\underset{\sim}{r}-s\ell(\underset{\sim}{r},\underset{\sim}{s}),\underset{\sim}{s})$. Then, with $R_k \equiv r_k - s_k\,\ell(\underset{\sim}{r},\underset{\sim}{s})$,

$$\underset{\sim}{s}\cdot\nabla_{\underset{\sim}{r}} I_{in} = -\gamma(\underset{\sim}{s}\cdot\nabla_{\underset{\sim}{r}}\ell) I_{in} + (\exp-\gamma\ell)(\partial I_{in}^{\Sigma}(\underset{\sim}{R},\underset{\sim}{s})/\partial R_k)(s_i\ \partial R_k/\partial r_i) \qquad \text{(C-5)}$$

but $\underset{\sim}{s}\cdot\nabla_{\underset{\sim}{r}}\ell = 1$, and $s_i\ \partial R_k/\partial r_i = s_i(\delta_{ki} - s_k\ \partial_i\ell) = s_k(1-\underset{\sim}{s}\cdot\nabla_{\underset{\sim}{r}}\ell) = 0$,

so indeed $I_{in}(\underset{\sim}{r},\underset{\sim}{s})$ satisfies Eq. (2).

Now, consider Eq. (4), the expression for the total intensity. Since $\underset{\sim}{s}$ is a unit vector, it is clear that

$$\underset{\sim}{s}\cdot\nabla_{\underset{\sim}{r}} I(\underset{\sim}{r}-\xi\underset{\sim}{s},\underset{\sim}{s}') = -\partial I(\underset{\sim}{r}-\xi\underset{\sim}{s},\underset{\sim}{s}')/\partial\xi. \qquad \text{(C-6)}$$

Using this, and Eq. (4), and $\underset{\sim}{s}\cdot\nabla_{\underset{\sim}{r}}\ell(\underset{\sim}{r},\underset{\sim}{s}) = 1$,

$$\underset{\sim}{s}\cdot\nabla_{\underset{\sim}{r}} I(\underset{\sim}{r},\underset{\sim}{s}) = \underset{\sim}{s}\cdot\nabla_{\underset{\sim}{r}} I_{in} + (4\pi)^{-1}\gamma\, e^{-\gamma\ell}\int d\Omega_{s'}\, p(\underset{\sim}{s},\underset{\sim}{s}') I(\underset{\sim}{r}-\ell\underset{\sim}{s},\underset{\sim}{s}')$$

$$- (4\pi)^{-1}\gamma\int_0^{\ell} d\xi\, \frac{\partial}{\partial\xi}\left[e^{-\gamma\xi}\int d\Omega_{s'}\, p(\underset{\sim}{s}\underset{\sim}{s}') I(\underset{\sim}{r}-\xi\underset{\sim}{s},\underset{\sim}{s}')\right]$$

$$- (4\pi)^{-1}\,\gamma^2\int_0^{\ell} d\xi\, e^{-\gamma\xi}\int d\Omega_{s'}, p(\underset{\sim}{s},\underset{\sim}{s}') I(\underset{\sim}{r}-\xi\underset{\sim}{s},\underset{\sim}{s}').$$

The last term on the RHS of this equation is just $-\gamma(I(\underset{\sim}{r},\underset{\sim}{s})-I_{in}(\underset{\sim}{r},\underset{\sim}{s}))$; the third term on the RHS is integrable, and yields two terms, one of which cancels the second term. These results yield

$$\underset{\sim}{s}\cdot\nabla_{\underset{\sim}{r}} I(\underset{\sim}{r},\underset{\sim}{s}) = \underset{\sim}{s}\cdot\nabla_{\underset{\sim}{r}} I_n + (4\pi)^{-1}\gamma\int d\Omega_{s'}, p(\underset{\sim}{s},\underset{\sim}{s}') I(\underset{\sim}{r},\underset{\sim}{s}') - \gamma(I(\underset{\sim}{r},\underset{\sim}{s})-I_{in}(\underset{\sim}{r},\underset{\sim}{s})).$$

But $\underset{\sim}{s}\cdot\nabla_{\underset{\sim}{r}} I_n + \gamma I_{in} = 0$, (Eq. 2), so the final result is

$$\underset{\sim}{s}\cdot\nabla_{\underset{\sim}{r}} I(\underset{\sim}{r},\underset{\sim}{s}) + \gamma I(r,s) = (4\pi)^{-1}\gamma\int d\Omega_{s'}, p(\underset{\sim}{s},\underset{\sim}{s}') I(\underset{\sim}{r},\underset{\sim}{s}'), \qquad \text{(C-7)}$$

which is just Eq. (1).

The formal implicit solution of Eq. (C-1) given by Eq. (C-4) is simply a coordinate-dependent realization of a familiar form given by Chandrasekhar [32]. The authors of this report believe that this form (Eq. C-4) has not previously been reported in the literature.

Addendum: Most routines used and developed under this contract have been placed in a special file in WSMR's system B. That file is "8201NMSU*NMSFINAL". Some notes on the contents of that file follow.

Notes on File 8201NMSU*NMSFINAL

This file contains various source codes, data elements, mapping and running elements developed or modified during 1978.

There are two principal types of programs:

(1) ATRAN - the high resolution code
(2) assorted single-scattering (Mie) codes.

ATRAN: The main program is ATRAN14. A sample 1108 run-stream will be found in element ATRUNF. That element either contains (or will direct one to an element which contains) compilation, mapping and running instructions. Reference to ATRUNF or elements called by it (via @ADD statements) will define which source codes, etc., in file 8201NMSU*NMSFINAL belong to "ATRAN".

[Requires about 63K-words of core]

Mie-Codes: There are several of those:

1) AGAUS9 - an NMSU version of PGAUSS, including computation of "scattering fractions" (documented in final report).

Uses subroutines: AG9PT1,AG9PT2,AG9PT3,AG9PRT,GAUS,GUSET, WATER,MIEGX,TIMB,ANGLE.
Runstream: element = RUNAG9
Sample Data: elements = TYPE0,TYPE1,TYPE6,TYPE10,TYPE12,AGXC1 (type = 5).

[Requires about 60K of core]

2) AGAUSX (documented in the final report as AGAUS10) - a "halving" version of AGAUS9.

Uses Subroutines: AGXPT1,AGXPT2,AGXPT3,AGXPRT,GAUS,GUSET,ANGLE, MIEGX,TIMB,WATER
Sample Runstream: element = RUNAGX

[Requires about 60K of core]

Sample Data Elements: Same as for AGAUS9

3) MAIN1S (AGAUS10S, no documentation furnished). This is a version of AGAUS10 which uses double-precision arithmetic only in the Mie-subroutine (MIEGXS) and the routine (SGUSET) used to get the Gauss-Legendre quadrature weights and abscissae. It is logically identical to AGAUSX, except that it performs the convergence checks on the ave. Intensity as well as on the extinction coefficient. For similar conditions AGAUS10S results will agree with those of AGAUS10 to six or more digits, but it needs only about 40K words of core.

Uses Subroutines: PART1S,PART2S,PART3S,AGPRTS,MIEGXS,SGAUS, SGUSET,ANGLES,TIMBS,WATERS
Sample Rustream: element = RUN10S
Sample Data: same as AGAUS9 or AGAUS10

4) AGAUSXL - A version of AGAUS10 which uses the RRA Mie-routine instead of Querfeld's forward-recursion variant (MIEGX). The RRA routine DOWN42 is used in a slightly modified form called RRAMIE.

Requires Subroutines: AGXPT1,AGXPT2L,AGXPT3,AGXPRT,GAUS, GUSET,WATER,TIMB,RRAMIE,SETUP,ANGLE
Sample Runstream: RUNXL
Sample Data: Same as AGAUS9,10,10S.

[Core Requirement ≃ 64K]

Note: No documentation has been prepared for AGAUSXL, but most of the logic is the same as for AGAUS10. However, some improvements contained in AGAUS10 may not have been incorporated into AGAUSXL and subroutine AGXPT2L.

5) MIE2 - this is the RRA aerosol extinction routine supplied to NMSU by ASL. It is in file 8201NMSU*NMSFINAL more for reference than for any other reason. It uses elements FIRST(≡ DOWN42) and SECOND(≡ IPLAW). A sample data element is ME2C1.

#SPECIAL NOTES#

Programs ATRAN14 and AGAUS10S exist at NMSU in IBM 360/370 compatible versions. The other routines listed above are extant only in Univac 1108 tested forms.

[The Univac 1108 version of ATRAN at WSMR expects a 7-track (BCD) copy of the AFGL data-tape, while the IBM 360/370 version uses a 9-track (EBCDIC) version of the tape. Some Job Control Language (JCL) differences also exist, but IBM 360/370 JCL instructions could be supplied if desired].

AGAUS10S has also been successfully modified at NMSU to run (with slightly restricted capabilities) on a DEC/PDP-1160 computer. That version will run within a 32K-word memory allocation. Program listings could be supplied to ASL without much difficulty, but tape or card copies are not presently available.